

**Making the smart watershed-to-lake connection: using high-frequency sensors and process-based aquatic ecosystem models to predict nearshore greening in Lake Tahoe**



**FINAL REPORT**

**SUBMITTED TO:  
NEVADA DIVISION OF STATE LANDS**

June 30, 2024

Making the smart watershed-to-lake connection: using high-frequency sensors and process-based aquatic ecosystem models to predict nearshore greening in Lake Tahoe

Final Report

Submitted to:

Nevada Division of State Lands

Submitted by:

University of Nevada, Reno's Global Water Center, Departments of Natural Resources and Environmental Sciences and Biology, and Graduate Program of Hydrologic Sciences

Dr. Joanna Blaszczak, Kelly Loria, Jasmine Krause, Dr. Heili Lowman, Dr. Sudeep Chandra

June 30, 2024

# Table of Contents

Acknowledgements.....	6
Acronyms.....	7
I. Introduction.....	8
II. Objective 1: Dissolved oxygen and estimated nearshore ecosystem metabolism time series at the outlets of Glenbrook and Blackwood Creeks.....	10
II.A Introduction.....	10
II.B Methods.....	11
II.B.1 Site Description.....	11
II.B.1 Sensor deployment and maintenance.....	12
Stage I Sensor Deployment.....	13
Stage II Sensor Deployment.....	14
Sensor calibration.....	14
Sensor maintenance.....	15
II.B.2 Data cleaning.....	15
II.B.3 Covariate Data.....	15
II.B.4 Ecosystem metabolism modeling.....	16
Gas exchange estimates (k).....	16
Characterizing benthic light.....	17
II.C Results.....	17
II.C.1 Dissolved oxygen and temperature at multiple depths in the nearshore.....	17
II.C.2 Ecosystem metabolism estimates from the nearshore.....	21
II.C.3 Spatial and temporal variation in upland and lake processes.....	23
II.D Conclusion.....	25
III. Objective 2: Stream and lake water chemistry monitoring.....	27
III.A Introduction.....	27
III.B Methods.....	27
III.B.1 Sampling Site Description.....	28
III.B.2 Sample Collection.....	29
Survey methods and sample collection:.....	29

III.B.3 Laboratory Analysis .....	30
III.B.4 Data Analysis .....	31
Characterizing flow regimes .....	31
Statistical methods for analyzing stream and lake water chemistry .....	31
III.C Results .....	32
III.C.1 Inflowing stream water chemistry .....	32
Variation in stream water flow .....	32
III.C.2 Nearshore lake chemistry .....	35
III.C.3 Standing stock biomass AFDM and chl-a in the streams and nearshore .....	38
Standing stocks of biomass .....	38
Seasonal stream metabolism trends .....	40
III.D Conclusion .....	42
IV. Objective 3: Quantifying rates of ammonium and nitrate uptake.....	44
IV.A. Introduction.....	44
IV.B. Methods.....	45
IV.B.1 Sampling Locations.....	45
IV.B.2 Field Sampling .....	45
IV.B.3 Laboratory Incubations .....	46
Incubation array .....	46
Vial filling.....	47
Nitrogen additions.....	47
IV.B.4 Laboratory Sample Analysis.....	47
IV.B.5 Data Analysis .....	49
Nitrogen uptake calculations.....	49
IV.C Results.....	50
Environmental conditions during sample collection.....	50
Nitrate and ammonium uptake rates .....	53
Comparison to historic uptake rates.....	57
IV.D Conclusion .....	57
V. Objective 4: Predicting nearshore ecosystem productivity.....	59
V.A Introduction.....	59

V.B Methods .....	61
V.B.1 Data structure .....	61
V.B.2 Data analysis and time series modeling .....	61
Time series - generalized linear mixed models.....	61
Structural Equation Modeling (SEM).....	62
Structural Equation Modeling - Precipitation Effects.....	63
V.C Results .....	63
V.C.I Relative influence of environmental drivers of nearshore metabolism .....	63
Stream dynamics within the nearshore .....	63
Other environmental drivers of nearshore ecosystem metabolism .....	67
V.D Conclusion.....	69
VI. Conclusions and Recommendations .....	71
VII. References .....	72
Appendix 1. Supplementary Figures.....	80

## **Acknowledgements**

We are grateful for the assistance and contributions of the many individuals who helped make this project possible. In no particular order, we thank Dr. Leon Katona, Rob Miller, Meredith Brehob, Taryn Elliot, Ian Halterman, Molly Ferro, Keenan Seto, Dillon Ragar, Emily Carlson (M.S.), Elizabeth Everest, Zachary Bess (M.S.), Erin Suenega (M.S.), Helen Lei, Dr. Wubneh Belete Abebe, and Rija Masroor for their assistance with field and lab work related to this project. We thank Marine Taxonomic Services Ltd. and the Tahoe Regional Planning Agency (Dan Segan) for their assistance with diving to maintain and retrieve sensors. We thank the residents of Glenbrook, Nevada, especially Gary and Susan Clemons for their support of this work. We thank the Nevada Division of State Lands and the Lake Tahoe License Plate Program (Chris LaCrosse) for funding this project. Additional support for sensor equipment and personnel was provided by the National Science Foundation award to PI Blaszcak (OIA-2019528).

## Acronyms

AFDM	Ash free dry mass
BW	Blackwood Creek
Chl-a	chlorophyll-a
DO	dissolved oxygen
DOC	dissolved organic carbon
ER	Ecosystem Respiration
GB	Glenbrook Creek
GPP	Gross Primary Productivity
$K_d$	Light extinction coefficient
km	kilometer
PAR	Photosynthetically active radiation
$PO_4^{3-}$	phosphate (measured as orthophosphate)
$NH_4^+$	ammonium
$NO_3^-$	nitrate
r	Pearson correlation coefficient
$R^2$	coefficient of determination
SPC	Specific conductance
SH	Slaughterhouse
SS	Sunnyside
SWE	Snow water equivalent

## I. Introduction

Lake Tahoe is a world-renowned large oligotrophic lake valued for its water clarity and deep blue color that attracts millions of visitors every year. The majority of visitors interact with the edge or nearshore of the lake by spending time on Lake Tahoe's beaches or walking along its shores. While calendar year mid-lake mean lake water clarity in Lake Tahoe by Secchi disk has been relatively stable with a slight decline since around 2000, there have both been declines in summer mean water clarity (Naranjo et al. 2022) and increasing reports of declines in nearshore water quality due to increased algae growth in the littoral zone, or what is known colloquially as "nearshore greening" (Naranjo et al. 2019, Vadeboncoeur et al. 2021). There is mixed evidence regarding the extent to which these changes in nearshore greening are occurring along the perimeter of Lake Tahoe (Atkins et al. 2021), but regardless, this issue has highlighted our limited understanding of what controls temporal and spatial variation in nearshore algae growth. High spatial heterogeneity in nearshore ecosystem productivity originates in part from variation in the degree of hydrologic connectivity with upland landscapes, which supply allochthonous nutrients and organic matter that support productivity and diversity in the littoral zone (Vander Zanden & Vadeboncoeur 2020). Thus, the goal of our project was to address the question, **how do watershed processes contribute to temporal variation in Lake Tahoe's nearshore water quality and which hydroclimatic factors and within-nearshore processes influence nearshore algal growth?**

Given the economic and ecological importance of clarity in the nearshore of Lake Tahoe, it is critical to understand the interactive controls which contribute to algal growth, the timing of peak growth rates, and what management actions may be implemented to improve water quality. Over the past decade, agency supported research activities to detect the presence of algal biomass along the nearshore of the lake included approaches such as remote sensing (Pearson & Huntington 2019), aerial imagery (Hackley et al. 2020), and in-situ boat driven transects with turbidity and chlorophyll-a sensors (Heyvaert et al. 2016). This prior work was an important first step in determining variation in the intensity and timing of algal growth, but scientists and managers still lack process-based understanding of variation in nearshore greening.

Previous work in Lake Tahoe has suggested that nearshore productivity may be limited by nitrogen (i.e., nitrate ( $\text{NO}_3^-$ ) and ammonium ( $\text{NH}_4^+$ )) availability (Reuter et al. 1986). Since 2005, ammonium (i.e., a form of nitrogen (N) used and sometimes preferred by algae (Axler et al. 1983)) delivery has increased to the nearshore of the lake (Domagalski et al. 2021). Changes in nitrogen loading and uptake by benthic algae could be a factor contributing to the observed changes in algae growth because if nearshore algae is N-limited, algal growth will increase with N delivery.

Current methods of directly quantifying periphyton biomass through time cannot match the spatial and temporal resolution of daily gross primary productivity (GPP) estimates because of destructive sampling techniques (e.g., scrubbing rocks), complications of scaling up to understand regional patterns of production when growth is patchy, and intensive labor requirements (e.g., diving and laboratory processing of biofilms samples). Instead, ecosystem metabolism time series models fit to high frequency dissolved oxygen and temperature sensor data can advance our understanding of year-round productivity dynamics. We can then infer underlying variables (e.g., periphyton biomass) using mathematical models (Blaszczak et al. 2023), thereby overcoming spatiotemporal inadequacies in physical sampling.

The overarching goal of this project was to build a process-based understanding of how watershed-to-lake connections drive nearshore algal growth dynamics in Lake Tahoe. We addressed this goal through a combined approach of the following objectives:

1. Generate time series of daily rates of modeled ecosystem gross primary productivity (GPP), an integrative metric of algal growth, at depths throughout the photic zone by monitoring dissolved oxygen, water temperature, light, and wind from weather stations.
2. Monitor streamwater  $\text{NH}_4^+$  and  $\text{NO}_3^-$  concentrations to determine watershed loading. Streamwater  $\text{NH}_4^+$  is currently no longer monitored as part of the USGS Lake Tahoe Interagency Monitoring Program (LTIMP) despite increases in this chemical species.
3. Quantify rates of  $\text{NH}_4^+$  and  $\text{NO}_3^-$  uptake and N-fixation in benthic samples collected quarterly using established laboratory incubation methods.
4. Modify and test time series models which integrate the results from objectives 1 and 2 to generate predictions of site-specific nearshore GPP through time.

We describe our approach and findings in detail corresponding to each objective below.

## **II. Objective 1: Dissolved oxygen and estimated nearshore ecosystem metabolism time series at the outlets of Glenbrook and Blackwood Creeks**

### **II.A Introduction**

Historically, measurements of productivity dynamics in lakes have focused on the mid-water column and samples collected from the center of a lake; however, this sampling schema may underestimate the influence of nearshore (i.e., littoral) zones on total lake productivity (Vander Zanden and Vadeboncoeur, 2020). Nearshore zones can be more strongly influenced by upland processes that disconnect nearshore dynamics from those measured in the center of lakes. Recently, there have been reports of increases in filamentous green algae growth on the benthos (i.e., bottom) of nearshore zones in otherwise clear, oligotrophic lakes (Vadeboncoeur et al., 2021), including Lake Tahoe (Naranjo et al., 2019). However, the extent to which filamentous green algal growth might be increasing around the edge of Lake Tahoe is debated as periphyton biomass monitored at 54 locations around the lake at 0.5 m depth did not show widespread increases since 1982 (Atkins et al. 2021). Yet, in the littoral fringe zone at 0.5 m depth, periphyton biomass might be considerably impacted by wave action and therefore further investigation is needed to understand how representative shallow zones are of the nearshore.

Because of these discrepancies in determining whether the nearshore is experiencing changes in benthic productivity, high-frequency year-round measurements of nearshore productivity are needed to establish a baseline understanding of how littoral fringe zone (0.5 m) dynamics differ from those further offshore and examine which environmental factors (e.g., climate, nutrient inputs) may be influencing the changes in benthic algal productivity. Daily gross primary productivity (GPP) can be estimated from diel changes in dissolved oxygen (DO) and temperature which can be measured using high frequency sensors (Winslow et al. 2016, Lottig et al. 2021). GPP is a reflection of the amount of underlying autotrophic biomass as well as the responses of photosynthetic activity to variation in light, temperature, and hydraulic disturbances that might remove the biomass (Blaszczak et al. 2023). Daily ecosystem respiration (ER) can also be estimated using diel variation in dissolved oxygen as this process consumes oxygen throughout the day and night. Together, GPP and ER are collectively known as ecosystem metabolism and monitoring of their collective dynamics can improve understanding of the timing and magnitude of biological activity year-round to inform management actions (Jankowski et al. 2021).

Here, we deploy a series of instruments in the nearshore region of Lake Tahoe to quantify the differences in dissolved oxygen (DO) and metabolism dynamics (1) on contrasting east and west shore sites surrounding stream outlets and with depth, and (2) at locations located closer to and further from stream inlets (i.e., watershed outlets to the lake). We deployed instruments that continuously measured DO and water temperature in the nearshore at multiple water depths at the time of deployment including 3 m (shallow littoral), 10 m (mid-shallow littoral), 15 m (mid-

deep littoral), and 20 m (deep littoral). All depths were instrumented and monitored from October 2021 to February 2023 (Project Stage I), while the shallow littoral zone was monitored until the fall of 2023 (Project Stage II).

## **II.B Methods**

### II.B.1 Site Description

Lake Tahoe is an oligotrophic mountain lake situated at 1,898 meters above sea level and a maximum depth of 505 meters (Goldman 1988). The watershed surrounding the lake (800 km<sup>2</sup>) is primarily forested and comprises 63 different streams that drain into the lake (Goldman 1988). Recently, reports of seasonal periphyton blooms in nearshore regions of Lake Tahoe have increased, particularly during the late winter and early spring seasons (Naranjo et al., 2019), although long-term monitoring of periphyton blooms has not found evidence of correlations between increased human development along the lakeshore and periphyton biomass (Atkins et al., 2021).

We focused sampling to the contrasting shores of Lake Tahoe that encompass varying levels of development, watershed slope, lake bathymetry, exposure to alongshore lake currents, and precipitation (Figure 1). The nearshore region of Lake Tahoe (<150 m depth) represents 19% of the overall surface area of the lake (Loeb et al. 1983) and can receive high nutrient inputs following winter storms and spring snowmelt (Naranjo et al., 2022) as well as wind-driven upwelling events in late spring and early summer (Roberts et al., 2021). The Blackwood Creek watershed on the west shore (29 km<sup>2</sup>) is primarily undeveloped and forested (Leonard et al, 1979; Coats et al., 2016) and drains a more gradually sloping catchment that enters Lake Tahoe north of Tahoe Pines, California (39.107009, -120.158221) in a relatively steep and exposed nearshore region of the lake. The Glenbrook Creek watershed on the east shore (11 km<sup>2</sup>) is primarily forest at higher elevations with some development and wetlands at lower elevations (Leonard & Goldman 1981), and it drains a much steeper catchment that enters Lake Tahoe near Glenbrook, Nevada (39.088019, -119.940094) into the gently sloping and protected Glenbrook Bay. Although most annual precipitation in the larger Lake Tahoe watershed falls as winter snow, it may vary significantly between the west (mean annual precipitation [MAP] = 140 cm yr<sup>-1</sup>) and east (MAP = 67 cm yr<sup>-1</sup>) shores (Coats et al., 2008).

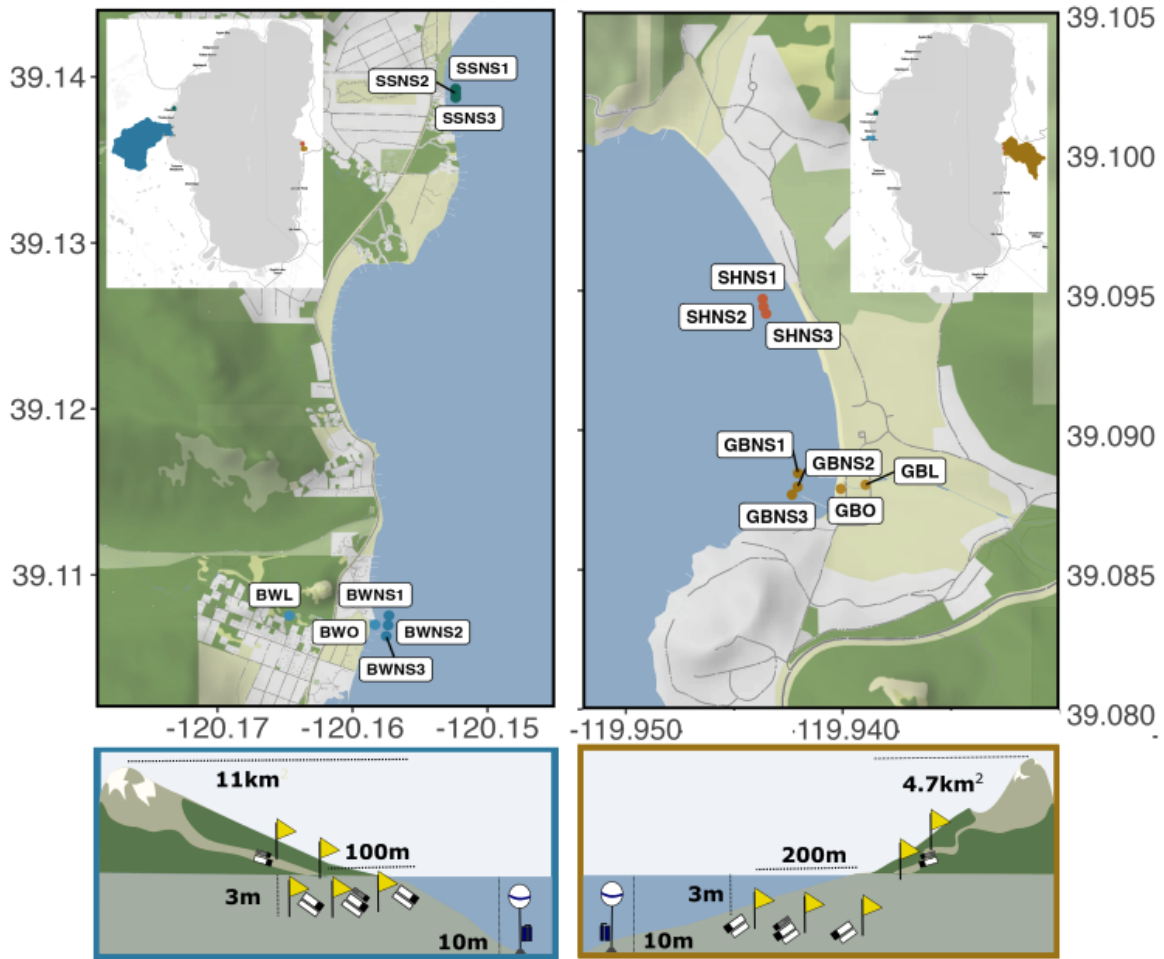


**Figure 1.** Map of nearshore sampling locations, Blackwood (BW in blue), Glenbrook (GB in yellow), Sunnyside (SS in green), and Slaughterhouse (SH in orange). The conceptual diagram of catchment morphology depicts locations of instrumentation (miniDOTs, conductivity loggers, and PAR sensors) and sampling locations (yellow flags).

### II.B.1 Sensor deployment and maintenance

Between 2021 and 2023, we deployed sensors in the littoral zone of Lake Tahoe in two stages - Stage I and Stage II as described below (Figure 2).

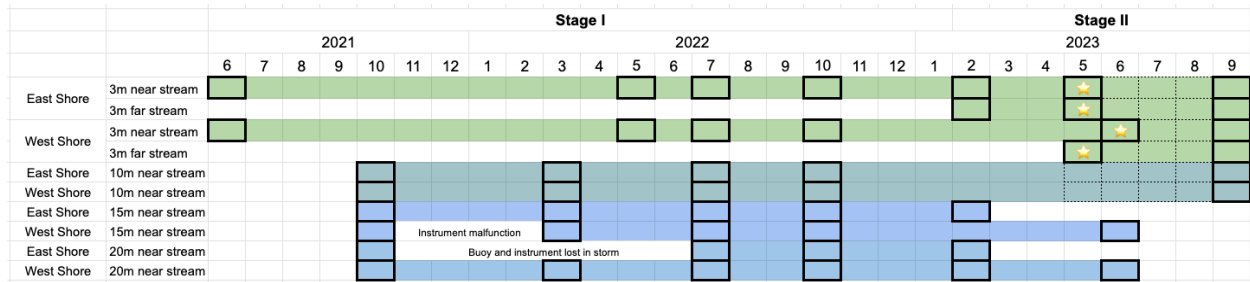


**Figure 2.** A timetable depicting instrument deployment on east and west shores of the lake and at various water depths during stages I and II of the project. Shaded boxes signify instrument deployment, black outlines indicate dates of instrument servicing, dotted outlines indicate dates of cleaning, and reasons for pauses in deployment are detailed in text boxes. Months containing stars indicate that cinder blocks coated with anti-fouling paint were deployed at that time.

### *Stage I Sensor Deployment*

During Stage I, miniDOT DO and water temperature loggers with wipers (Precision Measurement Engineering, Inc.) were deployed via SCUBA at the mouth of two stream outlets, one on the east shore (Glenbrook Creek; GB) and another on the west shore (Blackwood Creek; BW). We deployed sensors in a “t-shaped” pattern, with three instruments deployed parallel to shore in a nearshore location (approximately 3m water depth at the time of deployment in June 2021) 50 m apart from one another and three instruments deployed perpendicular to shore at increasing water depths. At the time of deployment by October 2021, the approximate total water depths included mid-shallow littoral (10 m), mid-deep littoral (15 m), and deep littoral (20 m) locations offshore of the stream mouths. The three shallowest sensors parallel to shore were each attached horizontally to cinder blocks with PVC and placed on the bottom, where the sensors were positioned approximately 0.25 m off of the lake bottom. We placed sensors immediately in front (NS2) of and approximately 50 m north (NS1) and south (NS3) of inflowing creeks to capture variable surface water inflow dynamics. To deter algal growth, we installed copper plates on all miniDOTs in October 2022 and sealed cinder blocks with waterproof masonry paint in June 2023. The three deeper sensors perpendicular to shore were attached to a moored buoy line; initially these sensors were deployed in the mid-water column (approximately 2m from the surface) but were moved to deeper positions in March 2022 (approximately 1m from the bottom). Data collection from these benthic, “t-shaped” arrays (n = 6 instruments each) continued until February 2023 on the east shore and June 2023 on the west shore. We deployed Odyssey Submersible Photosynthetic Active Radiation (PAR) Loggers with Odyssey PAR Wipers (Dataflow Systems Ltd, Christchurch New Zealand) vertically on the mid-shallow littoral zone depth (~10 m) directly offshore from the central miniDOT at each stream mouth recording PAR at every 15 minutes in October 2021 to September 2023.

### *Stage II Sensor Deployment*

After one year of data collection across all sites (October 2021 - October 2022), we examined the dissolved oxygen and temperature data and found limited diel variation indicative of biological activity at the mid-deep littoral and deep littoral locations. Therefore, we determined that a more efficient use of the miniDOT sensors, given the resources at hand and to meet the project objectives of understanding temporal and spatial variability in nearshore productivity, was to redeploy those sensors at a shallow littoral depth at a location paired with our existing sensor array but far from inflowing streams.

Thus, during Stage II, we retained the same shallow littoral zone miniDOT sensors at the mouth of the same two stream outlets (Glenbrook Creek on the east shore and Blackwood Creek on the west shore), but removed miniDOT sensors from the deeper depths where a biological signal was not being detected. Instead, we shifted sensors from deeper locations to new shallow locations that were chosen to be away from a stream outlet (Figure 1). On the east shore, we deployed three miniDOTs (SHNS1, SHNS2, SHNS3) approximately 1.05 to 1.15 km north of the inflow of GB Creek but south of the inflow of the intermittent Slaughterhouse Creek (SH) in Glenbrook Bay in February 2023. On the west shore, we had already deployed one miniDOT with a wiper on a cinder block at the Sunnyside (SS; SSNS1) marina as part of another project in collaboration with Sudeep Chandra which is approximately 2.8 km north of BW in August 2021, and we then deployed two additional miniDOTs (SSNS2 and SSNS3) in June 2023. On both shores, we retained a single miniDOT deployed via the mid-shallow littoral moored buoy. We removed the remaining four deep buoys from both shores.

To further characterize the environmental conditions in the nearshore of the lake, in 2023 (February for GBNS2 and SHNS2, and June for BWNS2, and SSNS2) we added electrical conductance and temperature sensors (Onset HOBO U24, Bourne, Massachusetts) and light and temperature loggers (Onset HOBO Pendant MX Temperature/Light Pendant, Bourne, Massachusetts) onto the central cinder blocks at all four shores. Because of sensor issues, we only recorded PAR data from June 2021 to May 2022 at Glenbrook and lost DO data from our southernmost sensor at Sunnyside. All instruments were deployed and maintained via SCUBA and downloaded at least twice a year, and cleaned approximately every 3-4 months, except in 2023 where sensors were cleaned every month (June to September). Data collection from these arrays parallel to shore ( $n = 7$  instruments each) continued until September 2023.

### *Sensor calibration*

All instruments arrived with factory calibration settings prior to deployment. However, to account for issues with sensor accuracy, we intercalibrated miniDOT sensors following the user manual. In brief, we saturated a bucket full cold of tap water with oxygen using a Micro Bubble Diffuser (Pentair Aquatic Eco-Systems, Apopka, FL), air, and ice to cool water temperatures to roughly 4 °C. We monitored water temperature and DO with a handheld meter to saturate the

water with DO. Once conditions plateaued, we turned off the bubblers and allowed sensors to continue recording every 1 minute. We averaged plateau concentrations of DO (mg L) at 100% DO saturation for 10 minutes across all DO sensors. We used a Extech SD700 barometer to measure the precise local barometric pressure, and calculated the theoretical DO saturation concentration using the Garcia-Benson model in the ‘calc\_DO\_sat’ function in the streamMetabolizer R package (Appling et al. 2018). We then determined how far off each sensor was from the theoretical DO saturation concentration and corrected data from each sensor using a sensor-specific offset.

### *Sensor maintenance*

We serviced all sensors approximately every 3-4 months. We deployed wipers with each miniDOT and PAR logger to routinely wipe the sensor surface of the instrument. During servicing, divers would collect each sensor, bring it to the boat for physical cleaning and data download, and then return it to its previous location.

### II.B.2 Data cleaning

Prior to using the data collected by the dissolved oxygen sensors in any data analysis or metabolism modeling efforts, we performed several steps to clean and filter the data. First, we removed any data from the days on which instrument deployment or retrieval occurred. Second, we removed data due to poor quality indicators from the instrument (sensor quality [Q] < 0.7) and wiper (wipe time < 4 seconds and/or average current > 140 mA) readings. Third, we compared raw dissolved oxygen data with diver photographs and removed data at times during which we suspected severe biofouling may have occurred; we took a conservative approach with this last filter, so if dissolved oxygen signals displayed greater-than-average diel changes but there were no photographs of the site available, we retained the data. Finally, we removed all data that fell outside of 3 times the standard deviation of a given deployment location (e.g., cinder block or buoy). Together, these four filters removed 376,249 observations or 24% of the data collected. Although Stage I began in October 2021, we focused our analyses beginning in March 2022 because of various equipment adjustments (e.g., missing wiper data) and malfunction (e.g., lack of data at Blackwood mid-deep littoral) that needed to be fixed. Therefore, the most complete version of Stage I data is from March 2022 to February 2023.

### II.B.3 Covariate Data

We aggregated hourly light data (surface shortwave radiation flux downwards,  $W m^{-2}$ ) from the North American Land Data Assimilation System (Xia et al. 2012, NLDAS project 2021; [NLDAS\\_FORA0125\\_H](#)) converted it to PAR ( $\mu mol m^{-2} s^{-1}$ ) based on the conversion factor in Savoy et al. 2021 (multiplying it by 2.114), and interpolated 3-hour observations of barometric pressure (surface air pressure, Pa) and wind speed (near surface wind speed,  $m s^{-1}$ , Beaudoin & Rodell 2020; [GLDAS\\_NOAH025\\_3H](#)). We aggregated precipitation (mm) and air temperature

(°C) data from the Parameter-elevation Relationships on Independent Slopes Model (PRISM Climate Group 2024 <https://prism.oregonstate.edu/>) and Snow Telemetry (SNOTEL) station data from sites [848](#) (Ward creek 39.14°N, -120.22°W, and at 2,056 m ASL) and [615](#) (Marlette lake 39.16°N, -119.9°W, and at 2,403 m ASL); these data include precipitation events, accumulated precipitation, and snow water equivalent (SWE).

#### II.B.4 Ecosystem metabolism modeling

We estimated daily nearshore metabolism by implementing metabolism models “LakeAnalyzer” and “LakeMetabolizer” (Winslow et al. 2018) with recommended modifications based on Lottig et al. (2021) as well as Scordo et al. (2022) at each shallow littoral miniDOT location, including the locations surrounding the stream outlets at Glenbrook and Blackwood and the additional miniDOT arrays at Slaughterhouse (3) and Sunnyside (2, with 11 total). This model differs from many other models (e.g., the standard LakeMetabolizer R package) in that instead of fitting each day individually, the model is fit to the entire time series to generate daily metabolism estimates and model parameters are constrained to ecologically feasible ranges (i.e., GPP and ER must be positive and negative, respectively).

We aggregated high-frequency (15 minute) measurements of DO from PME miniDOTs (in mg L<sup>-1</sup>), water temperature (°C), light from Odyssey® photosynthetic irradiance recording systems (PAR; μmol m<sup>-2</sup> s<sup>-1</sup>), wind speed (m s<sup>-1</sup>), and barometric pressure (mbar) at roughly lake level (1,897 m ASL) to mean hourly observations. We constrained the degree of autocorrelation in the parameters through time using hierarchical variance parameters in the random walk components of the model. We fit the model to our observed dissolved oxygen and water temperature time series separately for all years (2021, 2022, and 2023) for each site via Stan (Carpenter et al. 2017) run in R (R Core Team, 2020) using the ‘rstan’ package (Stan Development Team, 2020) as described in Phillips (2020), and Lottig et al. (2021). Lastly, we used the median of the posterior for each parameter for interpreting daily patterns in either GPP or ER (Scordo et al. 2022).

#### *Gas exchange estimates (k)*

We estimated final gas transfer velocity (k in h<sup>-1</sup>) using a bivariate model based on wind speed and lake area to estimate K<sub>600</sub> in (m day<sup>-1</sup>) (Vachon & Prairie 2013; Dugon et al. 2016):

$$k_{600} = 2.51 + (1.48 * U_{10}) + 0.39 * U_{10} * \log_{10} (LA).$$

Where U<sub>10</sub> is wind speed (m s<sup>-1</sup>) at a 10 m height above the lake, and LA is lake area (m<sup>2</sup>). Then we converted K<sub>600</sub> values to k using the ‘k600.2.kGAS’ function in the R package LakeMetabolizer, and normalized k by sensor-specific depth and observation frequency. We removed days with observations of wind speeds greater than 5.9 m s<sup>-1</sup> in accordance with recommendations for the appropriate range of input data for estimating reasonable values of k (Vachon & Prairie 2013; Dugon et al. 2016). Lastly, we reduced the lake area to a third of

Tahoe's size (165.4 km<sup>2</sup>) to more appropriately estimate these parameters for a smaller nearshore zone.

### *Characterizing benthic light*

We estimated the diffuse attenuation of PAR as  $K_d$  (m<sup>-1</sup>) at depth for each sensor based the log linear function (Rose et al. 2009):

$$K_d = \frac{\ln\left(\frac{E_0}{E_z}\right)}{Z}$$

where  $E_z$  is PAR data from Odyssey PAR loggers ( $\mu\text{mol m}^{-2} \text{s}^{-1}$ ) at depth  $Z$  (m) which varied from 9.5 m to 11 m depending on lake level. We converted incoming shortwave radiation data (NLDAS project 2021; [NLDAS FORA0125 H](#)) from  $\text{W m}^{-2}$  to PAR to get surface irradiance ( $E_0$  in  $\mu\text{mol m}^{-2} \text{s}^{-1}$ ). Additionally, we used publicly available data for 2021 and 2022 “1% depth PAR” from the “Tahoe\_LTP\_UV” station (Watanabe & Schladow 2023) which is roughly 200 m south of our instrumentation at 4.6 m depth to compare an infill missing estimates of daily  $K_d$ . We used these daily PAR  $K_d$  estimates to calculate the amount of hourly incoming PAR likely to reach each individual sensor depending depth as:

$$I = E_0 - E_0 * \exp\left(\frac{-K_d * Z_i}{K_d * Z_i}\right)$$

where  $I$  is light intensity ( $\mu\text{mol m}^{-2} \text{s}^{-1}$ ) and sensor depth  $Z_i$  for each sensor ranged from 2.5 m to 5.7 m depending on lake level depth (Winslow et al. 2018).

Lastly, we used the photoinhibition photosynthesis-irradiance (P-I) curve (Steele 1962) to describe the relationship between GPP and light based on Lottig et al. (2021), and Scordo et al. (2022) implementation:

$$P_I = P_{max} \frac{I}{I_{opt}} \exp\left(1 - \frac{I}{I_{opt}}\right)$$

where  $P_I$  is the production rate at light intensity  $I$ ,  $P_{max}$  is the maximum production rate, and  $I_{opt}$  is the optimal light intensity. Photoinhibition of productivity is common in lakes (Staehr et al. 2016). We allowed  $P_{max}$  and  $I_{opt}$  to vary through time at a daily time scale.

## **II.C Results**

### II.C.1 Dissolved oxygen and temperature at multiple depths in the nearshore

Dissolved oxygen (DO) concentrations measured between March 2022 and September 2023 displayed a wide range (5.2-12.5 mg/L and 58-122 % saturation) as did water temperatures (1.5-

24.7°C). During the Stage I deployment (March 2022 - February 2023), the nearshore sites displayed the greatest daily variability in DO, particularly during later winter and early spring (Figures 3 & 4). Conversely, temperature displayed the greatest daily variability during summer months and at deeper sites (mid-deep and deep littoral locations, Figures 3 & 4). During the Stage II deployment (March - September 2023), variability in daily DO was greatest at nearshore sites located near stream outlets, and this pattern was more pronounced on the east shore at the mouth of Glenbrook Creek (Figure 4). Similar to the first phase of deployment, there was greater variability in daily temperature during summer months in Stage II and typically at either the deeper site (i.e., shallow littoral) or at the site nearest the stream outlet (Figures 4-7).

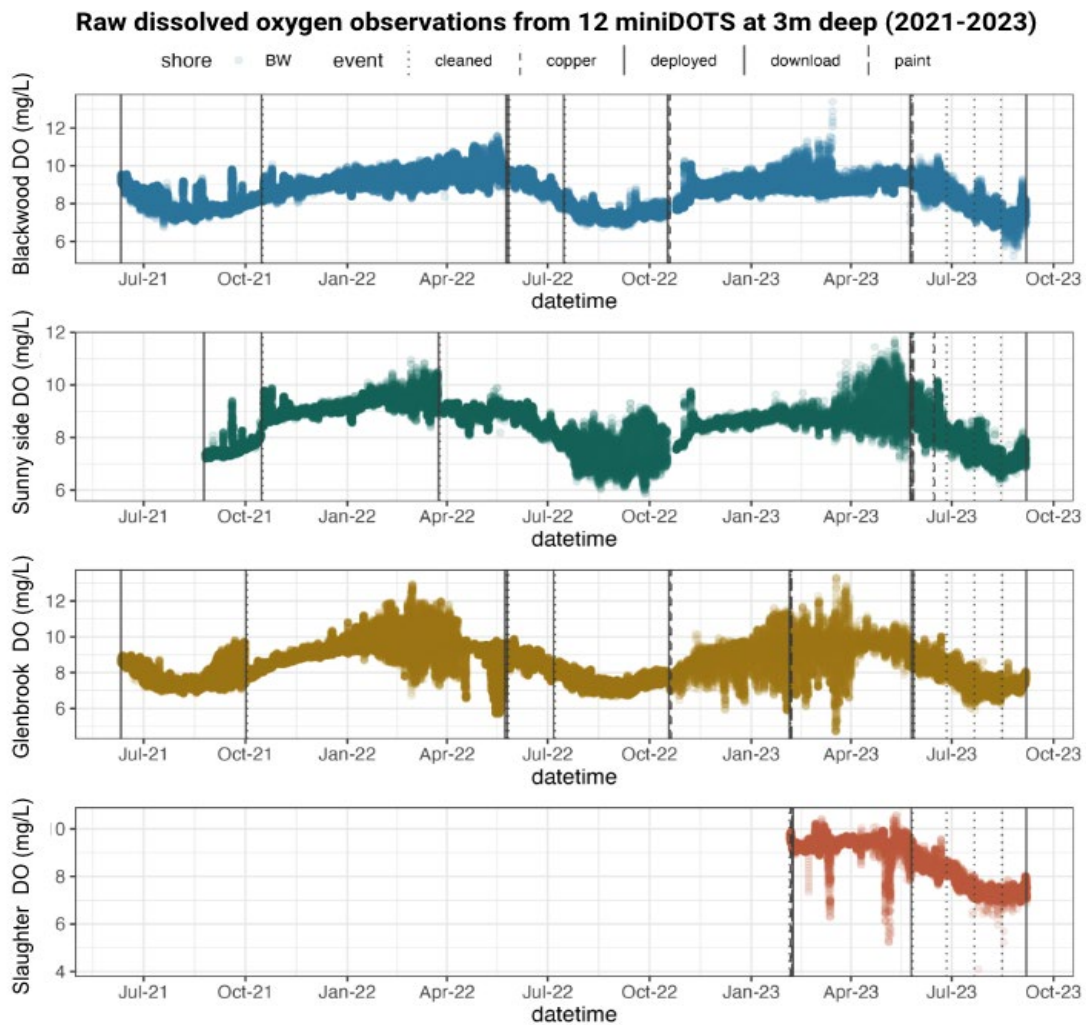


**Figure 3.** Unfiltered (no data removed) 15 minute dissolved oxygen data ( $\text{mg L}^{-1}$ ) from three miniDOTs across four instrumented shores (2021-2023). Where color represents site location, and dotted lines represent cleaning, solid lines represent deployment and downloads, and dashed lines represent copper plate installation and painted sealed block deployments.

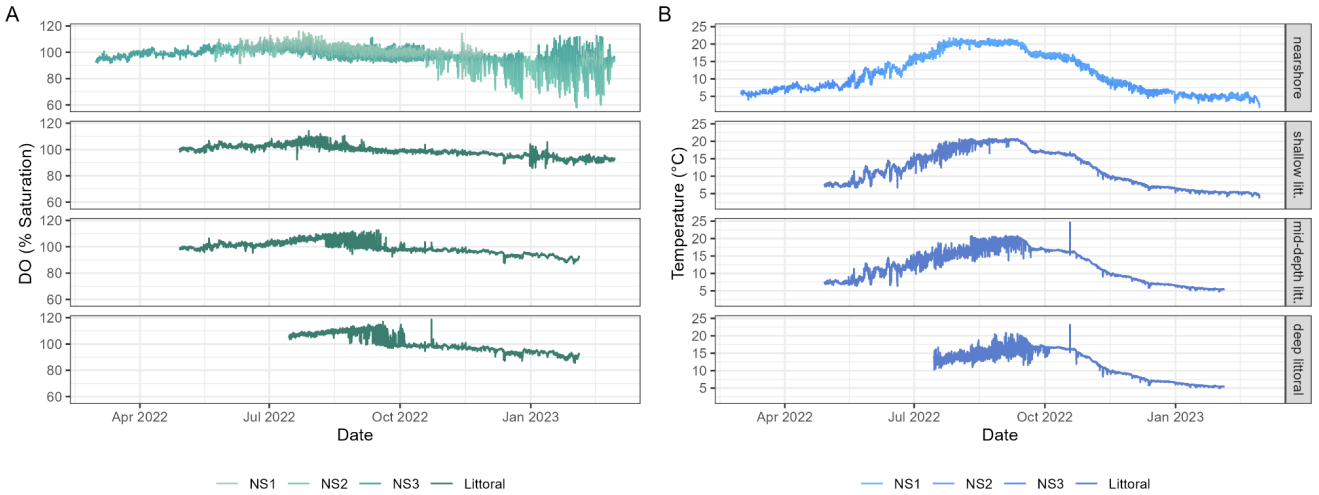


**Figure 4.** Cleaned (A) Dissolved oxygen (% Saturation) and (B) temperature (°C) collected along the east shore near the Glenbrook Creek outlet during Stage I of the project (March 2022 - February 2023). Each panel presents data from the four depths instrumented in a separate row (shallow littoral (labeled as “nearshore”), mid-shallow littoral (labeled as “shallow lit.”), mid-deep littoral (labeled as “mid-depth lit.”), and deep littoral). At the shallow littoral depth, data from all three cinder blocks is shown (NS1, NS2, NS3).

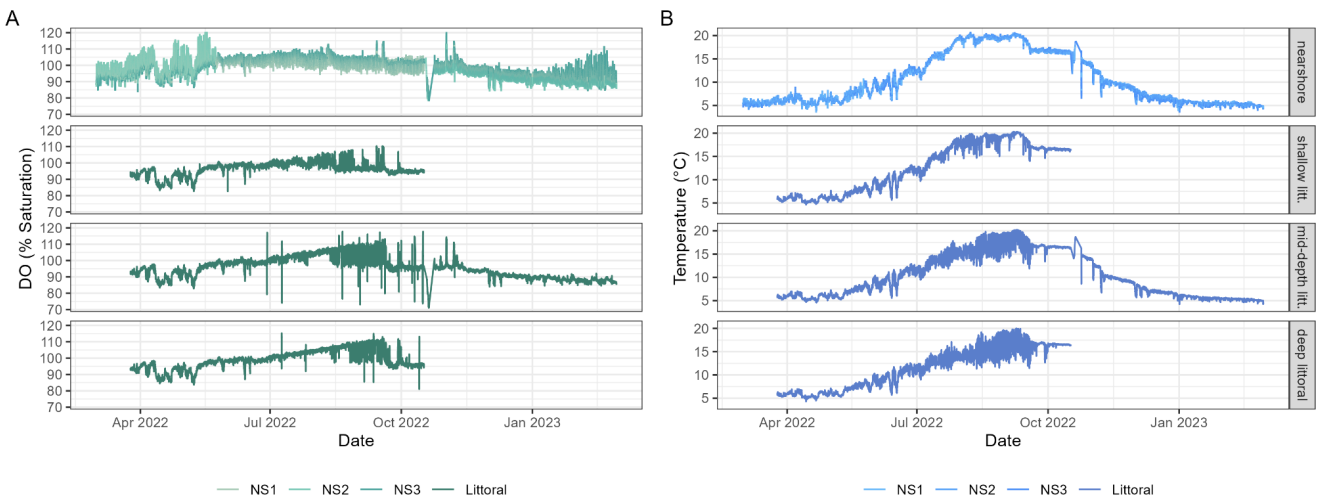


**Figure 5.** (A) Dissolved oxygen (% Saturation) and (B) temperature (°C) collected along the west shore near the Blackwood Creek outlet during Stage I of the project (March 2022 - February 2023). Each panel presents data from the four depths instrumented in a separate row (shallow littoral (labeled as “nearshore”), mid-shallow littoral (labeled as “shallow lit.”), mid-deep littoral (labeled as “mid-depth lit.”), and deep littoral). At the nearshore depth, data from all three cinder blocks is shown (NS1, NS2, NS3).

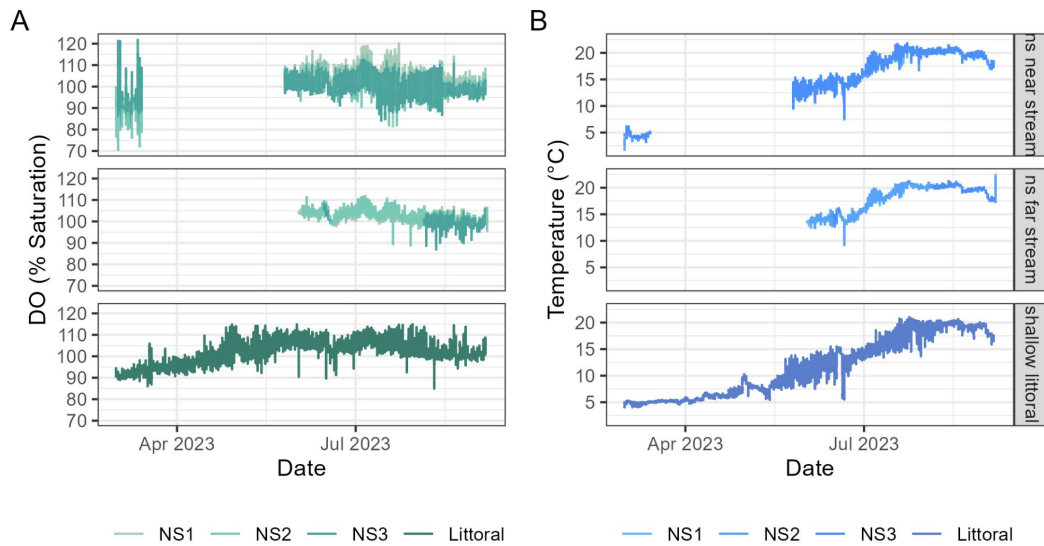


**Figure 6.** (A) Dissolved oxygen (% Saturation) and (B) temperature (°C) collected along the east shore near the Glenbrook Creek outlet during Stage II of the project (March - September 2023). Each panel presents data from the depths and locations instrumented in a separate row (nearshore (i.e., shallow littoral) near stream, nearshore (i.e., shallow littoral) far from stream, and shallow littoral (i.e., mid-shallow littoral)). At the nearshore locations, data from all cinder blocks is shown (NS1, NS2, NS3).

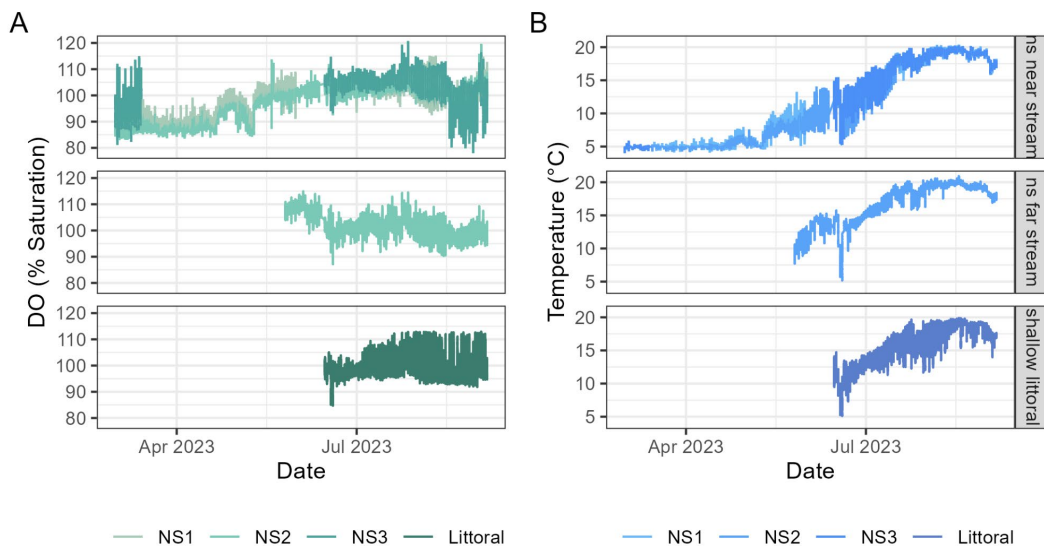


**Figure 7.** (A) Dissolved oxygen (% Saturation) and (B) temperature (°C) collected along the west shore near the Blackwood Creek outlet during Stage II of the project (March - September 2023). Each panel presents data from the depths and locations instrumented in a separate row (nearshore (i.e., shallow littoral) near stream, nearshore (i.e., shallow littoral) far from stream,

and shallow littoral (i.e., mid-shallow littoral)). At the nearshore locations, data from all cinder blocks is shown (NS1, NS2, NS3).

### II.C.2 Ecosystem metabolism estimates from the nearshore

Nearshore benthic metabolism estimates varied across different shore areas through time, yet all sites were heterotrophic ( $ER > GPP$ ; Figures 8 & 9). Comparing fluxes for net ecosystem productivity (NEP) for sensors around either BW or GB creeks we found greatest amount of NEP tended to occur in early February 2023 ( $23.41 \pm 5.17 \text{ nmol O}_2 \text{ m}^{-3} \text{ d}^{-1}$ ) and that GPP ranged 0.06 to  $29.30 \text{ nmol O}_2 \text{ m}^{-3} \text{ d}^{-1}$  and ER ranged from  $-29.80$  to  $-3.44 \text{ nmol O}_2 \text{ m}^{-3} \text{ d}^{-1}$ . In contrast, GB had the highest amount of NEP in October of 2021 ( $6.51 \pm 0.12 \text{ O}_2 \text{ m}^{-3} \text{ d}^{-1}$ ), and have slightly higher productivity where GPP ranged 0.44 to  $19.37 \text{ nmol O}_2 \text{ m}^{-3} \text{ d}^{-1}$  and ER ranged from  $-19.26$  to  $-4.35 \text{ nmol O}_2 \text{ m}^{-3} \text{ d}^{-1}$ .

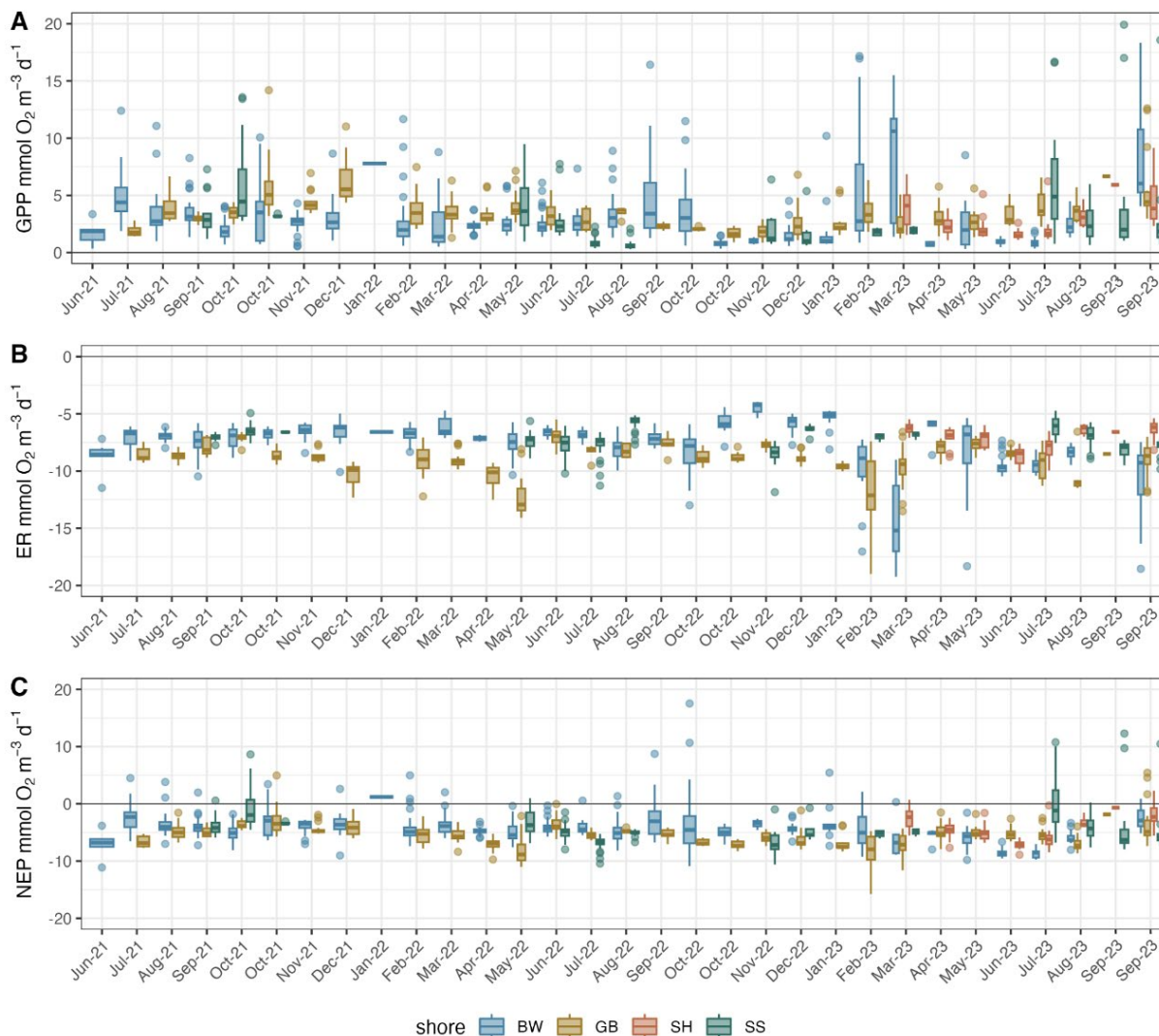


**Figure 8.** Nearshore metabolism estimates as A) GPP, B) ER, or C) NEP in  $\text{nmol O}_2 \text{ m}^{-3} \text{ day}^{-1}$  for every four weeks (~monthly) June 2021 to September 9th 2023 for shallow depths (nearshore)

or 3 m depth) across full time series June 2021 to September 9th 2023. Color represents shore location (BW in blue, GB in yellow, SH in orange, and SS in green).

When comparing the magnitude of ecosystem metabolism for overlapping observations from four different shore areas in summer 2023 (June-September) we found that Sunnyside had the highest mean GPP (GPP:  $4.03 \pm 0.49$  nmol O<sub>2</sub> m<sup>-3</sup>d<sup>-1</sup>, and ER:  $-7.11 \pm 0.12$  nmol O<sub>2</sub> m<sup>-3</sup>d<sup>-1</sup>), followed by Glenbrook (GPP:  $3.82 \pm 0.15$  nmol O<sub>2</sub> m<sup>-3</sup>d<sup>-1</sup>, ER:  $-9.27 \pm 0.24$  nmol O<sub>2</sub> m<sup>-3</sup>d<sup>-1</sup>), and Blackwood (GPP:  $3.26 \pm 0.37$  O<sub>2</sub> m<sup>-3</sup>d<sup>-1</sup> and ER:  $-9.97 \pm 0.34$  nmolO<sub>2</sub> m<sup>-3</sup>d<sup>-1</sup>); with Slaughterhouse having the lowest relative fluxes of both GPP and ER (GPP:  $3.05 \pm 0.16$  nmol O<sub>2</sub> m<sup>-3</sup>d<sup>-1</sup>, and ER:  $-7.07 \pm 0.09$  nmol O<sub>2</sub> m<sup>-3</sup>d<sup>-1</sup>). Interestingly our stream location on the east shore (GB) tended to have much higher productivity relative to the site further away from an inflowing stream (SH), while this pattern was reversed for west shore locations as SS tended to have greater productivity relative to the western stream location (BW), which also had higher ER.

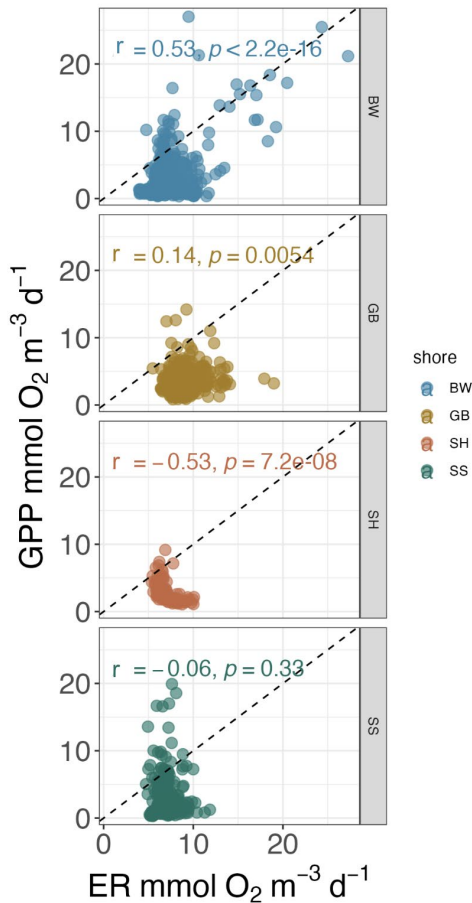


**Figure 9.** The relationship of GPP to absolute value of ER in nmol O<sub>2</sub> m<sup>-3</sup> day<sup>-1</sup> for every four weeks June 2021 to September 9th 2023 for shallow depths (nearshore or 3 m depth) across full time series June 2021 to September 9th 2023. The dashed line represents the 1:1 line where points above represent autotrophy and points below represent heterotrophy. Pearson's correlation coefficient (r) between GPP and ER for each shore location is depicted in the top left corner of each plot. Color represents shore location (BW in blue, GB in yellow, SH in orange, and SS in green).

### II.C.3 Spatial and temporal variation in upland and lake processes

Across the monitoring period, average daily air temperature tended to be the greatest in mid-August and ranged from 10.60 to 23.9°C (Figure 10). Similarly, average daily PAR at the lake's surface ranged from 44.77 to 363.92  $\mu\text{mol m}^{-2} \text{s}^{-1}$  and tended to be highest in May and remained high until early August (Figure 10). The highest rates of wind speed and precipitation rates occurred outside of the summer months, with average daily wind speeds ranging from 0.63 to 10.81  $\text{m s}^{-1}$  and average daily precipitation ranging from 0 to 159 mm across all sites (Figure 10). Wind speeds were similar across all sites (mean values: GB: 2.3  $\text{m s}^{-1}$ ; BW: 2.4  $\text{m s}^{-1}$ ; SH: 2.3  $\text{m s}^{-1}$ ; SS: 2.6  $\text{m s}^{-1}$ ).

**Table 1.** Annual hydroclimatic metrics for accumulated SWE (mm), surface water yield in ( $\text{m}^3 \text{km}^{-1}$ ) and average air temperature ( $^{\circ}\text{C}$ ) from SNOTEL stations and stream gage data from Blackwood and Glenbrook catchments.

Water year	Site	SWE (mm)	Annual water yield ( $\text{m}^3 \text{km}^{-1}$ )	Mean air temp ( $^{\circ}\text{C}$ )
2021	BW	75988	808629	7.06
2021	GB	38754	125615	6.32
2022	BW	74451	2316451	6.44
2022	GB	54028	156622	5.86
2023	BW	204311	4493548	5.04
2023	GB	146517	1081897	4.20

Examining variation in hydroclimatic conditions 2021-2023, we observed large differences in snow-water equivalence (SWE), melt rates, and stream flow both across years and shore locations. The Blackwood catchment on the west shore accumulated 32% more SWE on average and generated 82% more surface water relative to the Glenbrook catchment on the east shore, in part because of its larger size (Table 1). SWE accumulation and annual water yield varied strongly from 2021 to 2023 (Figure 11). 2021 was a dry year with early snowmelt and relatively low stream flow at both Glenbrook and Blackwood. 2022 had more precipitation events, but also more mid-winter melting events, especially at Glenbrook which had a relatively low annual water yield and less SWE accumulation relative to Blackwood (Table 1, Figure 11). In contrast, 2023 was one of the top five wettest years in the Sierra Nevada (California Department of Water Resources 2023), and we observed 67% more SWE and 83% more annual surface water yield at both Glenbrook and Blackwood relative to 2021.

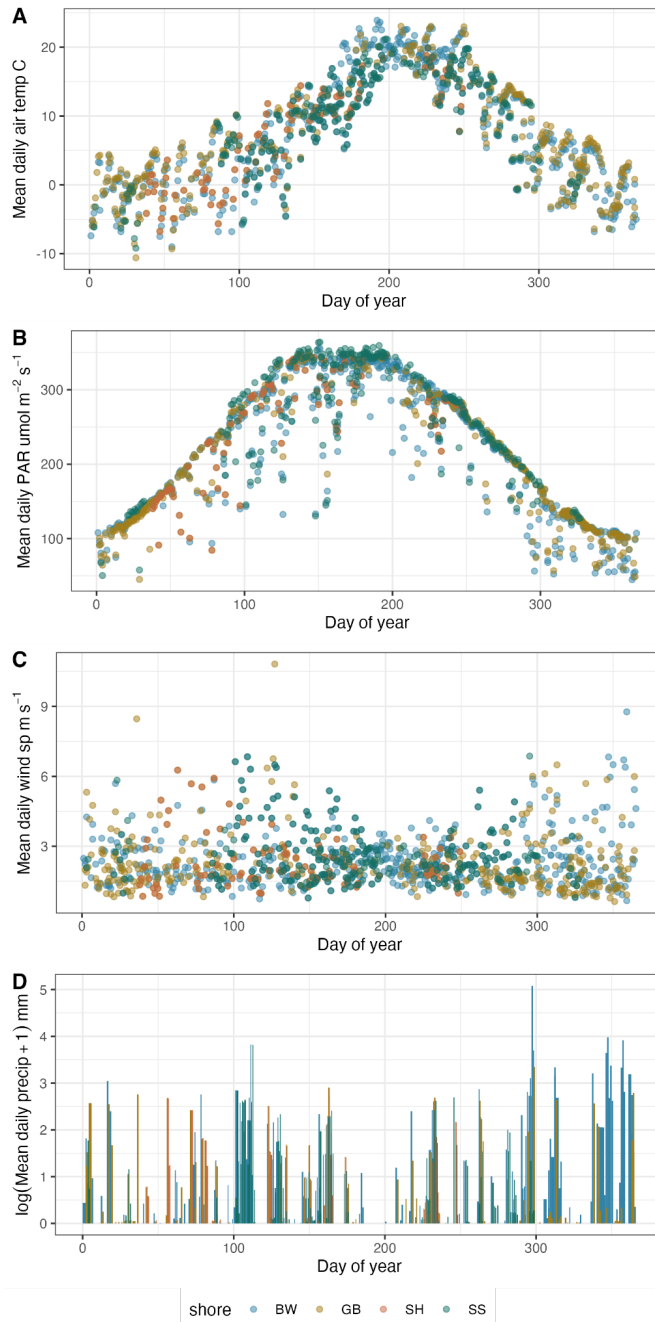


**Figure 10.** Seasonal climate trends of mean daily A) air temperature ( $^{\circ}\text{C}$ ), B) incoming solar radiation as PAR ( $\mu\text{mol m}^{-2} \text{s}^{-1}$ ), C) wind speed ( $\text{m s}^{-1}$ ), and D) log precipitation (+1) (mm) for years 2021-2023 across our four shore locations. Color represents shore (BW in blue, GB in yellow, SH in orange, and SS in green).

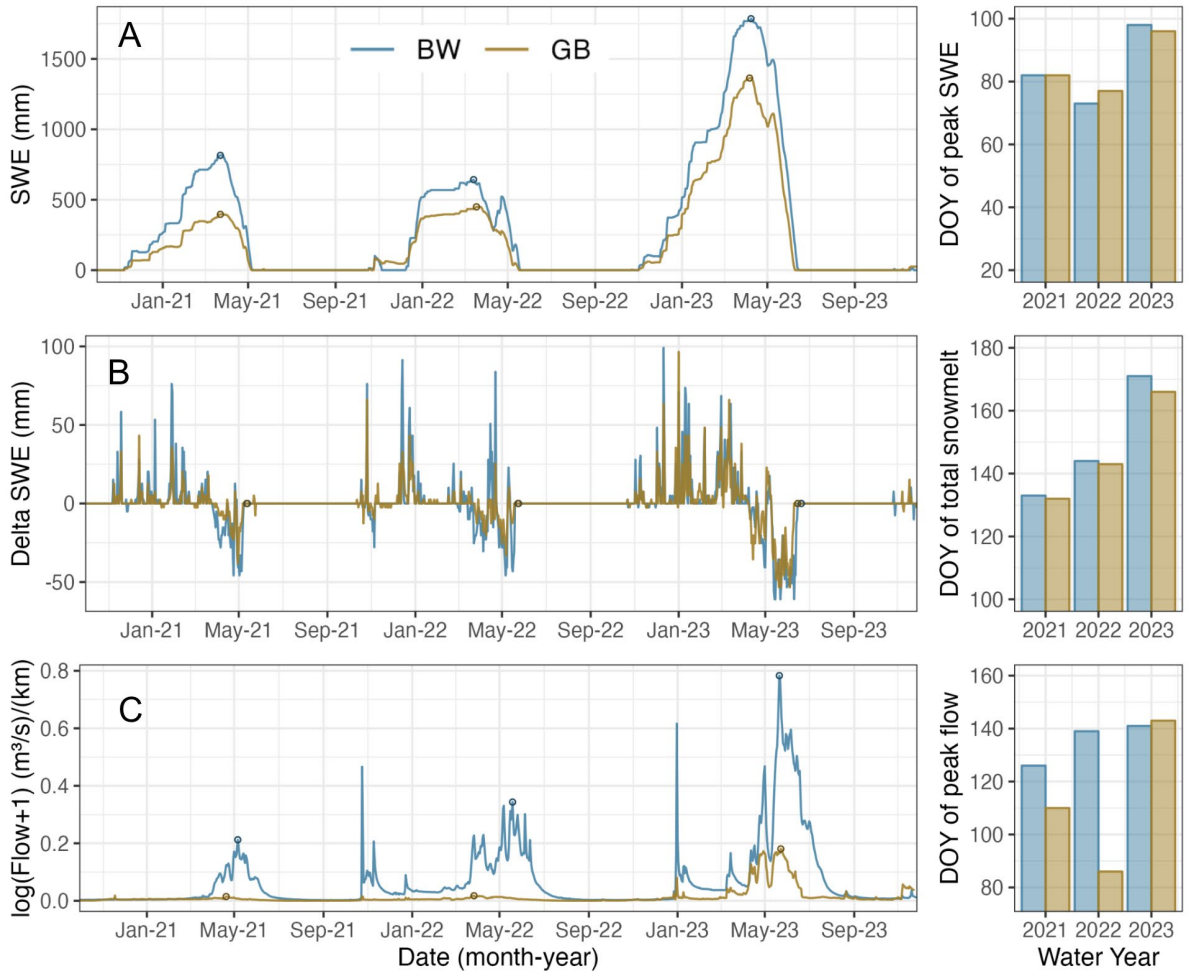


**Figure 11.** Hydroclimatic conditions over time (October 1st 2021 to September 30th 2023) in the upland areas around our two sites near streams Blackwood (BW) and Glenbrook (GB). A) annual accumulated snow water equivalent (SWE) (mm). Days of peak SWE occurrence are indicated by small circles and also in the barplot for the day of year of peak SWE. B) Delta SWE or the net change in SWE for each day (mm), where positive values indicate that precipitation accumulated as snowpack, and negative values indicate snow melt. The accompanying bar plot depicts the day of year of total snowpack melt. C) Log- transformed stream (+1) normalized to catchment area in  $\text{m}^3 \text{s}^{-1} \text{km}^{-1}$ . The accompanying bar plot depicts the day of year of total peak streamflow. SWE data is from SNOTEL stations (848 and 615) and streamflow was transformed from USGS gages (10336660 and 10336730).

## II.D Conclusion

Over the course of both stages of instrument deployment, sites located nearest to shore, particularly those located closer to stream outlets, displayed the highest daily variability in measured dissolved oxygen (DO) concentrations. Although the timing of changes and variability

in both DO and temperature varied across the east and west shore sites, the seasonal patterns generally mirrored one another. Past research has found benthic algal growth in nearshore regions of Lake Tahoe to be greatest in late winter and early spring (Naranjo et al., 2019), which may be one reason that, during the first stage of the project, DO variability was greatest at the shallowest sites from approximately February through May 2022. During the second stage of the project, we also found higher daily summer DO concentrations near the outlet of Glenbrook Creek compared to the site further away from an inflowing stream (called Slaughterhouse, but which is south of the actual intermittent stream inlet). This increase in daily fluctuations may be a result of increased flow from snowmelt entering the lake during the day (Kirchner et al., 2020), that can be highly-oxygenated because of turbulence and from being colder which increases oxygen solubility (i.e., oxygen solubility decreases with increasing temperature). Snowmelt in the summer of 2023 was delayed due to the large snowpack the previous winter (19.14 m, UC Berkeley Central Sierra Snow Lab, <https://cssl.berkeley.edu/>), which may have contributed to the increased DO variability measured through August near the Glenbrook Creek outlet. Together, our results suggest that these nearshore regions may be subject to strong physical and biological drivers of DO throughout the year, dynamics that might otherwise be missed if only limnetic, or deeper portions of the lake where the photic zone does not reach the bottom, are monitored.

We found pronounced differences in the metabolic regimes across the two different shorelines, with higher episodic GPP and ER on the westshore. Throughout our monitoring period littoral GPP was somewhat synchronous with ER with BW having a slightly greater heterotrophic signal. Additionally, we expect these temporal differences to vary between water years, where we expect increases in streamflow to delay stream GPP with unknown consequences for the timing of peak littoral GPP.

## **III. Objective 2: Stream and lake water chemistry monitoring**

### **III.A Introduction**

High-elevation streams are thought to be nitrogen (N) limited as the microbial (uptake, assimilation, and fixation) and hydrologic processes (wet deposition, snowmelt, and streamflow) that control inorganic N availability and demand tend to be disconnected (temporally and spatially), allowing episodic nitrate losses despite biotic community activity (Stoddard 1995; Sickman et al. 2003). In areas like the Lake Tahoe Basin, years with greater precipitation have been associated with greater nitrogen deposition (Coats et al. 2016), and yet differences in precipitation retention, forest cover, and geology can lead to variable stream based N export (Domagalski et al. 2021). The pelagic environment in Tahoe is currently co-limited by both P and N, while the nearshore has shown patterns of N limitation (Coats et al. 2016; Naranjo et al. 2019; Domagalski et al. 2021). Regional management agencies are concerned about the lake's biogeochemical potential to facilitate algal blooms and threaten Lake Tahoe's world famous water clarity. As such, there is a need to understand the extent to which inflowing streams can deliver nutrients to the nearshore of Lake Tahoe to contextualize the patterns of nutrient supply and subsequent growth in nearshore algae.

It is well understood that nutrient and organic matter concentrations follow seasonal patterns of precipitation, surface water, and groundwater transport (Hagedorn et al. 2000; Johnson et al. 2009); conceptual models of transport are based on historically cold and consistent winters where soils are thought to be frozen and hydrologically disconnected from downstream rivers, lakes, or groundwater (Brooks et al. 2011; Seybold et al. 2022). However, warming trends and the variability of precipitation timing and intensity in mountain regions can alter the availability of key resources like nitrogen, with unknown interactions with ecosystem energy fluxes (i.e., primary productivity and ecosystem respiration). Therefore, we set out to characterize seasonal rates of carbon and nitrogen cycling within paired catchments in the Lake Tahoe basin that accumulate different amounts of precipitation and subsequently have unique flow regimes.

### **III.B Methods**

We collected regular samples (weekly to monthly) for water chemistry (porewater and surface water measurements of dissolved organic carbon,  $\text{NO}_3^-$  - N,  $\text{NH}_4^+$  - N, TDN, and  $\text{PO}_4^{3-}$  - P), stream productivity (water chlorophyll-a, epilithic ash-free dry mass, and chlorophyll-a), sediment quality (pH, bulk density, and organic matter), and used in situ sensors to monitor reach water chemistry (DO (mg/L), temperature ( $^\circ\text{C}$ ), and specific conductance (SPC in  $\mu\text{S cm}^{-1}$ )). Specifically, we instrumented streams with miniDOT DO sensors (5-minute observation intervals) to model daily stream metabolism (Appling et al. 2018), and HOBO U24 conductivity sensors to measure SPC.

### III.B.1 Sampling Site Description

The mountain streams that flow into Lake Tahoe occupy drainages composed of igneous rocks, mainly granite and andesite along the southern, eastern, and northern shores; while the western shore contains large outcrops of volcanic rock. The eastern shore has steeper slopes and creates smaller watersheds with steeper streams, while the western shore has more gradual valley formations and larger drainages. The topography in the basin also plays a role in directing orographic precipitation via a rain-shadow effect and causes the western catchments to accumulate up to twice as much winter precipitation allowing for strong intra-annual surface water variation in inflow streams (Reuter & Miller 2000). Therefore, we focused our monitoring efforts on contrasting a western drainage area Blackwood Creek, and an eastern drainage area Glenbrook Creek. Blackwood's drainage area can receive 35% more average annual precipitation relative to Glenbrook based on point data from SNOTEL (Figure 12). Blackwood Creek flows through a 29 km<sup>2</sup> largely undeveloped watershed underlain by volcanic and surficial deposits. It has a history of activities such as logging (1880s-1920s), gravel excavation from the streambed/streambank (1960s), grazing, and fire (Reuter & Miller 2000). In contrast, Glenbrook Creek flows through a 10.65 km<sup>2</sup> watershed primarily composed of decomposed granitic rock. The upper watershed has historical logging (1860s-1900s), while the middle regions feature extensive highway road cuts. The lower watershed area is relatively flat and exhibits light to moderate development, including a golf course (Leonard & Goldman 1981). Both drainages are predominantly forested with conifers, including nitrogen-fixing species like mountain alder (*Alnus incana*), which may influence stream nitrogen loads (Leonard et al. 1979; Coats et al. 2016).

The geologic history that shaped the mountainous ridges above Lake Tahoe also played a large role in creating the unique patterns of bathymetry along the benthic environment of the nearshore. Lake Tahoe is thought to have formed 3.5 million years ago and was impacted by a fault line causing steep sloping shorefaces along the western edge while the Glenbrook Apron acts as a shallow shelf formation along the eastern shoreface (Gardner et al. 1998). These dramatic differences along the shoreline in bathymetric depth are expected to allow for variation in off-shore water circulation. The alluvial depositional zone around the stream-to-lake interfaces are mostly composed of permeable andesitic and basaltic sandy soils, rocky cobbles, as well as sporadic chunks of woody debris, with most hard substrates disappearing after three meters in depth (Naranjo et al. 2019). We focused our monitoring effort immediately around the creek mouths of both Glenbrook and Blackwood within the littoral zone (0–150 m lake depth for any distance within ~105 m or 350 ft of shore). While this area represents only 19% of the lake surface area but can contribute >60% of the total primary production (Loeb et al. 1983).

We targeted our stream survey efforts near United States Geological stream gauge stations to get precise estimates of streamflow and average reach depth. We used USGS stations for ([10336660](#), 39.11°N, -120.16°W, and at 1900 m ASL) and ([10336730](#), 39.09°N, -119.94°W, and 1901 m

ASL) for 15 minute observations of streamflow and water depth. We used daily stream metabolism models from Blackwood and Glenbrook creeks (Appling et al. 2018) for estimates of stream GPP or ER ( $\text{g O}_2 \text{m}^{-2} \text{d}^{-1}$ ). We used Onset HOBO U24 conductivity sensors to estimate groundwater influence and water density near the stream lake interface and in the nearshore. These high-frequency measurements of water chemistry were complimented by regular water and sediment nutrients ( $\text{NO}_3$ ,  $\text{NH}_4$ ,  $\text{PO}_4$ , and DOC) and organic matter (epilithic and sediment biomass and chlorophyll-a) sampling (bi-monthly May- September, and monthly October-April) at the lower stream reaches, the inlet, as well as 0.5 m deep directly in front of the stream for each shore.



**Figure 12.** Map of stream monitoring locations at Blackwood and Glenbrook creeks. The stream is highlighted in blue for Blackwood or gold for Glenbrook and sensor positions are noted with circles for in-stream miniDOTs and HOBO conductivity loggers. Upper photos depict the upper stream reaches and lower photos depict the downstream or lower reach location.

### III.B.2 Sample Collection

#### *Survey methods and sample collection:*

At each stream reach (Blackwood lower - BWL, Blackwood upper - BWU, Glenbrook lower- GBL, Glenbrook - GBU), we established five transects above the sensor station, perpendicular to the flow of water, and spaced 10 meters apart for a total reach length of 50 m. For shallow shoreline littoral sampling, we set up three transects, one directly in front of the inlet and two 10 m north and south of the inlet all at 0.5m depth. We also set up three transects to sample the inlet: (1) directly at the stream-lake interface, (2) 5 m upstream, and (3) 10 m upstream to collect sediment and rocks from. We always collected water samples and measurements 5 m upstream of the inlet and directly in front of the stream inlet at the lake. For off-shore sample collection, we used a combination of boat-based Van Dorn water sampling, and direct SCUBA collection when possible. We sampled water from the surface (0.5m) and benthos (3m), and when possible,

sediment adjacent to each of the three littoral DO sensors (NS1, NS2, & NS3). We collected all off-shore water samples in acid washed 1L bottles which were kept on ice and filtered the same day through combusted Whatman GF/F filters (0.7  $\mu\text{m}$  pore size) into acid-washed 60 mL HDPE bottles. Water samples were frozen at  $-20^{\circ}\text{C}$  for chemical analyses at a later date. We collected sediment by scooping the top 5-10 cm of sediment from three random locations within 1 m of each DO sensor into a ziploc lock bag for later sieving in the lab (see below).

We measured water DO, temperature, SPC, and pH, within 1 m of the stream sensor deployments using a multiparameter sonde (YSI Professional Plus, Yellow Springs, OH, USA; Orion pH probe, Thermo Fisher Scientific, Waltham, Massachusetts, USA). We collected duplicate filtered water samples from the same location using acid-washed syringes and combusted Whatman GF/F filters (0.7  $\mu\text{m}$  pore size, Whatman, Piscataway, NJ, USA) and stored in acid-washed 60 mL HDPE bottles frozen at  $-20^{\circ}\text{C}$  for later chemistry analysis. We passed a total of 300 mL of water on each filter and stored them frozen at  $-20^{\circ}\text{C}$  for later chlorophyll-a analysis. We sampled epilithic biomass by scraping three rocks selected at a random transect using a 6  $\text{cm}^2$  plastic delimiter and toothbrush. We poured the composite scrape slurry into a 1000-500 mL volume plastic bottle, diluted the slurry to the final bottle volume using stream water, and kept it chilled for later AFDM and chlorophyll-a analysis. We sampled sediment with a hand shovel to collect composite samples of the top 5-10 cm at three randomly selected transects, collecting three scoops per transect. We sieved using a stainless steel #10 2 mm opening sieve (VWR, Radnor, PA, USA) and collected subsamples off of this composite for bulk density, AFDM, pore water, sediment pH, and sediment chlorophyll-a.

### III.B.3 Laboratory Analysis

In the lab, we weighed 10 mL of wet sediment to determine bulk density of every sediment sample collected. For sediment AFDM, we dried sediment samples at  $60^{\circ}\text{C}$  for 48 h and then combusted them at  $500^{\circ}\text{C}$  for 8 h to determine ash free dry mass (AFDM) and percent organic matter ( $\%OM = ((\text{dry weight} - \text{AFDM})/\text{dry weight}) \times 100$ ). For epilithic AFDM, we filtered 100-250 mL of composite epilithic material on to a combusted Whatman GF/F filter (0.7  $\mu\text{m}$ ), dried the filtrate at  $60^{\circ}\text{C}$  for 48 h, and then combusted it at  $500^{\circ}\text{C}$  for 8 h to determine ash free dry mass and percent organic matter. We corrected for the amount of diluted composite processed and the area scraped (108  $\text{cm}^2$ ) ( $\%OM = ((\text{dry weight} - \text{AFDM})/\text{dry weight}) \times 100 \times \text{percentage analyzed of total sample} / 108 \text{ cm}^2$ ). For soil pH, we used an Orion Star A211 Benchtop pH Meter (Thermo Fisher Scientific, Waltham, Massachusetts, USA) to measure the pH of a mixture of 3 g of dried sediment in 5 mL of 0.01 mol/L  $\text{CaCl}_2$ , the addition of which lowers sediment pH by  $\sim 0.5$  pH units compared to water pH but is advantageous for taking measurements (Carter & Gregorich, 2008). For porewater solutes, we added  $3 \pm 0.25$  g of wet sediment and 25 mL of deionized to a falcon tube and vortexed it every 30 minutes for 4 h. We then rested the falcon tubes in a fridge overnight and centrifuged them the next day. We then

filtered the supernatant through Whatman GF/F filters (0.7  $\mu\text{m}$ ) and stored it in acid-washed 60 mL HDPE bottles in a freezer at  $-20^{\circ}\text{C}$ , until analyzed.

We analyzed pore water solutes and filtered water samples for dissolved organic carbon (DOC), total dissolved nitrogen (TDN), ammonium, orthophosphate, and nitrate. We used a TOC analyzer with a TN module (TOC-V CPH; Shimadzu, Kyoto, Japan) for DOC and TDN. Additionally we used SEAL AQ2 discrete analyzer (SEAL Analytical, Mequon, Wisconsin, USA) to analyze samples for ammonium ( $\text{NH}_4^+ - \text{N}$ ) with a detection limit of  $0.002 \text{ (mg N L}^{-1}\text{)}$ , orthophosphate (o-P) concentrations based on US EPA method 350.1 revision 2.0 and USEPA method 365.1 revision 2.0 (US EPA, 1993a, 1993b) with a detection limit of  $0.402 \text{ (}\mu\text{g P L}^{-1}\text{)}$ , as well as nitrate ( $\text{NO}_3^- - \text{N}$ ) based on US EPA Method 353.2, Revision 2.0. with a detection limit  $0.003 \text{ (mg N L}^{-1}\text{)}$  respectively. Chlorophyll-a was analyzed on a Turner Designs Trilogy benchtop fluorometer.

### III.B.4 Data Analysis

#### *Characterizing flow regimes*

We calculated the portion of streamflow as baseflow or quickflow using the Eckhardt digital filter method based on the ‘EcoHydRology’ package in R to characterize baseflow conditions and help identify potential groundwater signals in surface water quality (Fuka et al., 2018).

#### *Statistical methods for analyzing stream and lake water chemistry*

We used generalized linear mixed-effects models (GLMMs) to evaluate how nitrogen concentrations (as either  $\text{NO}_3^- - \text{N}$  or  $\text{NH}_4^+ - \text{N}$ ) and stream metabolism (GPP and ER) vary within stream catchments as a function of hydrologic conditions. We organized all data (collected, modeled, or aggregated from online sources) based on the water year (October 1st to September 30th). To assess the relationship between metabolism and hydroclimate we used GLMMs (Gaussian distribution with an identity link) on either ER data or log-transformed GPP data (with the addition of + 1 to minimize log biases). In each model, we included fixed effects for average daily observations of discharge (cms), SPC as proxy for water source ( $\mu\text{S cm}^{-1}$ ), water temperature ( $^{\circ}\text{C}$ ), and light ( $\mu\text{mol m}^{-2} \text{ s}^{-1}$ ), as well as a random intercept term for reach location to account for the non-independence of specific reach identity (Blackwood lower as BWL, Blackwood upper as BWU, Glenbrook lower as GBL and Glenbrook upper as GBU). To avoid collinearity, we evaluated pairwise correlations between predictor variables and ensured all relationships were low ( $\rho \leq |0.60$ ) before including predictor variables into models. To examine trends in N availability and hydroclimate, we built individual GLMMs with responses for either stream water or pore water concentrations of  $\text{NO}_3^- - \text{N}$  ( $\text{mg L}^{-1}$ ) or  $\text{NH}_4^+ - \text{N}$  ( $\text{mg L}^{-1}$ ), a mixed effect for streamflow (cms), and a random intercept term for reach location (BWL, BWU, GBL, and GBU).

All models were built using the lme4 package (Bates et al. 2014) and implemented in R version 4.3.1. We evaluated model fit by assessing the histogram of the residuals and comparing the variance residual model variance to the variance encompassed by the random intercept terms. Additionally, we checked for variance inflation using VIF (implemented in the car R package) and estimated the significance of individual terms using likelihood ratio tests (implemented in the lmerTest R package; Fox and Weisberg 2011; Kuznetsova et al. 2017), and obtained approximate  $R^2$  values for each model using the 'rsquaredglmm' function (implemented in the MuMin package, Barton and Barton 2015).

### **III.C Results**

#### III.C.1 Inflowing stream water chemistry

##### *Variation in stream water flow*

Both Blackwood and Glenbrook creeks showed a strong association to snow melt and precipitation. During our monitoring period, base flow was highly correlated with quickflow in GB ( $R^2 = 0.89$ ) relative to BW ( $R^2 = 0.78$ ) with a greater amount of unexplained variance in BW surface water likely coming from snowmelt (Figure 13).

GB creek has significantly higher (up to 88% higher) SPC relative to BW. Exploration into within catchment variation shows that specific conductance (SPC) is 70% higher at Glenbrook lower and water temperatures are 12% lower than the upper location, indicating there may be a stronger groundwater influence in the lower reach of Glenbrook. At all sites, SPC concentrations increased under base flow conditions (BW:  $\beta_Q: -15.59 \pm 0.31$ ,  $p < 0.001$ ,  $R^2 = 0.48$  and GB:  $\beta_Q: -96.45 \pm 2.26$ ,  $p < 0.001$ ,  $R^2 = 0.52$ ) and are indicative of groundwater contributions (Figures 14 & 15). In general, SPC tends to decrease (dilute) with precipitation events for both the upper and lower reaches at BW, however this relationship may be reversed at GB, could indicate that terrestrial watershed processes may mediate the influence of precipitation on stream flow (Figure 15).

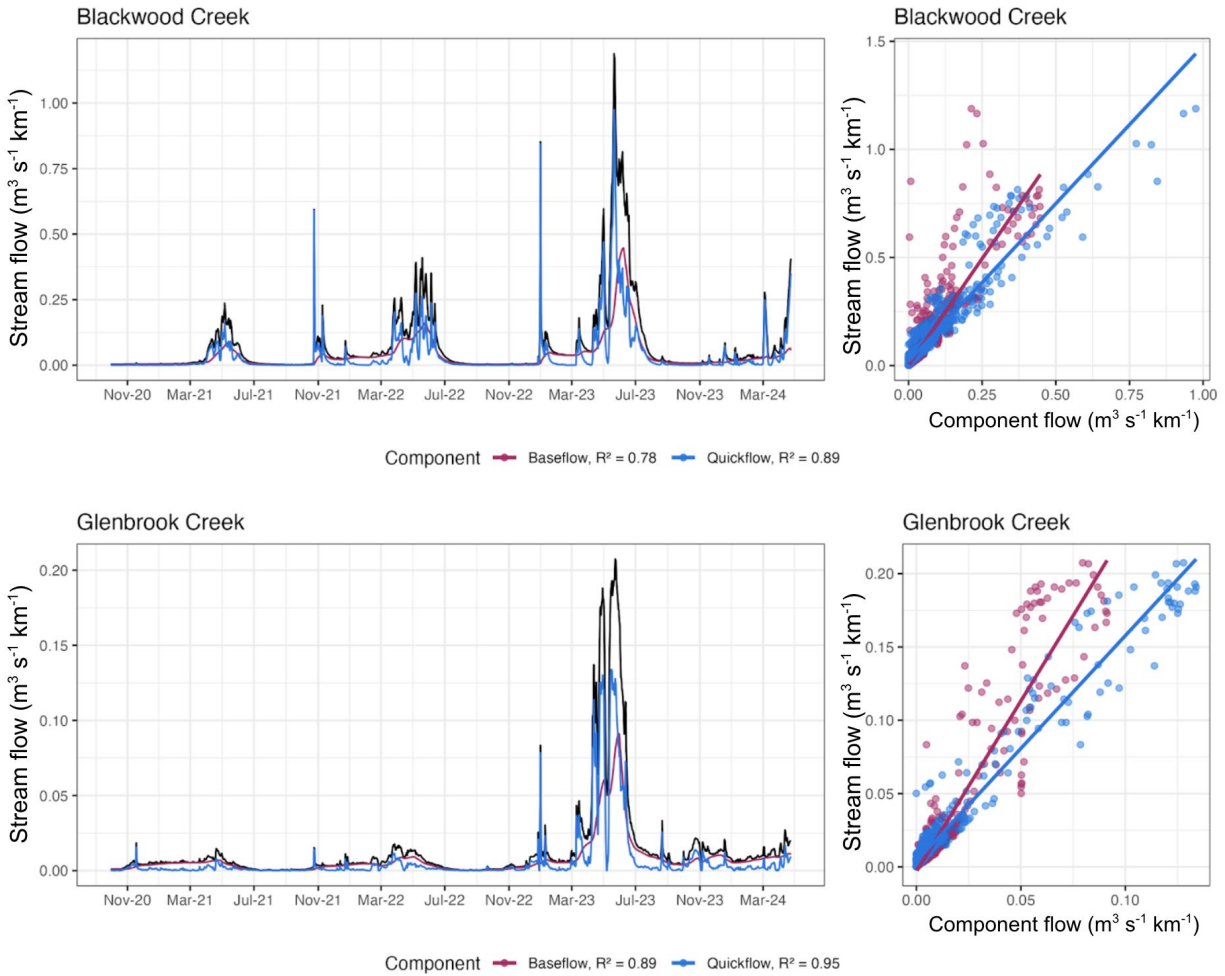


**Figure 13.** Base flow and quickflow components of daily streamflow (cms) normalized for catchment area (km<sup>2</sup>) as for BW (top) and Glenbrook (bottom) as time series (left) or as correlations (right). Color represents flow component total streamflow (black), baseflow (pink), and quickflow (blue). The coefficient of determination (R<sup>2</sup>) of total flow to individual flow components is listed in the legend.

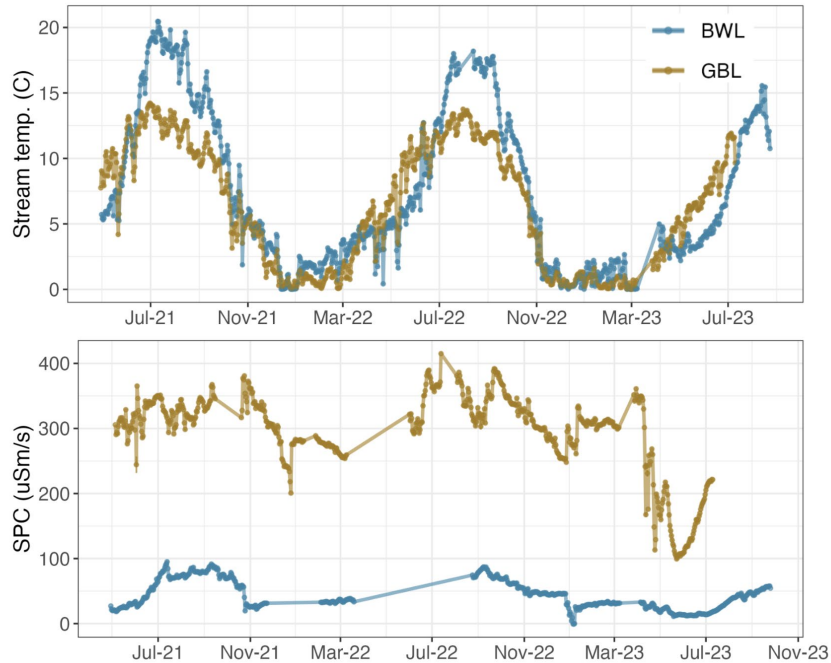


**Figure 14.** Time series of daily water temperature ( $^{\circ}\text{C}$ ) and specific conductance (SPC in  $\mu\text{Scm}^{-1}$ ) in lower reaches of BW (blue) and GB (yellow) from May 2021 to September 2023.

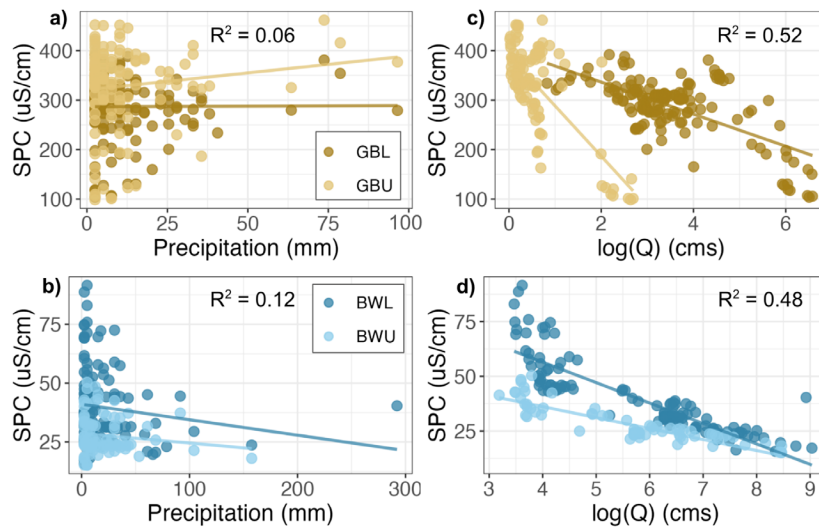


**Figure 15.** Trends in specific conductance and catchment hydrology. Relationships between specific conductance (SPC in  $\mu\text{Scm}^{-1}$ ) and precipitation at a) Glenbrook lower (gold points) and upper (light gold) and b) Blackwood lower (blue) and upper (light blue). Relationships between specific conductance (SPC in  $\mu\text{Scm}^{-1}$ ) and  $\log$  (discharge) as  $Q$  ( $\text{cms}^{-1}$ ) at c) Glenbrook lower (gold points) and upper (light gold) and d) Blackwood lower (blue) and upper (light blue) where higher discharge is associated with decreased SPC in both creeks.  $R^2$  represents the overall GLM fit.

### III.C.2 Nearshore lake chemistry

Across all sampling locations (stream, interface, nearshore, and offshore) nutrient concentrations were low (Figures 16-19). At Blackwood and Glenbrook, surface water  $\text{NO}_3^-$  ranged from 0.003 to 0.047 ( $\text{mg L}^{-1}$ ) and 0.015 to 0.034 ( $\text{mg L}^{-1}$ );  $\text{NH}_4^+$  ranged from 0.002 to 0.080 ( $\text{mg L}^{-1}$ ) and 0.002 to 0.044 ( $\text{mg L}^{-1}$ ),  $\text{PO}_4^{3-}$  ranged from 0.040 to 26.164 ( $\mu\text{g L}^{-1}$ ) and 5.308 to 28.010 ( $\mu\text{g L}^{-1}$ ), DOC ranged from 0.312 to 8.065 ( $\text{mg L}^{-1}$ ) and from 0.987 to 25.481 ( $\text{mg L}^{-1}$ ), and sediment organic matter ranged from 11.68 to 43.54 ( $\text{mg mL}^{-1}$ ) and from 18.88 to 68.82 ( $\text{mg mL}^{-1}$ ), respectively. We found  $\text{NO}_3^-$  and to a lesser degree  $\text{NH}_4^+$  were sensitive to seasonal patterns of snowmelt with spring pulses and fall declines in concentrations. Despite differences in discharge volume, Blackwood had lower average concentrations of nitrogen (0.012  $\text{mg L}^{-1}$   $\text{NO}_3^-$  and 0.012  $\text{mg L}^{-1}$   $\text{NH}_4^+$ ) relative to Glenbrook (0.017  $\text{mg L}^{-1}$   $\text{NO}_3^-$  and 0.033  $\text{mg L}^{-1}$   $\text{NH}_4^+$ ). These differences were slightly more pronounced in the sediment porewater.

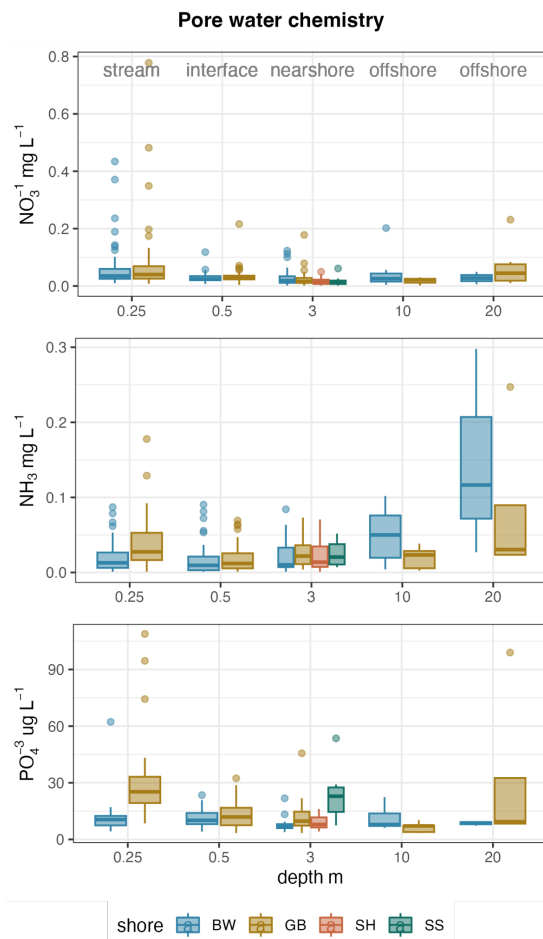


**Figure 16.** Pore water nutrients  $\text{NO}_3^-$  (top),  $\text{NH}_3$  (middle), and  $\text{PO}_4$  (bottom) for stream (at 0.25 m), interface (0.5 m), nearshore (3 m), and offshore (10 m or 20 m) locations. Where color represents BW (blue), GB (yellow), SH (orange), and SS (green).

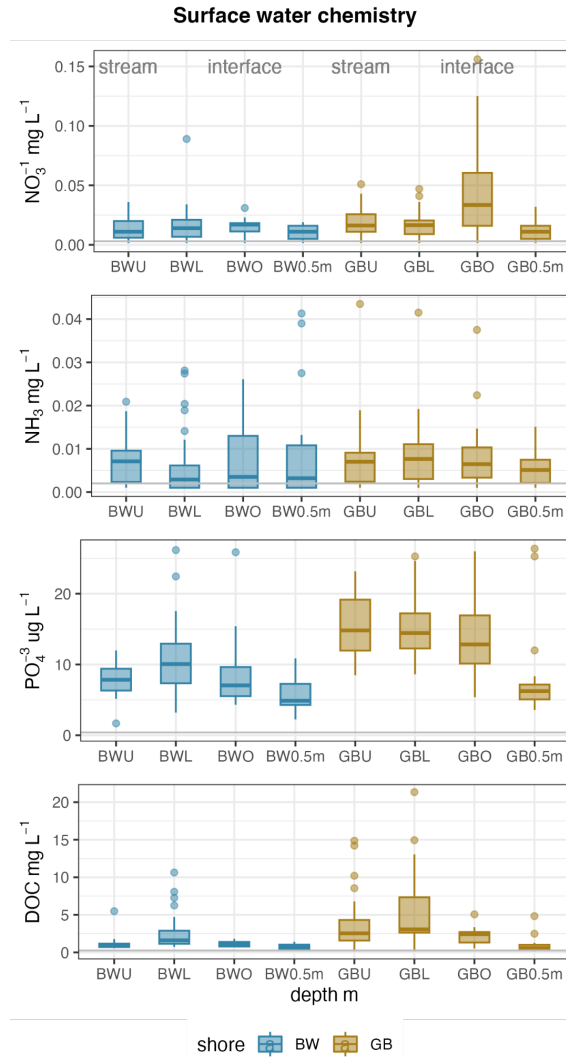


**Figure 17.** Surface water chemistry nutrients  $\text{NO}_3^-$  (top),  $\text{NH}_3$  (second from the top),  $\text{PO}_4$  (second from the bottom), and DOC ( $\text{mg L}^{-1}$ ) for just stream (at 0.25 m) and interface (0.5 m) locations. Where color represents BW (blue) and GB (yellow). Horizontal gray lines represent detection limits.

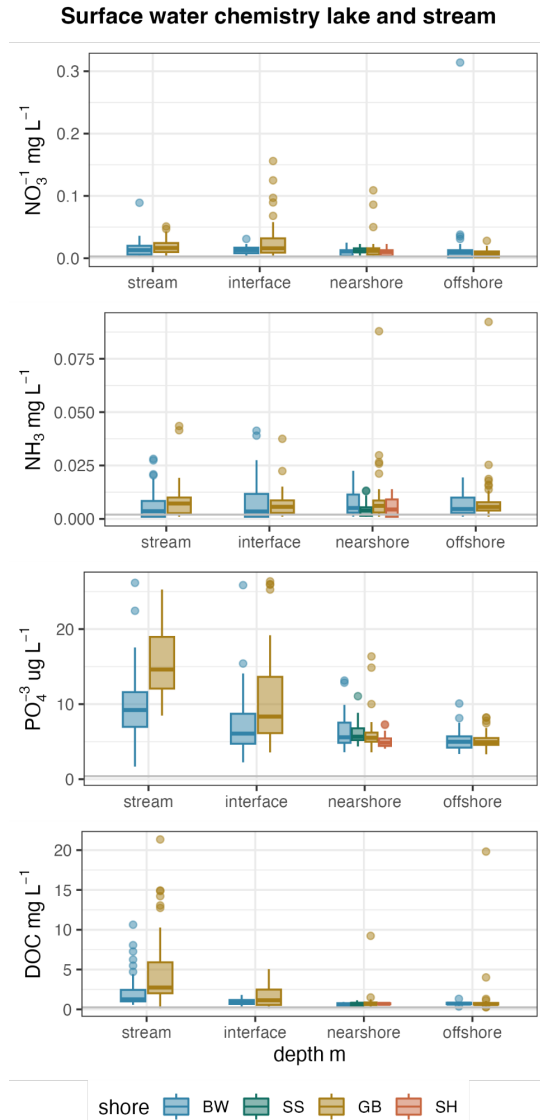


**Figure 18.** Surface water chemistry nutrients  $\text{NO}_3^-$  (top),  $\text{NH}_3$  (second from the top),  $\text{PO}_4$  (second from the bottom), and DOC ( $\text{mg L}^{-1}$ ) for just stream (at 0.25 m) and interface (0.5 m), nearshore (3 m), and offshore (10 m, 15m, or 20 m) locations. Where color represents shore BW (blue), GB (yellow), SH (orange), and SS (green). Horizontal gray lines represent detection limits.

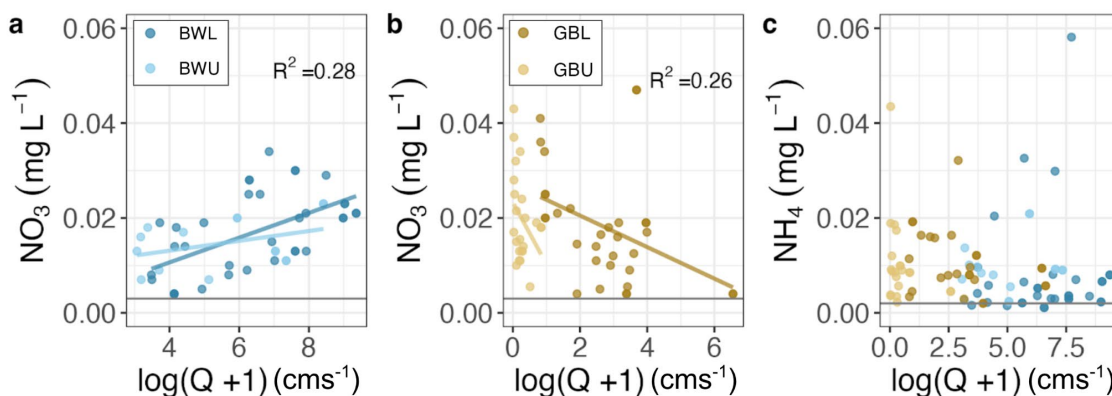


**Figure 19.** Contrasting relationships between nitrogen as  $\text{NO}_3^-$  - N in stream water at either a), BW reaches (blue) or b) GB (yellow) reaches and log transformed discharge as  $\log(Q+1)$  in  $\text{cms}^{-1}$ . c) The relationship between nitrogen as  $\text{NH}_4^+$  - N at BW (blue) and GB (yellow) reaches, and log transformed discharge as  $\log(Q+1)$  in  $\text{cms}^{-1}$ . Trend lines represent a significant model fit ( $p < 0.05$ ), horizontal gray lines represent detection limits.

### III.C.3 Standing stock biomass AFDM and chl-a in the streams and nearshore

#### *Standing stocks of biomass*

The presence of cobbles tends to disappear after 1.5 m depth in the nearshore zones of Glenbrook (GB) and Blackwood (BW). We observed more epilithic (surface of rock) biomass and sediment organic matter in both the stream and interface locations at GB. This pattern changed in 2023 where BW accumulated greater amounts of sediment organic matter. Additionally, we consistently observed higher amounts of sediment organic matter at the nearshore location at BW relative to the GB (Figure 20).

We found that epilithic biomass (in the stream and interface) was not representative of photosynthetic capacity. Biomass can be composed of both dead and photosynthetically-active material, and we found that higher amounts of biomass were not indicative of greater GPP and instead may be indicative of higher ER. We observed the greatest standing stock of chl-a in June of 2021 in BW and in August in GB (Figures 20-22).

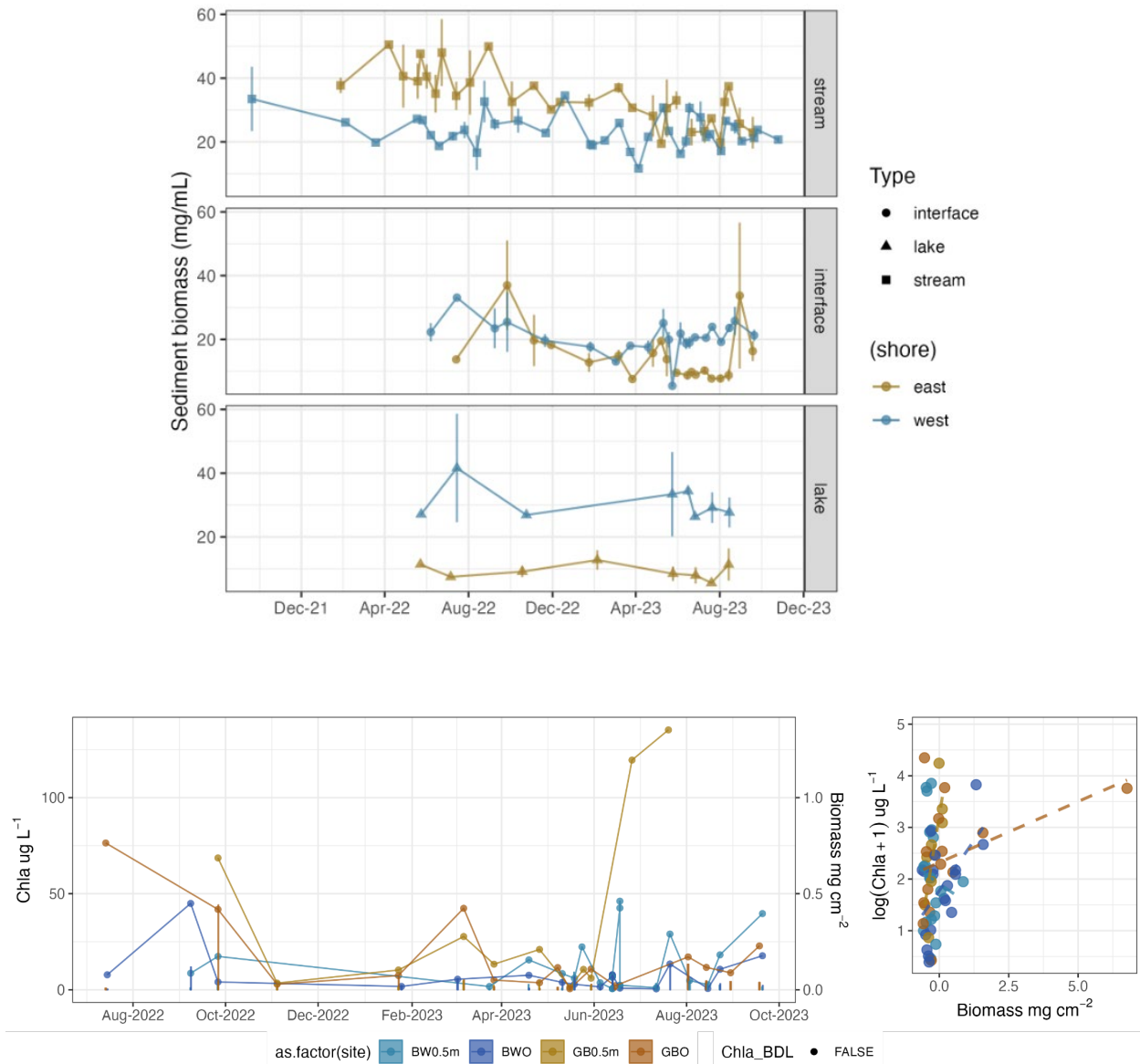


**Figure 20.** For epilithic (surface of rock) chlorophyll-a ( $\mu\text{g L}^{-1}$ ) and biomass ( $\text{mg cm}^{-2}$ ) overtime for interface sites from October 2022 to September 2023 (left). Points and lines represent chl-a samples that were above detection limits and bars represent biomass. The plot to the right represents log transformed +1 chl-a and biomass. The dashed line represents a marginal positive correlation. Where color represents shore BW (blue) and GB (yellow).

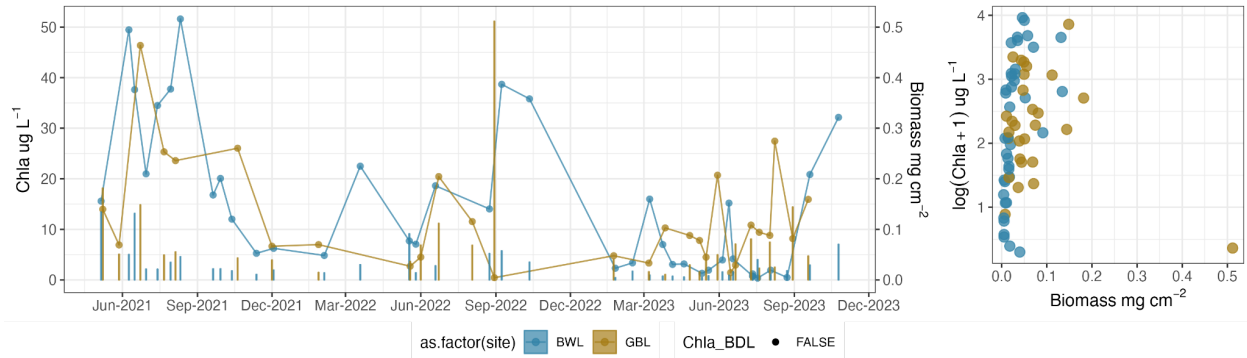


**Figure 21.** Epilithic (surface of rock) chlorophyll-a and biomass over time for the stream sites from May 2021 to September 2023 (left). Points and lines represent chl-a samples that were above detection limits and bars represent biomass. The plot to the right represents log transformed +1 chl-a and biomass. Color represents shore BW (blue) and GB (yellow).

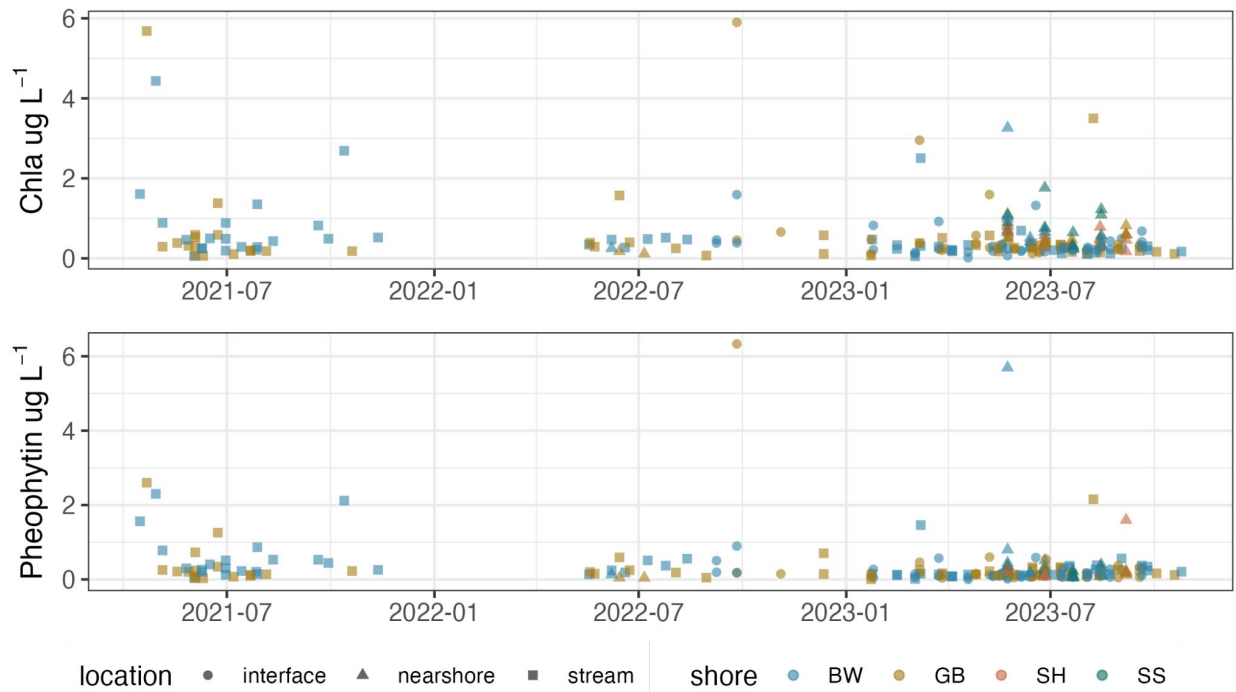


**Figure 22.** Surface water chlorophyll-a (top) and pheophytin (bottom) overtime for sites from May 2021 to September 2023. Shape represents location stream, interface, nearshore, and offshore (10 m, 15m, or 20 m) locations. Color represents shore BW (blue), GB (yellow), SH (orange), and SS (green)

*Seasonal stream metabolism trends*

We saw seasonal differences in modeled stream metabolism, but no clear trends in epilithic biomass or sediment organic matter. In general, all monitored stream reaches were heterotrophic ( $ER > GPP$ ). GPP tends to peak towards the end of summer or early fall, and occurred earlier in

2021, likely due to lower streamflow, a narrower stream width and high degree of shading, and great concentrations of sediment organic matter. The west shore sites tend to be more productive relative to the east shore sites, with the highest rates of both GPP ( $14.6 \pm 1.43 \text{ g O}_2 \text{ m}^{-2}$ ) and ER ( $31.74 \pm 3.77 \text{ g O}_2 \text{ m}^{-2}$ ) occurring at the upper station along Blackwood creek in August of 2021. The highest rates of GPP on the east shore occurred at Glenbrook in the lower reach in early June ( $2.78 \pm 0.55 \text{ g O}_2 \text{ m}^{-2}$ ) while the highest rates of ER occurred in October 2021 ( $16.39 \pm 1.87 \text{ g O}_2 \text{ m}^{-2}$ ) (Figure 23). We observed negative correlations between ER and GPP at BWL ( $R^2 = 0.03$ ), BWU ( $R^2 = 0.19$ ), and GBL ( $R^2 = 0.14$ ). In examining the influence of gas exchange, we found strong negative correlations between ER and  $K_{600}$  at GBL ( $R^2 = 0.69$ ), moderate negative correlations at BWL ( $R^2 = 0.41$ ), and no correlation at BWU or GBU.

Across all sites daily stream GPP was negatively correlated with discharge ( $\beta_Q: -0.11 \pm 9.04e^{-3}$ ,  $p < 0.001$ ), positively correlated with water temperature ( $\beta_{\text{Temp}}: 7.33e^{-3} \pm 1.13e^{-2}$ ,  $p < 0.001$ ), and incoming PAR ( $\beta_{\text{PAR}}: 8.05e^{-2} \pm 1.21e^{-2}$ ,  $p < 0.001$ ;  $R^2 = 0.64$ ; Figure 24). Similarly daily stream ER was positively associated with temperature ( $\beta_{\text{Temp}}: 2.17 \pm 1.13e^{-2}$ ,  $p < 0.001$ ), and discharge ( $\beta_Q: 1.72 \pm 0.10$ ,  $p < 0.001$ ), and negatively associated with incoming PAR ( $\beta_{\text{PAR}}: -0.70 \pm 0.14$ ,  $p < 0.001$ ;  $R^2 = 0.82$ ; Figure 24). The strong correlation with ER and  $K_{600}$  suggests that physical mixing of oxygen into the stream water, especially at GBL, could have biased our metabolism estimates, and so modeled outputs are still considered to be preliminary while we collect empirical gas exchange estimates.

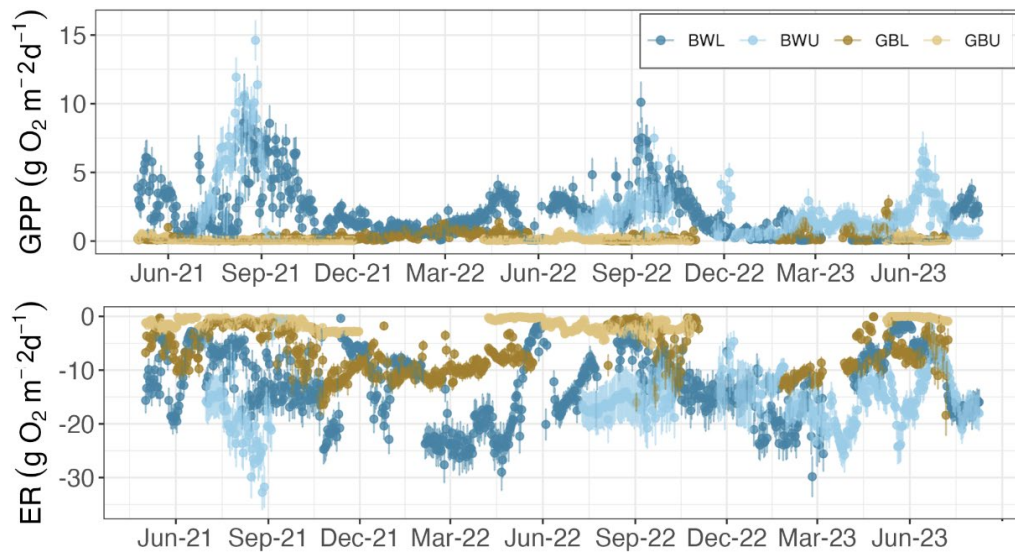


**Figure 23.** Modeled daily gross primary productivity (GPP top) and ecosystem respiration (ER bottom) in  $\text{g O}_2 \text{ m}^{-2} \text{ d}^{-1}$  from June 2021 to mid-July 2023 for all four instrumented reaches. Point color corresponds to site (Blackwood lower, Blackwood upper, Glenbrook lower, and Glenbrook), and bars represent standard error associated with each daily estimate of GPP or ER.

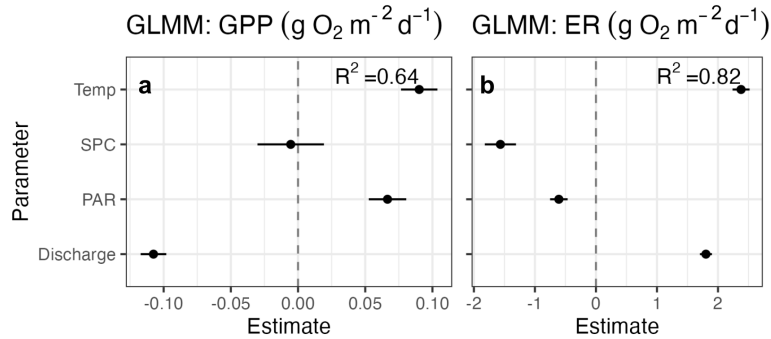


**Figure 24.** Coefficient plots of our parameter estimates associated with individual generalized linear mixed-effects models (GLMMs) for a) gross primary productivity (GPP) and b) ecosystem respiration (ER in  $\text{g O}_2 \text{ m}^{-2} \text{ d}^{-1}$ ) mixed effects for stream water temperature (Temp in C), specific conductance (SPC in  $\mu\text{Scm}^{-1}$ ), photosynthetically active radiation (PAR in  $\mu\text{mol m}^{-2} \text{ s}^{-1}$ ) and stream discharge (in  $\text{cms}^{-1}$ ) and random intercept terms for site. Horizontal bars represent standard error associated with each parameter estimate.

### III.D Conclusion

We observed a high degree of seasonality in streamflow from 2021 to 2023, but strong seasonal signals in stream metabolism were only observed in Blackwood Creek. We observed a high degree of variation in nutrient concentrations and biomass that was not coupled to other temporal surface water trends. The low levels of nutrients in our nearshore locations made detecting trends in nutrient dynamics challenging. Across the stream-lake interface, we observed higher concentrations of  $\text{NO}_3^-$ ,  $\text{NH}_4^+$ , o-phos, and DOC in streams relative to interface and nearshore areas.

We expected metabolism and nutrient cycling to be primarily controlled by streamflow and hydroclimatic conditions year to year. In mountain streams, variation in precipitation accumulation and run-off ratios determine stream discharge volumes and velocities (Poff & Ward 1992; Hammond et al. 2018). Stream discharge then acts as physical control on when and where in-stream communities can persist (Allan & Castillo 2021). Our observations of flow, precipitation, and SPC all suggest that Blackwood Creek is more sensitive relative to Glenbrook Creek to incoming precipitation and in regard to stream discharge as well as SPC changes. In Glenbrook, precipitation only explained 26% of variation in total annual water flow and 13% of variation in daily SPC. This greater precipitation signal could be a function of Blackwood's larger watershed area, but could also reflect Glenbrook's eastward slope orientation and higher percentage of forest cover which may create greater rates of evapotranspiration as well as canopy interception (Kirchner et al. 2020).

We expected to observe stream productivity peaks only in late summer and early fall, when there is slower streamflow, greater light availability, and water temperatures which are all known to be

conditions that are ideal for benthic biomass growth. The pronounced heterotrophy in Glenbrook may reflect a greater supply of organic matter entering the stream relative to Blackwood, as well as a higher degree of canopy shading which could facilitate microbial respiration relative to primary productivity. While we did observe summer and fall GPP peaks within the study stream reaches at both catchments, we also observed early spring increases in GPP and ER that correspond with potential under-ice algal growth at Blackwood in 2022 and 2023. These patterns in stream GPP suggest that biogeochemical cycling of nutrients through autotrophic organismal uptake could be occurring in the winter despite cold temperatures and reduced light availability from snow and ice cover.

Past work comparing winter nitrogen dynamics in the Sierra Nevada highlights the warmer marine snowpack as insulating above freezing temperatures in soil both facilitating large seasonal pulses of  $\text{NO}_3$  due to snowmelt transport of soil-nitrate (up to 75% of  $\text{NO}_3$  concentrations in stream water), as well as the rapid  $\text{NH}_4$  immobilization by active winter time heterotrophic activity (Sickman et al. 2003; Brooks et al. 2011). Patterns of snow insulation and winter soil temperature could explain the contradicting correlations between nitrate and flow in our two catchments, where Glenbrook may tend to lose lake level snowpack more easily and therefore experience colder soil temperatures that can suppress winter soil biogeochemical processing.

## IV. Objective 3: Quantifying rates of ammonium and nitrate uptake

### IV.A. Introduction

Periphyton plays a key role in lake ecosystems by cycling nutrients, providing energy to the food web through primary production, and benthic metabolism, and creating habitat space for other organisms (Wetzel 2001; Vadeboncoeur & Steinman 2002). Previous work in Lake Tahoe has suggested that periphyton growth is limited by nitrogen (nitrate ( $\text{NO}_3^-$ ) and ammonia ( $\text{NH}_4^+$ ) availability in the littoral zone of the lake (Reuter et al. 1986). Examining spatial and temporal variation in rates of  $\text{NO}_3^-$  and  $\text{NH}_4^+$  uptake can improve our understanding of how the benthic algal community responds to variation in N supply.

We measured benthic  $\text{NO}_3^-$  and  $\text{NH}_4^+$  uptake rates for the dominant substrate (sediment, or biofilm) across a range of habitat patches (the stream-lake interface at 0.5 m deep, the shallow littoral zone at 3 m deep, both directly in front of and away from streams) three times across the spring to summer transition (May, June, and July) for four different nearshore locations in Lake Tahoe (Figure 25).

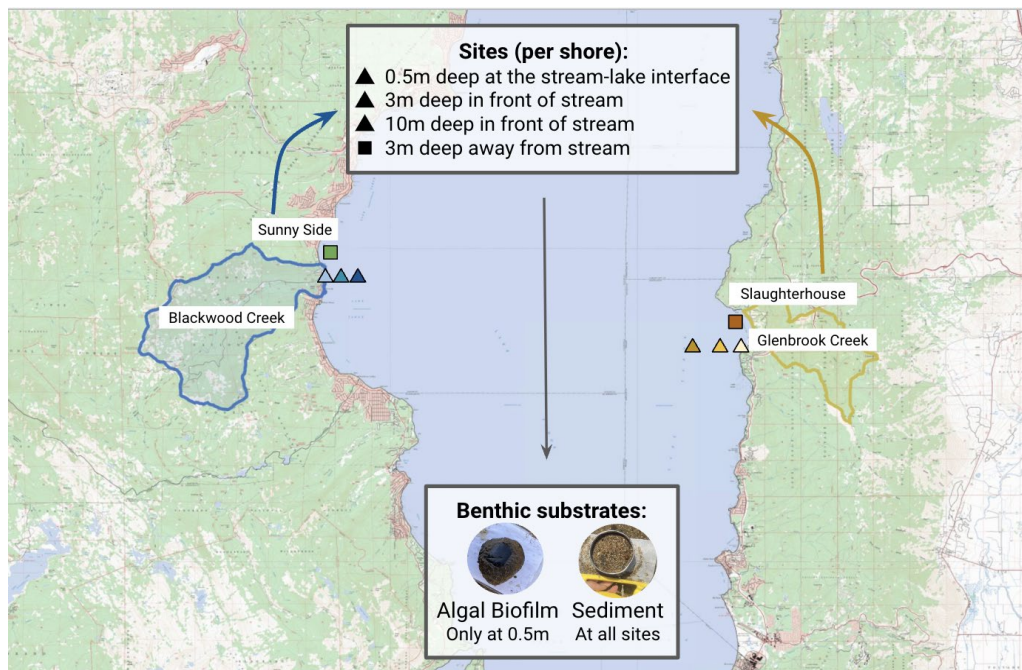


**Figure 25.** Sampling schematic of site locations on the east (Glenbrook and Slaughterhouse) and west shores (Blackwood and Sunnyside) of lake tahoe to collect benthic substrates to measure nitrogen uptake rates for either nitrate ( $\text{NO}_3^-$ ) or ammonia ( $\text{NH}_4^+$ ). The watersheds for the creek impacted sites are highlighted, and substrate collection locations are represented by triangles.

## IV.B. Methods

### IV.B.1 Sampling Locations

We monitored the littoral zone of both the east and west shores of the lake as described above (Figure 25). We collected samples from the dominant substrate (benthic algae or sediment) at four different sites on east (inlet of Glenbrook Creek and between Glenbrook Creek and Slaughterhouse meadow but hereafter called Slaughterhouse) and west (Blackwood Creek and Sunnyside) shores of the lake. Within each site, we collected samples from eight different patches, one patch at the stream-lake interface at (0.5 m deep), three patches in the nearshore directly in front of inflowing creeks (3 m deep), a patch farther offshore in front of creek (10 m deep) directly in front of each creek, and three patches from an area at least 500 m away from an inflowing stream (at Sunnyside and Slaughterhouse meadows and also 3 m deep).

### IV.B.2 Field Sampling

In order to characterize the seasonal heterogeneity in rates of nitrate and ammonia uptake for different littoral substrates we sampled the dominant substrate at the four sites in May, June, and July of 2023. For each incubation, we collected the dominant benthic substrate at each site (sediment, epilithic biofilm, or both) within five days of the incubation. The outlet (0.5 m) site demonstrated an equal mix of both sediment and biofilm, and so we performed incubation rates on both those materials. All other sampling locations (nearshore at 3 m deep and shallow littoral at 10m deep, both directly in front of and away from streams) were dominated by sediment which we sampled via SCUBA divers.

We sampled epilithic biomass at the watershed outlet (stream inlet to the lake) at 0.5 m depth by scraping twenty rocks selected across a transect using a 6 cm<sup>2</sup> plastic delimiter and toothbrush. To create a concentrated slurry, we squeezed a small volume of deionized water over the rock area that was scraped and the toothbrush. For every five rocks, we rinsed scraped material into 50 mL falcon tubes. Thus, for 20 scraped rocks, we collected a total of 200 mL composite epilithic biomass slurry. The samples were transported to the lab in a cooler on ice and then stored in a refrigerator at 4°C. We pipetted the slurry following shaking the tubes into designated incubation vials. We also subset the composite slurry for background biomass and chlorophyll-a concentrations.

We sampled sediment with a circular core (8 cm diameter) marked at 1 cm to standardize the volume of collected sediment. With minimal disturbance to the sediment, the core was pushed into the mark and a metal tray was placed underneath to keep the sediment intact. This process was repeated three times per site location and placed in a composite ziploc bag. The Glenbrook 10 m site was collected using a Ponar during the June and July incubations to prioritize safety. The samples were transported to the lab in a cooler on ice and then stored in a refrigerator at 4°C. We then homogenized sediment and siphoned water in excess of the sediment for each

composite sediment sample. For every samplin event, we collected lake water from the lake above the Blackwood 3m and Glenbrook 3m locations to be used for the incubations.

### IV.B.3 Laboratory Incubations



**Figure 26.** Replicate sediment and algal incubations in water baths in a temperature-controlled cold room and set under light conditions to mimic those in the nearshore zone of Lake Tahoe.

#### *Incubation array*

We incubated known quantities of sediment or epilithic biomass with lake water (and blanks with only lake water) in triplicate acid-washed 40 mL clear borosilicate glass vials in a light and temperature controlled environment to mimic the ambient temperature and light conditions observed at the time of sample collection. We used water baths and secured each vial to clear plastic racks to maintain a consistent orientation (45° angle) relative to the lamps and minimize variation in the light or temperature each vial might experience throughout the course of the incubation (Figure 26). We incubated vials for approximately six hours and agitated every two hours to prevent stratification in the vials. We tracked vial numbers to account for locations within each water bath, exact vial spike concentrations, replication, and start and end times specific to each vial. We instrumented the water baths with submerged temperature and light sensors (Onset HOBO Pendant MX Temperature/Light Pendant, Bourne, Massachusetts) to evaluate how well the conditions in the water baths mimicked the target ambient temperatures.

### *Vial filling*

Within 48 hours prior to the start of an incubation, we weighed out 2 g of wet sediment or epilithic biofilm into each vial and recorded the mass. We filtered lake water through a coarse 200 micron mesh to remove any large particles. We pipetted 25 mL of coarse filtered lake water into each vial 12 hours ahead of the nutrient additions and kept the samples in a dark and cold environment to allow for submerged substrates to equilibrate with the lake water. All west shore sites were incubated with water from Blackwood (0.5 m deep) and east shore sites were incubated with water from Glenbrook (0.5 m deep). We incubated ambient lake water alongside the incubation vials with sediment or biomass to account for any rates of pelagic uptake. Therefore, each of the three seasonal incubations included 288 individual vials for substrates, 144 vials for lake water, and three additional DI water blank vials for a total of 435 vials across 9 water baths (Figure 26).

### *Nitrogen additions*

For uptake kinetic experiments, each set of triplicates ( $n = 3$ ) received serial additions of ammonium chloride ( $\text{NH}_4\text{Cl}$ ) or sodium nitrate ( $\text{NaNO}_3$ ) to measure changes in nitrogen concentrations across six different nitrogen concentrations for either  $\text{NO}_3^-$  and  $\text{NH}_4^+$ . Serial addition concentrations ranged from 100-1,600  $\mu\text{g N L}^{-1}$ . We increased the spike concentrations from the first incubation in May 2023 (max: 1200  $\mu\text{L N}$ ) to the June 2023 incubation (max: 1600  $\mu\text{L N}$ ) to increase the likelihood of N saturation at the highest N concentration. After six hours of incubation, we filtered 10 mL of sample water from each vial with an acid washed syringe and 0.22  $\mu\text{m}$  nylon syringe filter into a labeled acid-washed 15 mL falcon tube and froze it ( $-20^\circ\text{C}$ ). We analyzed each filtered water sample ( $n = 435$ ), as well as the serial additions of either  $\text{NH}_4\text{Cl}$  or  $\text{NaNO}_3$  ( $n = 72$ ) on a SEAL AQ400 discrete analyzer to determine  $\text{NH}_4^+$  and  $\text{NO}_3^-$  values using methods described below.

### IV.B.4 Laboratory Sample Analysis

We calculated bulk density ( $\text{g mL}^{-1}$ ), percent of sediment organic matter (%), as well as chlorophyll-a ( $\mu\text{g L}^{-1}$ ) concentrations on collected substrates to standardize the material in each incubation replicate vial by the amount of biologically active material present in the sample. We weighed 10-15 mL of wet sediment to determine bulk density. For sediment biomass, we dried sediment samples at  $60^\circ\text{C}$  for 48 h and then combusted dried samples at  $500^\circ\text{C}$  for 12 h to determine organic matter. The wet weight of sediment was used for the experiment, so we corrected for the percentage of sediment that was water.

$$\begin{aligned}\text{OM \%} &= (\text{dry weight} - \text{combust weight})/(\text{dry weight}) * 100 \\ \text{\% water} &= (\text{wet weight} - \text{dry weight})/\text{wet weight} \\ \text{Dried sample weight (g)} &= \text{sediment weight} - (\text{sediment weight} * \text{\% water}) \\ \text{AFDW (g)} &= \text{OM \%} * \text{dried sample weight}\end{aligned}$$

For epilithic biomass, we filtered 25 mL of composite rock scrape on to a combusted Whatman GF/F filter (0.7  $\mu\text{m}$ ), dried the filtrate at 60°C for 48 h and then combusted it at 500°C for 12 h to determine organic matter.

For soil pH, we used an Orion Star A211 Benchtop pH Meter (Thermo Fisher Scientific, Waltham, Massachusetts, USA) to measure the pH of a mixture of 3 g of dried sediment in 5 mL of 0.01 mol L<sup>-1</sup> calcium chloride (CaCl<sub>2</sub>), the addition of which lowers sediment pH by ~0.5 pH units compared to water pH but is advantageous for taking measurements (Carter & Gregorich, 2007). We took background water quality measurements using a YSI ProSolo sonde prior to collecting samples (temperature, barometric pressure, dissolved oxygen, and specific conductance). We measured the pH of the water by collecting a sample with no head space and immediately reading values with the Orion Star A211 Benchtop pH Meter upon return to the lab.

For sediment chlorophyll-a, we subsampled 1-3 grams of wet sediment, which were then freeze dried, homogenized, and passed through a 180  $\mu\text{m}$  sieve. For epilithic chlorophyll-a, we filtered 10 mL of the composite epilithic biomass sample scraped from rocks onto a combusted Whatman GF/F filter (0.7  $\mu\text{m}$ ). We analyzed chlorophyll-a samples a Turner Designs Trilogy benchtop fluorometer using the hot ethanol extraction and acidification method (Roijackers 1981; Sartory 1985). Additionally, we preserved 2 mL of sediment and epilithic biofilms in a 25% glutaraldehyde solution for later taxonomic algal identification. We were unable to identify algae given the amount of sediment in each sample and therefore no taxonomic algal identification was possible.

To extract pore water from composite sediment samples, we added  $3 \pm 0.25$  g of wet sediment and 25 mL of deionized to a falcon tube and vortexed it for 60 seconds. We then rested the falcon tubes in a fridge overnight and centrifuged them the next day. We then filtered the supernatant through Whatman GF/F filters (0.7  $\mu\text{m}$ ) and stored it in acid-washed 50 mL falcon tubes in a freezer at -20°C, until analyzed. We collected filtered surface water samples each location using acid-washed syringes and combusted Whatman GF/F filters (0.7  $\mu\text{m}$  pore size, Whatman, Piscataway, NJ, USA) which were stored in acid-washed 60 mL HDPE bottles frozen at -20°C for later chemistry analysis.

We analyzed filtered surface and sediment pore water samples as well as water filtered from the incubation vials for dissolved organic carbon (DOC), total dissolved nitrogen (TDN), ammonium (NH<sub>4</sub><sup>+</sup>), orthophosphate (o-Phos), and nitrate (NO<sub>3</sub><sup>-</sup>). We followed the same methods outlined in Section III.B.3. We converted ammonia (NH<sub>3</sub>) concentrations determined by the AQ400 Discrete Analyzer to ammonium concentrations (NH<sub>4</sub><sup>+</sup>) using the ambient pH and temperature values (Emerson 1975). For values below detection (NO<sub>3</sub> < 0.003 mg/L; NH<sub>4</sub> < 0.002 mg/L; o-P < 0.402  $\mu\text{g/L}$ ) we set the concentration to half of the minimum detection limit (NO<sub>3</sub> < 0.0015 mg/L; NH<sub>4</sub> < 0.001 mg/L; o-P < 0.201  $\mu\text{g/L}$ ) for analyses.

Our efforts to quantify N-fixation did not result in reliable data and are therefore not included in this report.

#### IV.B.5 Data Analysis

##### *Nitrogen uptake calculations*

To get empirical estimates of added N spikes used as serial N additions for either  $\text{NH}_4^+$  and  $\text{NO}_3^-$  we measured the concentration of our serial dilutions in May (0, 100, 200, 500, 800, and 1200  $\mu\text{g/L}$ ), June (0, 100, 200, 800, 1200, and 1600  $\mu\text{g/L}$ ), and July (0, 100, 200, 800, 1600, and 2000  $\mu\text{g/L}$ ) in DI water. We determined the pelagic uptake in both Glenbrook and Blackwood lake water by calculating the change in N concentrations pre and post incubation. We conducted triplicates of each sample and took the mean concentration. To isolate the uptake rates associated with benthic substrates (sediment or biofilm), we subtracted any change in N concentration associated with the corresponding serial dilutions of incubated lake water. We tracked incubation start and end time for each individual vial and normalized rates by the actual incubation length as it varied from precisely six hours. Lastly, we normalized each vial by the percent of organic matter associated with the sample and volume of lake water.

Lake water uptake rate ( $\mu\text{g N/ L hr}$ ) = (N concentration post-incubation - N concentration pre-incubation)/time incubated

N uptake rate ( $\mu\text{g N/ L hr}$ ) = N concentration of sample/(time incubated - pelagic uptake)

N uptake rate ( $\mu\text{g N/ g AFDW hr}$ ) = (N uptake rate ( $\mu\text{g N/ L hr}$ ) \* 0.025 L) / g AFDW

We calculated  $\text{NH}_4^+$  and  $\text{NO}_3^-$  uptake rates by fitting dose-response curves to each of the eight location by substrate sets of incubations tested for either  $\text{NH}_4^+$  and  $\text{NO}_3^-$  uptake rates using the Michaelis Menten model implemented in via the drc package in R (Figure S1; Dugdale 1967; Reuter 1986; Ritz et al. 2015). These models calculate two parameters,  $V_{\text{max}}$  for the maximum asymptotic response, and  $K_s$  which represents the half-saturation constant based on an alpha level of significance ( $p < 0.05$ ) which we used to interpret whether uptake occurred (both  $V_{\text{max}}$  and  $K_s < 0.05$ ) or just possible (at least  $V_{\text{max}} < 0.05$  and  $K_s \leq 0.05$ ).

$$V = \frac{V_{\text{max}} \times S}{K_s + S}$$

Where  $V$  is the uptake rate,  $S$  is the concentration of our serial additions of either  $\text{NH}_4^+$  and  $\text{NO}_3^-$  (from 0 to 2,000  $\mu\text{g N/L}$ ),  $V_{\text{max}}$  is the rate of uptake at saturating levels of  $S$ , and  $K_s$ , is the half-saturation constant where  $V = V_{\text{max}}/2$ ). The drc package calculates a p-value for the model fit which indicates whether or not the mean model structure is appropriate (Ritz et al. 2015). Therefore, we only considered uptake rates as significant using the Michaelis Menten model when  $p < 0.05$ .

## IV.C Results

### *Environmental conditions during sample collection*

2023 was an above average year for winter precipitation and snowpack accumulation. The timing of peak snow water equivalent or (SWE, 1785.6 mm) for our west shore locations at the inlet of BW creek did not really change between years (only a 2 day difference), but the magnitude of peak SWE was 23% lower (1364.0 mm) than the previous year. Melt rates varied from April to June, with total melt occurring five days earlier on 2023-06-15 at GB, and on 2023-06-20 at BW (Figure 27 & 28). The exceedingly high snow year in 2023 corresponded to high stream water flows and similar timing in the peak flow across sites which occurred at the end of May for both sites (the 21st at  $1.188 \text{ m}^3 \text{ s}^{-1} \text{ km}^{-1}$  and the 23rd at  $0.198 \text{ m}^3 \text{ s}^{-1} \text{ km}^{-1}$  at Blackwood and Glenbrook respectively; Figure 28).

We collected samples for our uptake incubations on May 24th, June 26th, and July 21st of 2023. These dates corresponded to peak streamflow, receding limb, and baseflow conditions (Figure 28). Across all sites, background water temperature ranged from 5.19 to 14.46 °C in May, 6.00 to 15.04 °C in June, and from 9.02 to 20.18 °C in July. East shore sites Glenbrook and Slaughterhouse meadow were generally warmer than west shore sites Sunnyside and Blackwood (Figure 29). Similarly, we observed daily mean dissolved oxygen concentrations across all sites ranged from  $8.86 \pm 1.28 \text{ mg L}^{-1}$  in May,  $8.47 \pm 0.28 \text{ mg L}^{-1}$  in June, and from  $7.66 \pm 0.40 \text{ mg L}^{-1}$  in July. The west shore site (BW) had higher daily DO in both May and June relative to the east shore, while the east shore site (GB) had higher daily DO in July (Figure 30).

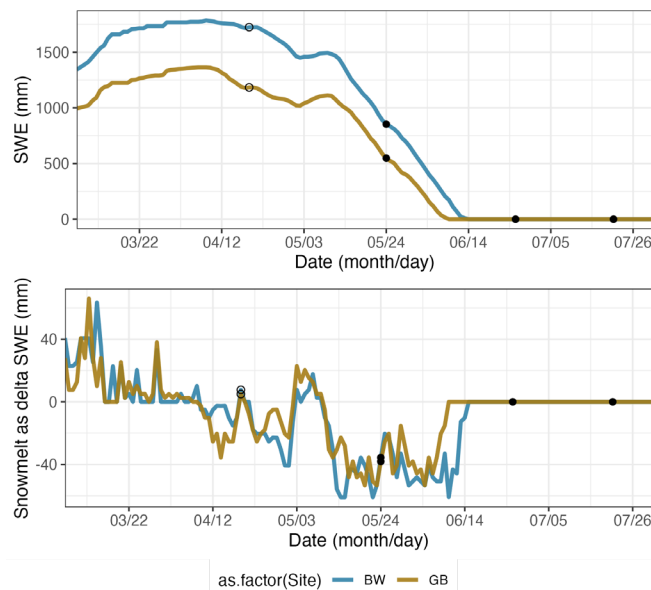


**Figure 27.** SNOTEL station estimates for snow water equivalent (SWE) in mm from nearby stations (BW: ward creek #3 represented in blue, and GB: marlette lake represented in yellow). Filled black circles represent incubation measurements, with the open circles representing the initial pilot incubation.

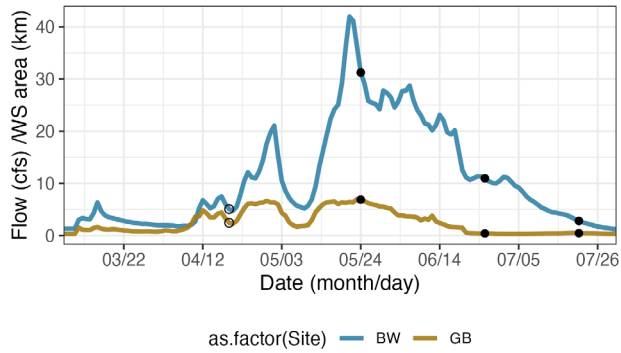


**Figure 28.** Streamflow (cfs) normalized by watershed area (in km) for BW in blue and GB in yellow. Filled black circles represent incubation measurements, with the open circles representing the initial pilot incubation.

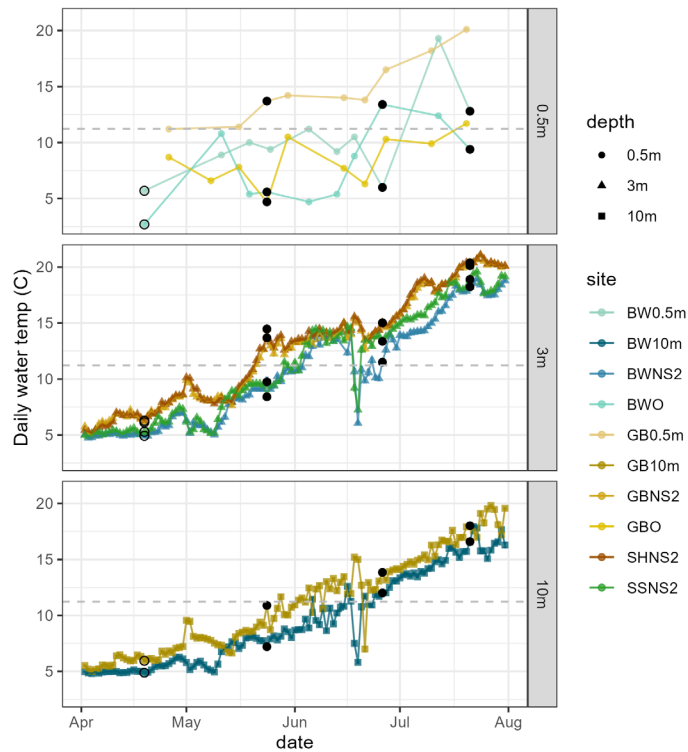


**Figure 29.** Mean daily water temperature from either YSI measurement at 0.5m depth or from miniDOT sensor at 3m and 10m depth with standard error bars present. Filled black circles represent incubation measurements, with the open circles representing the initial pilot incubation. The horizontal line represents the overall seasonal average across all the sites which was 11.22 (°C).

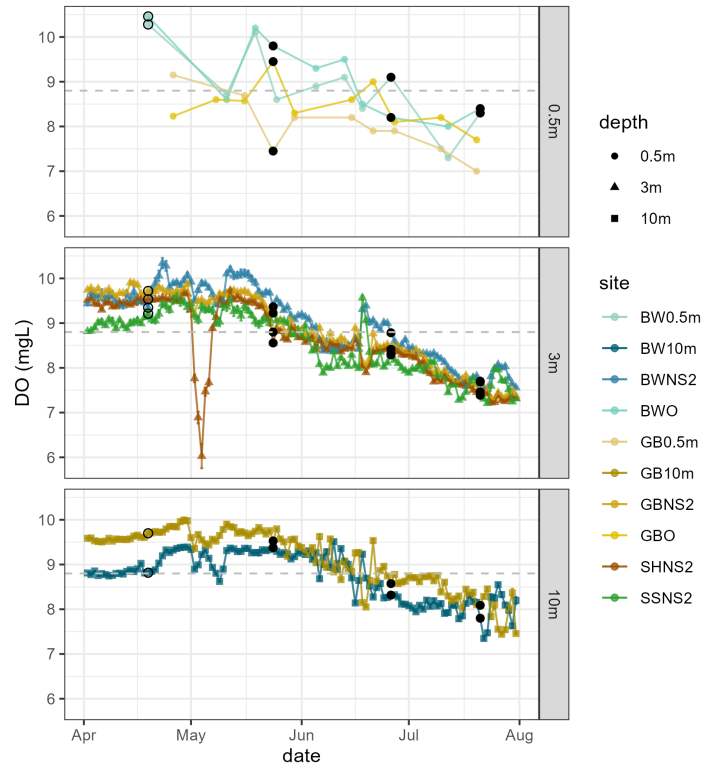


**Figure 30.** Mean daily dissolved oxygen ( $\text{mg L}^{-1}$ ) from either YSI measurement at 0.5m depth or from miniDOT sensor at 3m and 10m depth with standard error bars present. Filled black circles represent incubation measurements, with the open circles representing the initial pilot incubation. The horizontal line represents the overall seasonal average across all the sites  $8.80 \text{ (mg L}^{-1}\text{)}$ . Color represents unique site locations and shape represents the depth of the sampling area.

Background concentrations of water nutrients ( $\text{mg L}^{-1}$ ) were generally low (Figure 31). We observed the highest amounts of  $\text{NO}_3^-$ ,  $\text{NH}_4^+$ ,  $\text{PO}_4^{3-}$ , and DOC at the stream lake interface. DOC and  $\text{PO}_4^{3-}$  were highest in stream lake interface during May ( $\text{PO}_4^{3-}$ :  $0.014 \pm 0.009$ , and DOC:  $1.387 \pm 1.465$ ), while  $\text{NH}_4^+$  and  $\text{NO}_3^-$  concentrations increased in June ( $\text{NH}_4^+$ :  $0.001 \pm 0.001$  and  $\text{NO}_3^-$ :  $0.011 \pm 0.001$ ), and  $\text{NO}_3^-$  concentrations were highest in July ( $0.018 \pm 0.009$ ). For the immediately offshore sampling locations (3 m depth), we observed higher concentrations for nutrients in May ( $\text{NO}_3^-$ :  $0.013 \pm 0.001$ ,  $\text{NH}_4^+$ :  $0.007 \pm 0.003$ ,  $\text{PO}_4^{3-}$ :  $0.008 \pm 0.001$ , and DOC:  $0.569 \pm 0.150$ ) that tended to decline in June and July. We observed a similar temporal trend in the deeper sampling locations  $\text{NO}_3^-$ :  $0.014 \pm 0.004$ ,  $\text{NH}_4^+$ :  $0.015 \pm 0.004$ ,  $\text{PO}_4^{3-}$ :  $0.007 \pm 0.001$ , and DOC:  $0.711 \pm 0.267$ ) and at slightly higher concentrations.

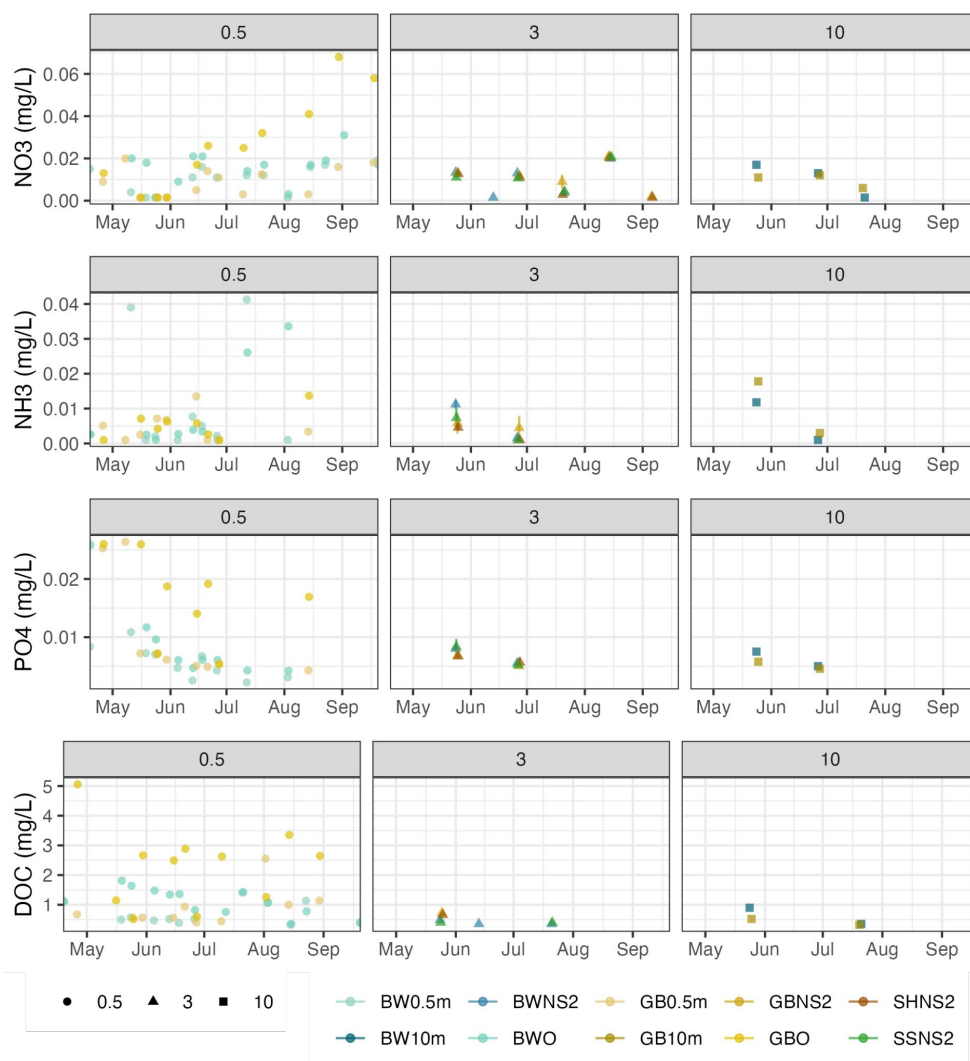


**Figure 31.** Concentration of NO<sub>3</sub>, NH<sub>4</sub> (converted from NH<sub>3</sub> in the figure), PO<sub>4</sub> (measured as o-Phos), and DOC from at 0.5m, 3m and 10m depth with standard error bars present for sites where replicate samples for the same location were collected. Color represents unique site locations and shape represents the depth of the sampling area.

### *Nitrate and ammonium uptake rates*

We attempted to replicate environmental conditions in each nitrogen uptake incubation in the water baths. Substrates collected in May were incubated at  $11.61 \pm 0.76$  °C, substrates collected in June were incubated at  $13.38 \pm 0.74$  °C, and substrates collected in July were incubated at  $17.31 \pm 0.52$  °C. We expected to have 48 measurements for either NO<sub>3</sub><sup>-</sup> and NH<sub>4</sub><sup>+</sup> uptake based on the eight unique site and substrate combinations in May, June, and July. We had a total of 60 possible combinations between months samples, site, substrate type, and analyte. Of those observations of converged uptake, only 35 contained probable estimates of either NO<sub>3</sub><sup>-</sup> and NH<sub>4</sub><sup>+</sup> uptake ( $p < 0.05$ ). Therefore, we also included estimates from uptake based on the average

net change in nitrogen concentrations after accounting for ambient water chemistry, organic matter, and incubation time differences.

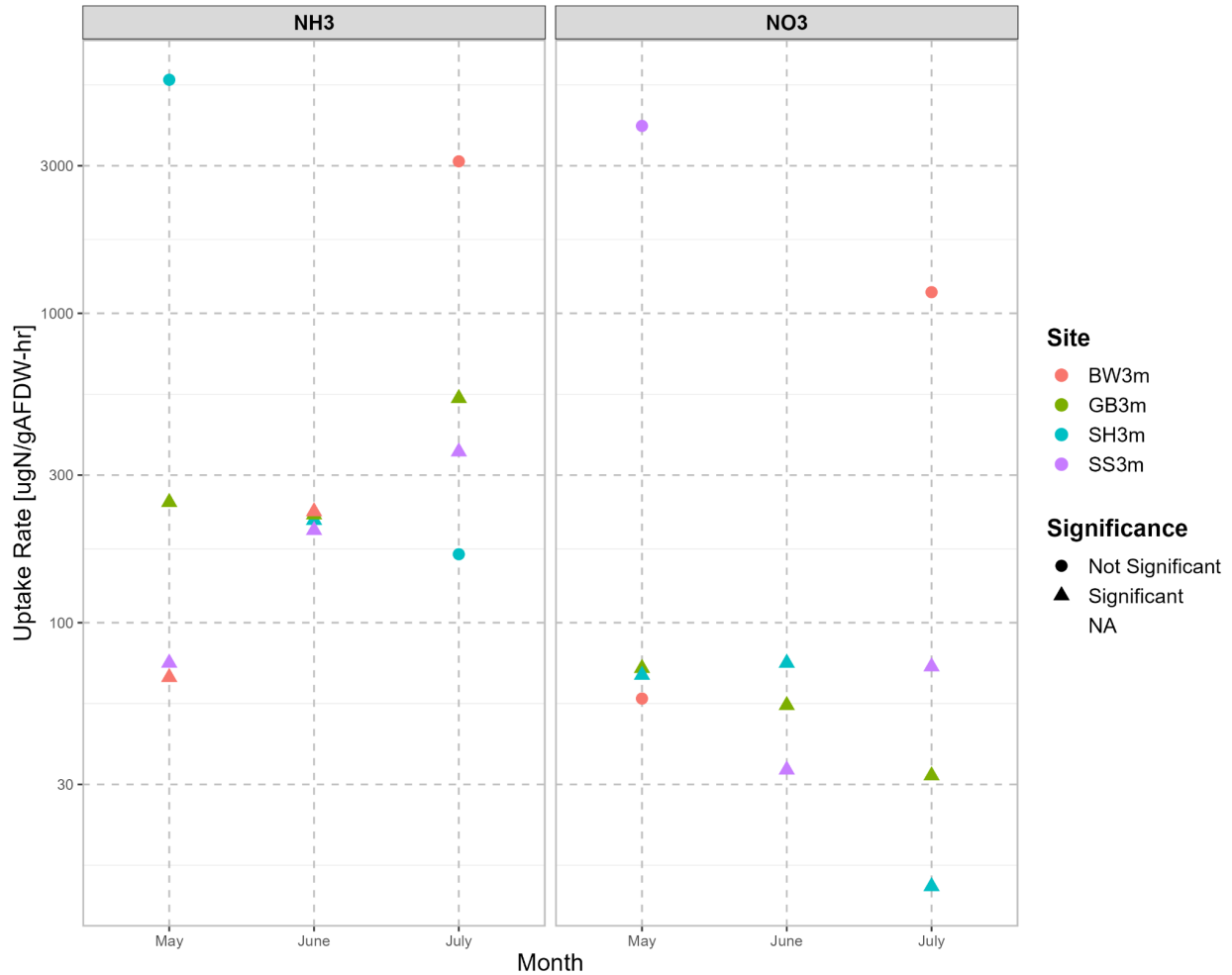


**Figure 32.** Estimates of  $\text{NH}_4^+$  and  $\text{NO}_3^-$  uptake from epilithic biofilm and sediment collected from all depths (0.5m, 3m, and 10m) at the stream lake interface. Triangle shapes represent whether the estimate of nitrogen uptake came from a significant p value ( $<0.05$ ) for Michaelis Menten models or not significant (circle) after accounting for ambient water chemistry, organic matter, and incubation time differences. The y-axis is on a log scale.

Overall, we found that biofilms had the greatest variability of nitrogen uptake from  $0.56$  to  $42.66 \pm 17.8$  for  $\text{NH}_4^+$  and  $0.40$  to  $225.03 \pm 91.28$  for  $\text{NO}_3^-$ , compared with sediments (Figures 32-35). Epilithic biofilms on the east shore tended to exhibit the highest nitrogen uptake rates, relative to biofilms collected from the west shore. Lastly, uptake rates for biofilms at both sites tended to increase in uptake rates from May to July for  $\text{NH}_4$  and decrease for  $\text{NO}_3$ .

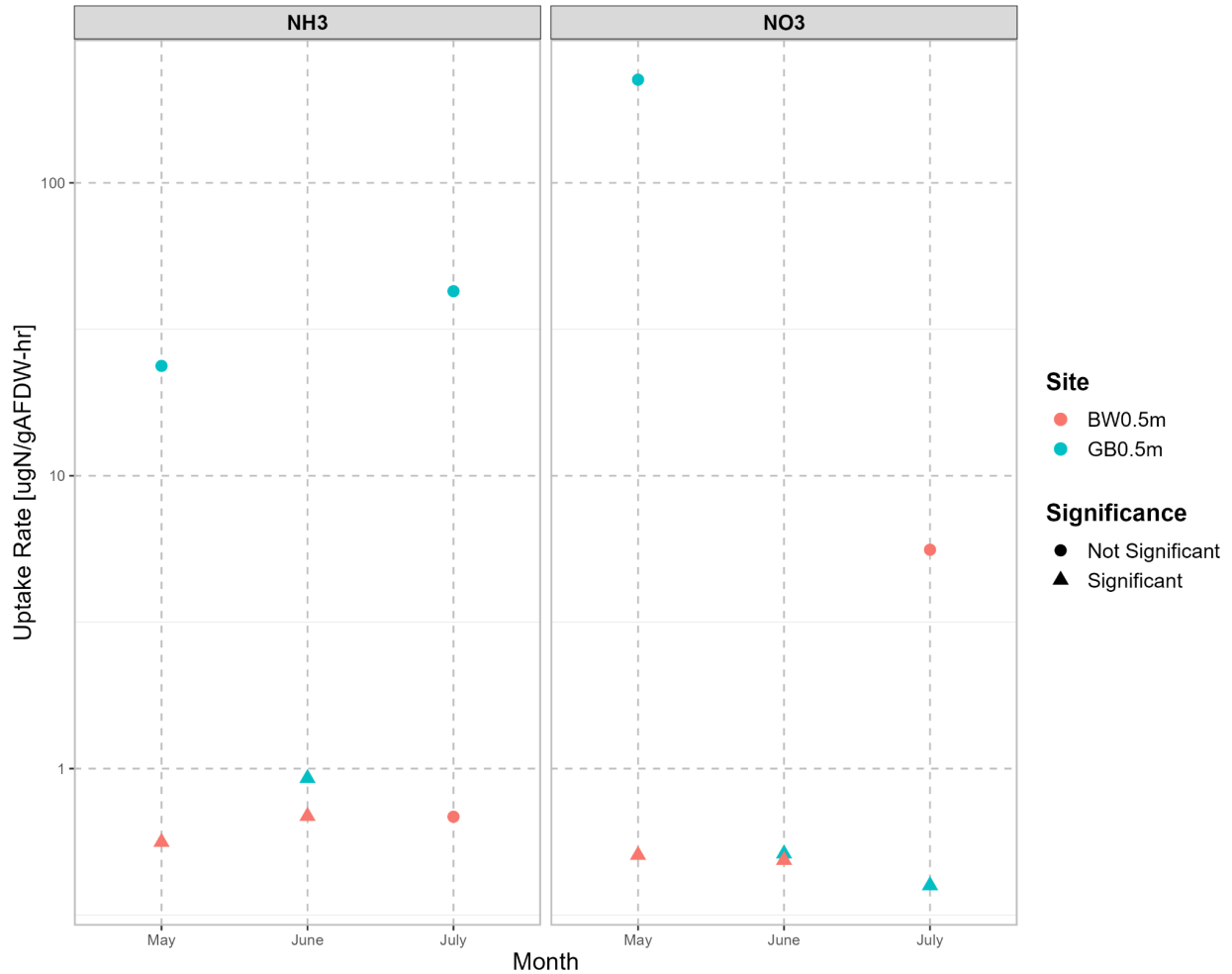


**Figure 33.** Estimates of  $\text{NH}_4^+$  and  $\text{NO}_3^-$  uptake from epilithic biofilm. Triangle shapes represent whether the estimate of nitrogen uptake came from a significant p value ( $<0.05$ ) for Michaelis Menten models or not significant (circle) after accounting for ambient water chemistry, organic matter, and incubation time differences. The y-axis is log scaled.

In contrast, west shore sediments tended to have higher rates of nitrogen uptake for both  $\text{NO}_3^-$  and  $\text{NH}_4^+$  relative to east shore sites. Across all sites we observed higher  $\text{NH}_4^+$  uptake rates relative to  $\text{NO}_3^-$ , with the greatest rates of  $\text{NH}_4^+$  occurring on the east shore at all sampled Glenbrook depths, as well as at Sunnyside (3m) on west shore. Additionally, rates of  $\text{NH}_4^+$  uptake increased from across all sites from May to July while rates of  $\text{NO}_3^-$  uptake did not appear to change.

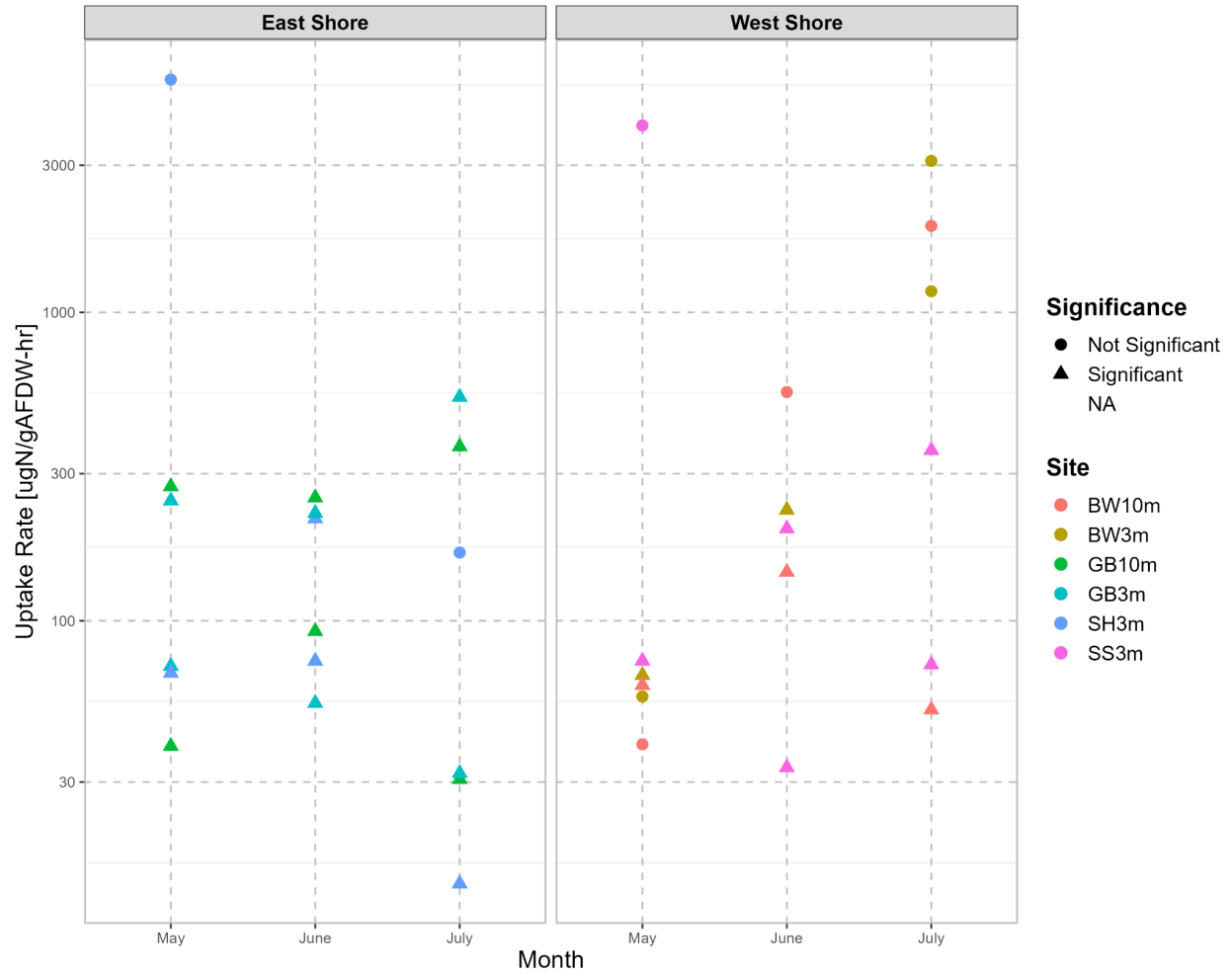


**Figure 34.** Estimates of nitrogen uptake  $\text{NH}_4^+$  and  $\text{NO}_3^-$  uptake from sediment collected from the east and west shores, where point color corresponds to sampling location. The y-axis is log scaled.

We observed comparable uptake rates on the west shore compared to the east shore (Figure 34), and at the stream-lake interface versus away (Figure 35).

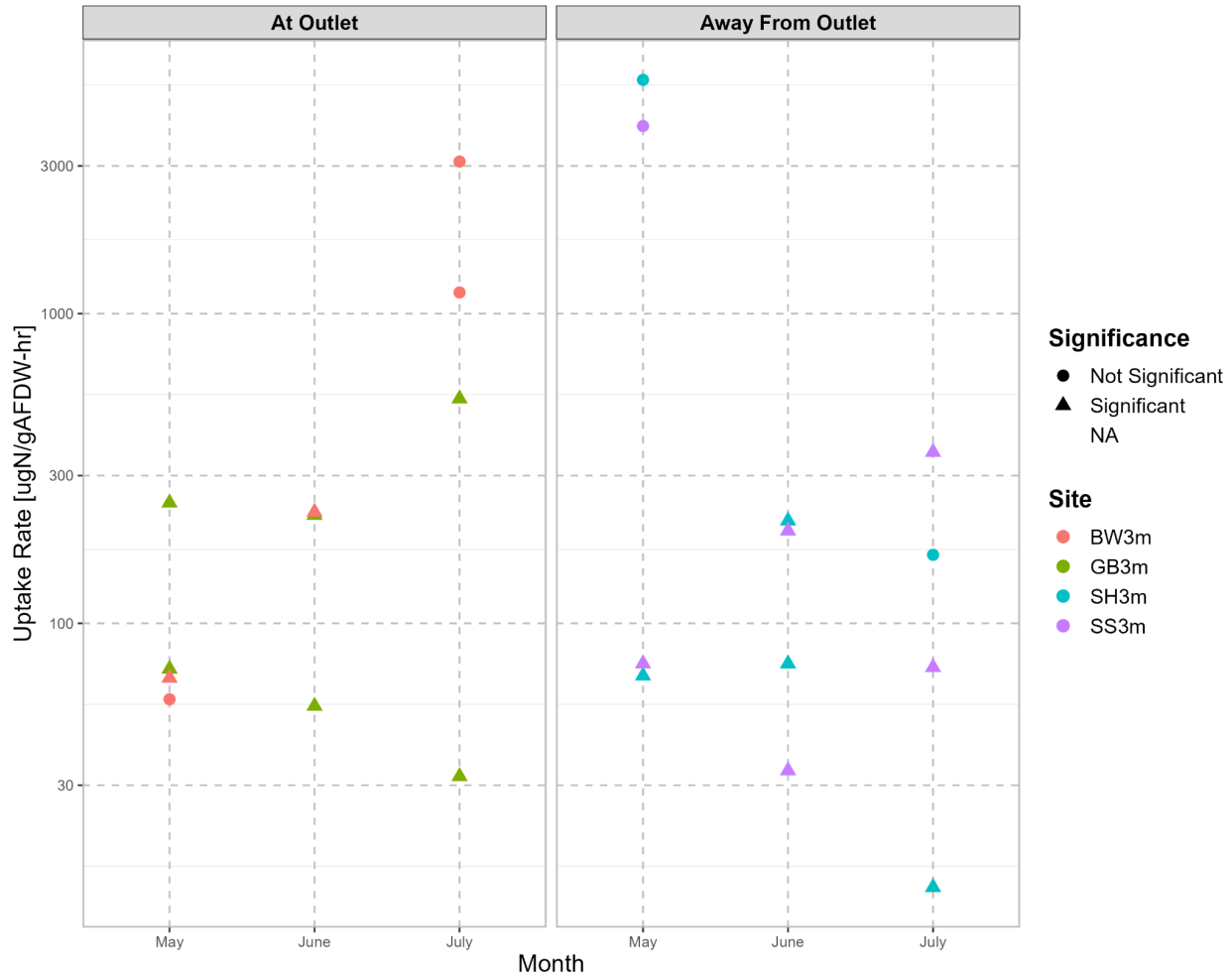


**Figure 35.** Estimates of nitrogen uptake  $\text{NH}_4^+$  and  $\text{NO}_3^-$  uptake from sediment collected at and away from the stream outlet, where point color corresponds to sampling location. The y-axis is log scaled.

#### *Comparison to historic uptake rates*

Reuter and others (1986) reported a maximum uptake of  $30.3 \pm 4.6 \mu\text{g N g}^{-1} \text{AFDW h}^{-1}$  for  $\text{NO}_3^-$  and  $18.7 \pm 3.2 \mu\text{g N g}^{-1} \text{AFDW h}^{-1}$  for  $\text{NH}_4$  during August 1981. We estimated substantially higher uptake rates for significant model fits, yet we attribute this discrepancy to very low amounts of AFDM that can inflate the uptake rate value. In addition, when only uptake rates that had a significant model fit are included, then rates are more comparable.

#### **IV.D Conclusion**

We quantified dissolved inorganic nitrogen uptake rates across four locations in the shallow littoral zone of Lake Tahoe. The dominant substrate for the sites was sandy apart from the outlet of the stream where larger cobble existed. We observed highly variable and high DIN uptake

rates, which were substantially greater than those reported in Reuter and others (1986). However, the very limited amounts of organic matter and biomass in the samples may have inflated the uptake rates and therefore we recommend further investigation before drawing substantial conclusions or using uptake rates in ecosystem models.

## **V. Objective 4: Predicting nearshore ecosystem productivity**

### **V.A Introduction**

Lakes are capable of integrating environmental processes from their surrounding landscapes, to reflect seasonal patterns of material transport, precipitation, and evapotranspiration (Adrian et al., 2009; Williamson et al., 2009). Within lakes, the nearshore habitat, or littoral zone, plays a key role in biogeochemical cycling and supporting biodiversity (Vadeboncoeur et al., 2003; Devlin et al., 2016; Vander Zanden & Vadeboncoeur 2020). The nearshore is characterized by greater substrate-surface water interactions which can elevate ecosystem productivity relative to the limnetic zone, but can also be highly heterogenous around a given lake perimeter (Vadeboncoeur et al., 2006; Cavalcanti et al., 2016). This high spatial heterogeneity in nearshore ecosystem productivity originates in part from variation in the degree of hydrologic connectivity with upland landscapes, which supply allochthonous nutrients and organic matter that support productivity and diversity in the littoral zone (Vander Zanden & Vadeboncoeur 2020). Here we examine how the degree of hydrologic connectivity as a function of streamflow and interannual precipitation influences the timing and magnitude of nearshore productivity.

Stream-to-lake transition zones within the nearshore are ecosystem control points (Bernhardt et al., 2017) that can create the right combination of environmental conditions and delivery of limiting nutrients to stimulate high rates of biogeochemical activity (Johengen et al 2008; Jones 2010). At the upland-lake interface, the direction and distance of stream water travels as a plume into the lake is determined by the streamflow velocity and temperature differences in the interacting waterbodies (Alavian et al., 1992; Roberts et al., 2018). In mountain lakes, cold stream water will sink into deep lake layers as underflow where suspended particles and dissolved matter can rapidly settle on in the benthos and facilitate hotspots of productivity (MacIntyre et al., 2006; Nielson & Henderson 2023). The processes responsible for streamflow generation in mountain ecosystems are strongly related to snowpack dynamics, evapotranspiration demands, and catchment morphology (Lyon et al., 2008; Harpold 2012; Kirchner et al., 2020). However, most mountainous regions in the United States are experiencing decreased snowpack persistence and earlier onset of melt (Musselman et al., 2021; Siirila-Woodburn 2021 ; Hale et al., 2023), subsequently altering the timing of surface water and solutes to lake ecosystems from year to year (Dodds et al., 2019; Oleksy et al., 2021). Therefore, the individual influence of inflowing streams on nearshore productivity reflects a combination of contemporary surface water hydrology and antecedent watershed loading patterns and can be highly variable across relatively short timescales (Hanson et al., 2015; Ward et al., 2022).

The degree to which a nearshore area is hydrologically connected to the uplands may result in heightened sensitivity to hydroclimatic variability. Past work has documented how hydroclimatic conditions can influence nearshore habitats through lake level rise and fall (Hofmann et al., 2008; Scordo et al., 2021), groundwater intrusion (Rosenberry et al., 2015; Naranjo et al., 2019),

and terrestrial runoff (Cassan et al., 2019; McCullough et al., 2019) Given expectations for climate change to severely alter the patterns of precipitation through watersheds (Stewart 2009; Dai et al., 2018; Hale et al., 2023), the degree to which nearshore ecosystem processes reflect changes in hydrologic connectivity within catchments relative to internal lake processes is unclear. This understanding is important for preserving the ecosystem function, safeguarding water resources, and maintaining the quality of recreation in lake ecosystems (Williamson et al., 2009; Moser et al., 2019).

Despite the potential impact of nearshore metabolism on whole-lake carbon cycling, much of past limnological theory and current monitoring efforts often rely on extrapolations from single, open water stations or pelagic energetic models, neglecting within-lake heterogeneity and variation in watershed contributions. This oversight can lead to substantial bias in whole lake metabolism estimates depending on the characteristics of the lake. Capturing the relative contribution of nearshore metabolism to whole lake estimates should also take the relative influence of inflowing streams at the monitoring location into account because areas around inflowing streams may have shorter water residence times and water chemistry that is more related to upland stream processes relative to other reaches of the shoreline further from streams (Chmiel et al., 2020; Ward et al., 2022).

This study investigates the relative influence of streams on variation in nearshore metabolism by measuring littoral water quality (water temperature, clarity, nutrients) and estimating ecosystem metabolism near and far from stream inlets continuously for 2.5 years. We conducted this work on two contrasting shores of Lake Tahoe (Nevada/California, USA), Patterns of nearshore water temperature warming (Ngai et al., 2013) are expected to facilitate summer algae growth, while it is thought that winter precipitation and corresponding groundwater recharge combined with wave action can enable nutrient fluxes that promote spring algal blooms (Naranjo et al., 2019; Vadeboncoeur et al., 2021). However, the high water clarity and possibility of UV- inhibition, combined with other environmental factors such as turbulence from high winds, precipitation, and streamflow, could disrupt these anticipated spring and summer peaks in algal growth.

Here, we compared seasonal variance in nearshore metabolism regimes for two paired catchments in Lake Tahoe and examined the relative influence of inflowing streams on those regimes. Specifically we asked three questions: (1) What is the relative influence of uplands versus internal lake processes on nearshore metabolism? (2) How do site characteristics mediate the influence of streams on nearshore metabolism? (3) How does the influence of streams on nearshore metabolism change from dry to wet years?. We hypothesize that upland streamflow will influence nearshore productivity (GPP and ER) through increased material transport during discrete periods immediately following snowmelt while the internal lake processes (benthic light and water temperature) will drive nearshore metabolism regimes for the remaining majority of the year. We additionally expect these patterns to vary based on specific site-attributes such as

substrate (sand or cobbles), bathymetry (steep or shallow), benthic nutrients and organic matter, catchment area, and weather (solar radiation, wind, rain events). We predict nearshore metabolism at the western locations will be more sensitive to stream-mediated processes, as this shore has steeper bathymetry, greater snow accumulation, and a larger inflowing stream relative to the eastern locations. Finally, we expect drier years will be associated with elevated autotrophic conditions in the nearshore zone due to higher light availability as well as less surface water run-off and turbulent inflow mixing. Conversely, wetter years are expected to have strong stream influence associated with greater inflow discharge and delayed GPP maxima. Our overarching objective is to quantify the respective contributions of upland and internal lake processes to nearshore metabolism over time and across distinct stream-to-lake transitional zones in order to provide a mechanistic understanding of how and when hydrologic connectivity with uplands drives nearshore productivity.

## **V.B Methods**

### V.B.1 Data structure

We fit our models to the daily gross primary productivity (GPP) and ecosystem respiration (ER) time series generated in Objective 1, and use covariate data from Objectives 1-3.

### V.B.2 Data analysis and time series modeling

#### *Time series - generalized linear mixed models*

We used autoregressive generalized linear mixed models (GLMMs) as well as structural equation models (SEM) to assess the different mechanisms for how streams influenced nearshore. Our goals were to characterize how streams could (1) influence nearshore metabolism through the magnitude, timing, and temperature of streamflow, (2) biogeochemically alter nearshore metabolism through the delivery of nutrients and organic matter, and (3) to investigate the relative influence of streamflow versus within-lake conditions (e.g., lake temperature, precipitation events, wind speed, and benthic light) that have been hypothesized drive GPP and ER. As metabolism is an inherently autoregressive processes relying on a 24 hour light cycle, we analyzed the autocovariance and partial autocorrelation of GPP and ER time series using the ‘acf’ and ‘pacf’ functions in R to establish appropriate lags and temporally de-trend the autocorrelation structure of our response variable from other measured covariates (Venables & Ripley 2002).

We modeled the direct effects of physical stream process on daily nearshore GPP or ER at either BW or GB using the glmmTMB package (Brooks et al. 2017), with log-normal error distributions, a nested random effect (Bolker et al., 2009) for site location (BWNS1, BWNS2, BWNS3, GBNS1, GBNS2, and GBNS3) within shore location (BW, GB, SH, and SS) as well as a random effect for year of observation (2021, 2022, and 2023). We transformed the absolute

value of ER (|ER|) to allow for both covariate effects to be interpreted at the same scale as GPP as well as the application of a log-normal error distribution. We subset our data for complete observations ( $n = 1464$ ) of scaled covariates for daily stream water SPC ( $\mu\text{S cm}^{-1}$ ), catchment area normalized stream flow ( $\text{cms}^{-1} \text{ km}^{-2}$ ), and stream water temperature ( $^{\circ}\text{C}$ ) and ensured collinearity relationships between scaled predictor variables was low ( $\rho \leq 0.60$ ) before proceeding with statistical models. For each GLM, we checked for variance inflation in each of our GLMs using VIF (implemented in the car package) (Fox and Weisberg, 2019), estimated the significance ( $P > 0.05$ ) of individual terms, used manual comparisons of model fit (residual distributions and AIC scores implemented in the lmerTest package) (Fox & Weisberg, 2011; Kuznetsova et al., 2017), and obtained model  $R^2$  values using the function rsquaredglmm (Barton & Barton, 2015). We implemented this approach in R version 5.0 (R Development Core Team, 2023).

### *Structural Equation Modeling (SEM)*

We modeled the combined direct and indirect effects of catchment normalized mean daily streamflow ( $\text{m}^3 \text{ s}^{-1} \text{ km}^{-1}$ ) on daily GPP and ER ( $\text{mmol O}_2 \text{ m}^{-3} \text{ d}^{-1}$ ) at both BW or GB by fitting three Bayesian SEMs for GPP and ER, benthic light ( $\mu\text{mol m}^{-2} \text{ s}^{-1}$ ), and water temperature ( $^{\circ}\text{C}$ ). We combined all models as Bayesian piecewise structural equation models (SEM) (Lefcheck 2016; Brown et al., 2023). SEMs can be used to evaluate a network of ecosystem processes to inform controls on ecosystem function while accounting for indirect pathways (Lefcheck et al., 2018). We tested the following models,

(1)

$$\log(\text{GPP}_{ti} \text{ or } |\text{ER}_{ti}| + 1) = \beta_0 + \beta_1 \times \log(\text{GPP}_{t-1 \ i} \text{ or } |\text{ER}_{t-1 \ i}| + 1) + \beta_2 \times \text{benthic PAR}_{ti} + \beta_3 \times \text{water temp.}_{ti} + \beta_4 \times \log(\text{streamflow})_{ti} + \mu_{ti} + \epsilon_{ti}$$

$$\mu_i \sim N(0, \sigma^2_{\mu}) \text{ and } \epsilon_{ti} \sim N(0, \sigma^2)$$

(2)

$$\text{benthic PAR}_{ti} = \delta_0 + \delta_1 \times \log(\text{streamflow})_{ti} + \mu''_{ti} + \epsilon''_{ti}$$

$$\mu''_i \sim N(0, \sigma^2_{\mu''}) \text{ and } \epsilon''_{ti} \sim N(0, \sigma''^2)$$

(3)

$$\text{water temp.}_{ti} = \gamma_0 + \gamma_1 \times \log(\text{streamflow})_{ti} + \mu'_{ti} + \epsilon'_{ti}$$

$$\mu'_i \sim N(0, \sigma^2_{\mu'}) \text{ and } \epsilon'_{ti} \sim N(0, \sigma'^2)$$

We constrained this analysis to days with streamflow less than flows with exceedance probabilities greater than 5% (BW = 1.11 and GB = 1.00  $\text{m}^3 \text{ s}^{-1} \text{ km}^{-1}$ ) to model log transformed catchment normalized streamflow as a Gaussian distribution. We fit models using the brms package (Bürkner 2021) with three chains, each running for 9,000 iterations (4,500 warm up), an autoregressive term for daily  $\text{GPP}_{t-1}$  or  $|\text{ER}_{t-1}|$ , and a random effect for site ( $i = 3$ ). We log

transformed (+1) GPP and |ER| to allow for Gaussian probability density functions, and scaled other model covariates, benthic light, lake temperature, and streamflow (catchment normalized) to allow for direct comparisons of path coefficient strength. We reported the mean posterior, and upper and lower credible interval for each parameter estimate with an  $\hat{R} > 1.05$ .

### *Structural Equation Modeling - Precipitation Effects*

To examine how the influence of streams on nearshore metabolism might change from dry to wet years, we contextualized how other hypothesized metabolism controls like benthic light ( $\mu\text{mol m}^{-2} \text{s}^{-1}$ ) and lake temperature ( $^{\circ}\text{C}$ ), and precipitation (mm) may impact nearshore metabolism (GPP or |ER|,  $\text{mmol O}_2 \text{m}^{-3} \text{d}^{-1}$ ). using We built individual Bayesian SEMs (Brown et al., 2023) using the brms package (Bürkner 2021) for each shore (BW, GB, SH, and SS) with parameters for log transformed benthic light, lake temperature, and precipitation (+1), on a subset of overlapping observations (February to September 2023, GPP = 750 and |ER|= 747) to include dynamics away from streams for 11 different sites across four different shores (BW, SS, GB, and SH) using the following model,

$$\log(\text{GPP}_{t,i} \text{ or } |\text{ER}_{t,i}| + 1) = \beta_0 + \beta_1 \times \log(\text{GPP}_{t-1,i} \text{ or } |\text{ER}_{t-1,i}| + 1) + \beta_2 \times \text{benthic PAR}_{t,i} + \beta_3 \times \text{water temp.}_{t,i} + \beta_4 \times \log(\text{precipitation})_{t,i} + \mu_{t,i} + \epsilon_{t,i}$$

$$\mu_i \sim \text{N}(0, \sigma^2_{\mu}) \text{ and } \epsilon_{t,i} \sim \text{N}(0, \sigma^2)$$

## **V.C Results**

### V.C.I Relative influence of environmental drivers of nearshore metabolism

#### *Stream dynamics within the nearshore*

From April to September 2023, stream water typically entered as underflow, as the difference between inflowing streamwater density and lake water density (i.e.,  $\Delta\rho$ ) was rarely positive (Figure 36). Therefore, inflowing stream water is likely to make contact quickly with the nearshore benthic zone. Our best fit model to explain variance on the full time series in either daily GPP or ER for the three locations immediately around the inlets of BW or GB creeks contained two day autoregressive terms, as well as covariates for average daily log-transformed streamflow, stream temperature, wind speed, benthic light, and log-transformed precipitation. We found that GPP was negatively correlated with stream flow ( $\beta_{\log(\text{flow})}$ :  $-0.245 \pm 0.088$ ,  $p = 0.006$ ,  $r^2 = 0.61$ ) and positively correlated with wind speed ( $\beta_{\text{wind sp.}}$ :  $0.020 \pm 0.007$ ,  $p = 0.007$ ,  $r^2 = 0.61$ ), and marginally correlated with stream water temperature ( $\beta_{\text{stream temp.}}$ :  $0.015 \pm 0.008$ ,  $p = 0.071$ ,  $r^2 = 0.59$ ). While daily ER was positively correlated with PAR ( $\beta_{\text{PAR}}$ :  $0.013 \pm 0.005$ ,  $p = 0.011$ ,  $r^2 = 0.66$ ).

When exploring these relationships for daily GPP or |ER| through Bayesian structural equation models (SEM), we observed that the influence of streamflow on nearshore productivity varied

with catchment, and was generally more robust for the west shore, BW (Figures 38 & 39). Streamflow had a direct positive influence on GPP at BW (mean; 95% credible interval,  $\beta_{\text{flow to GPPt}}$ : 0.05; 0.01 to 0.08), but only a marginal positive influence at our eastern catchment GB ( $\beta_{\text{flow to GPPt}}$ : 0.02; -0.02 to 0.06, Figure 38). Across both shores benthic water temperature had positive influence (BW:  $\beta_{\text{temp. to GPPt}}$ : 0.06; 0.01 to 0.10 and GB:  $\beta_{\text{temp. to GPPt}}$ : 0.03; 0.00 to 0.07) on nearshore GPP; while benthic PAR had a negative influence on nearshore shore GPP (BW:  $\beta_{\text{PAR to GPPt}}$ : -0.05; -0.08 to -0.01 and GB:  $\beta_{\text{PAR to GPPt}}$ : -0.05; -0.07 to -0.02). However, daily GPP at both shores was most strongly related to the day prior's GPP (BW:  $\beta_{\text{GPPt-1 to GPPt}}$ : 0.81; 0.77 to 0.85 and GB:  $\beta_{\text{GPPt-1 to GPPt}}$ : 0.78; 0.73 to 0.83).

In terms of confounding effects, streamflow decreased lake temperature (BW:  $\beta_{\text{flow to temp.}}$ : -0.52; -0.58 to -0.46 and GB:  $\beta_{\text{flow to temp.}}$ : -0.81; -0.85 to -0.76) and benthic PAR (BW:  $\beta_{\text{flow to PAR}}$ : -0.22; -0.29 to -0.16 and GB:  $\beta_{\text{flow to PAR}}$ : -0.39; -0.45 to -0.31) at both catchments. The indirect effect of streamflow on GPP can be estimated by multiplying the posterior distributions for streamflow based path coefficients. Here we found the indirect effects of streamflow on nearshore GPP was for BW was 0.005 increasing the overall effect of streamflow by 10% ( $\beta_{\text{flowT to GPPt}}$ : 0.06), while the indirect effect of streamflow on GPP at GB was slightly higher 0.007 increasing the overall stream effect of streamflow by 25% ( $\beta_{\text{flowT to GPPt}}$ : 0.03). We additionally evaluated the role of streamflow on ecosystem respiration (ER) for the same subset of data, but found streamflow did not influence ER at either shore (Figure 39). While streamflow maintained a negative influence on lake benthic temperature and light, benthic light marginally decreased ER (BW:  $\beta_{\text{PAR to |ERt|}}$ : -0.02; -0.03 to -0.00 and GB:  $\beta_{\text{PAR to |ERt|}}$ : -0.05; -0.07 to -0.02) and benthic temperature had no noticeable impact. Daily ER was also highly related to the day prior's ER at both shores (BW:  $\beta_{\text{|ERt-1| to |ERt|}}$ : 0.92; 0.90 to 0.95 and GB:  $\beta_{\text{|ERt-1| to |ERt|}}$ : 0.72; 0.67 to 0.77). The indirect effect of streamflow on nearshore ER was still marginal across both shores (BW:  $\beta_{\text{flowT to |ERt|}}$ : 0.002 and GB:  $\beta_{\text{flowT to |ERt|}}$ : 0.003).

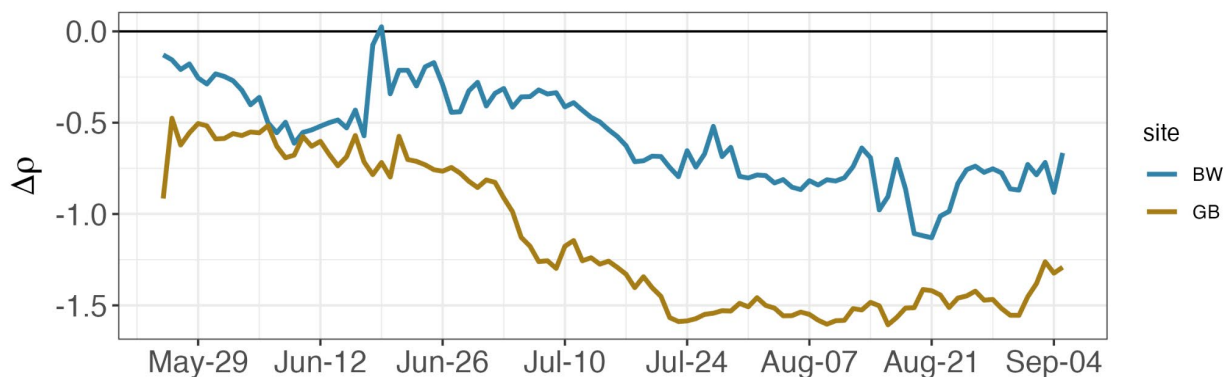


**Figure 36.** The difference between inflowing stream water density and lake water density as ( $\Delta\rho$ ) based on temperature and specific conductance of the streamwater and lake water using the

International Thermodynamic Equation of Seawater TEOS-10 (Feistel 2008; Roberts e al. 2018). Negative values indicate that stream water is entering the lake as underflow.

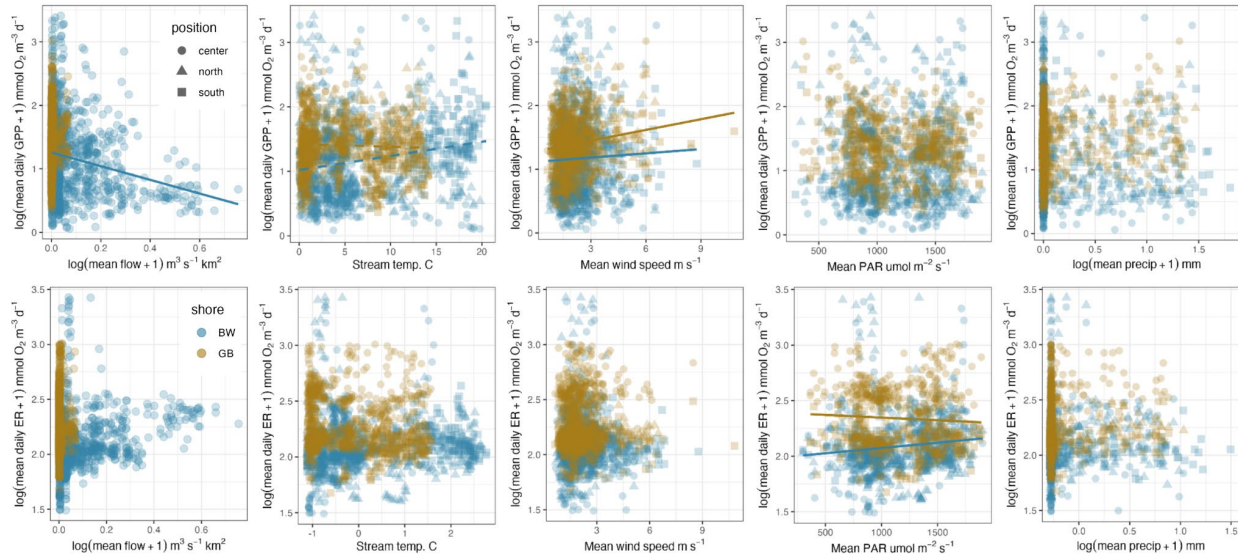


**Figure 37.** Relationships between log-transformed (+) daily GPP (top) or |ER| (bottom) and environmental covariates, average daily log-transformed streamflow, stream temperature, wind speed, benthic light, and log-transformed precipitation at BW (blue) and GB (yellow). Point shape represents sensor position; circles for sensors centrally located in front of streams, triangles for north of streamflow, and squares for south of streamflow. Solid lines represent statistically significant linear relationships, while dashed lines represent marginal relationships.

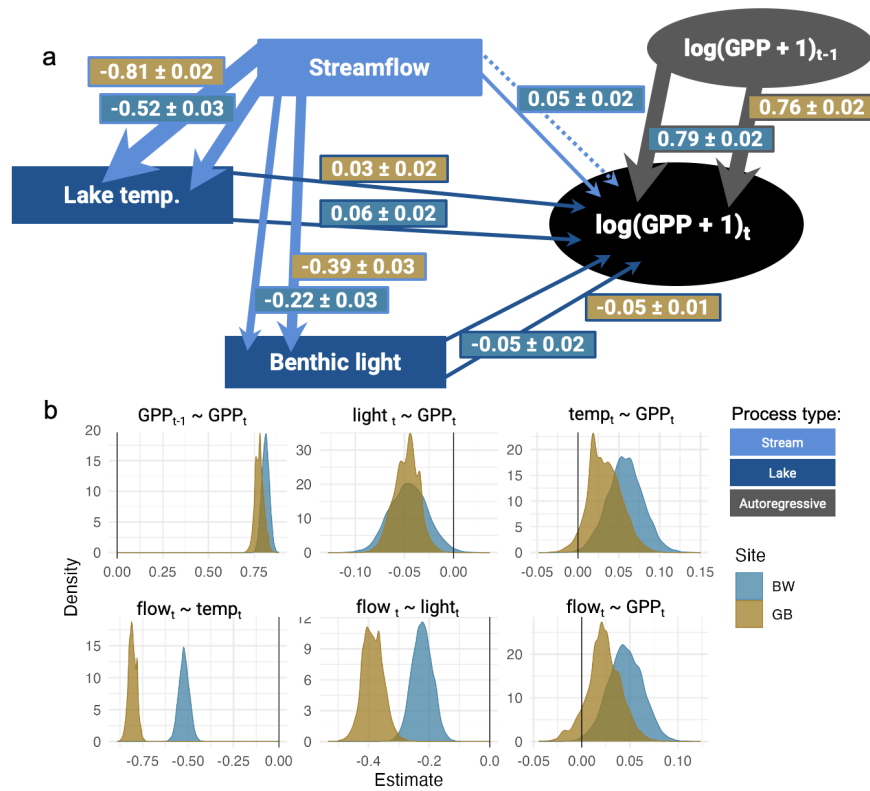


**Figure 38.** Results from Bayesian SEM for log transformed (+1) GPP at BW (in blue) and GB (in gold). a) The SEM structure for how  $\text{GPP}_t$  may be a function of streamflow, lake temperature, benthic light and  $\text{GPP}_{t-1}$ , with mean posterior estimates and standard error color coded by shore in boxes along the path coefficients. Arrow weight represents relationship strength and box color for each parameter represents the type of process associated with a given parameter (light blue for stream, dark blue for lake, and gray for autoregressive). b) the posterior estimates colored by shore BW (in blue) or GB (in gold) for each parameter relationship. The vertical line marks when posteriors overlap zero for any parameter.

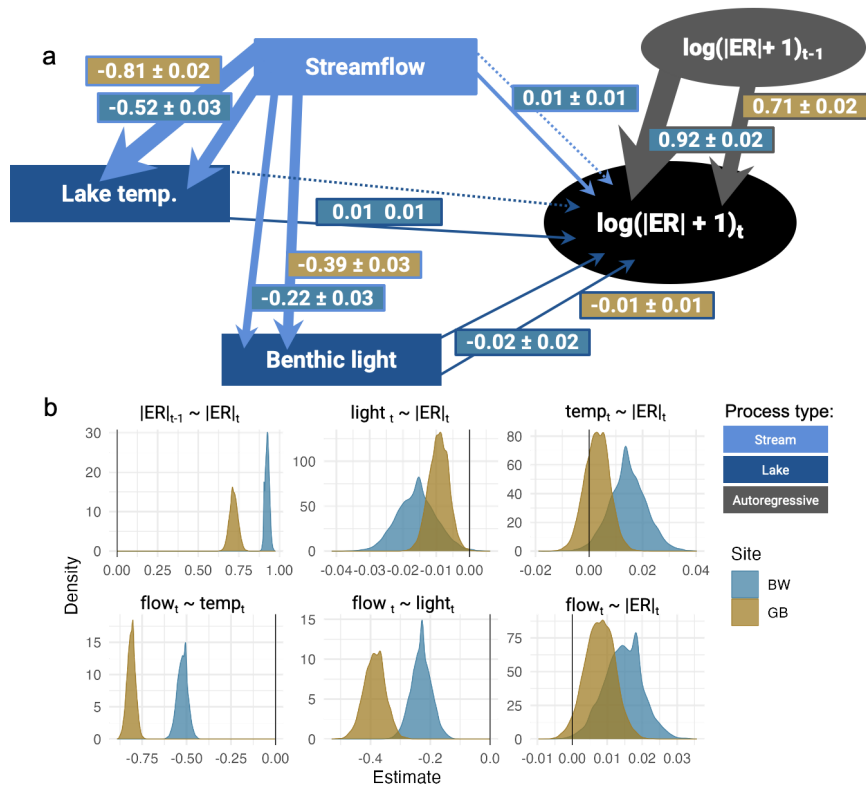


**Figure 39.** Results from Bayesian SEM for log transformed (+1) |ER| at BW (in blue) and GB (in gold). a) The SEM structure for how |ER| may be a function of streamflow, lake temperature, benthic light and |ER|<sub>t-1</sub>, with mean posterior estimates and standard error color coded by shore in boxes along the path coefficients. Arrow weight represents relationship strength and box color for each parameter represents the type of process associated with a given parameter (light blue for stream, dark blue for lake, and gray for autoregressive). b) The posterior estimates colored by shore BW (in blue) or GB (in gold) for each parameter relationship. The vertical line marks when posteriors overlap zero for any parameter.

#### *Other environmental drivers of nearshore ecosystem metabolism*

To contextualize other environmental drivers of nearshore metabolism, we calculated mean weekly fluxes of GPP and ER on a subset of observations (February to September 2023) and compared them to the metabolism estimates for shore locations away from inflowing streams (SH and SS). Our best fit model to explain variance in either weekly GPP or ER for 11 individual sites nested within four different shore locations for the summer of 2023 included an one temporally autoregressive term, as well as covariates for weekly average lake temperature, wind speed, benthic light as well as number of precipitation events. Weekly GPP was positively correlated with wind speed ( $\beta_{wind\ sp.}: 0.020 \pm 0.007, p = 0.007, r^2 = 0.61$ ) and lake water temperature ( $\beta_{lake\ temp.}: 0.018 \pm 0.009, p < 0.001, r^2 = 0.59$ ). While weekly ER was negatively associated with lake water temperature ( $\beta_{lake\ temp.}: -0.025 \pm 0.009, p = 0.006, r^2 = 0.65$ ).

Additionally, in SEMs for daily GPP or |ER| benthic light and precipitation had a small negative influence on both GPP and ER, while lake temperature had a small positive effect on GPP and ER. We observed GPP was potentially suppressed by light across all locations (BW:  $\beta_{PAR \text{ to } GPpT}$ : -0.24, -0.45 to -0.03; SS:  $\beta_{PAR \text{ to } GPpT}$ : -0.17, -0.64 to 0.30; and SH:  $\beta_{PAR \text{ to } GPpT}$ : -0.20, -0.53 to 0.12), except the stream-impacted east shore (GB:  $\beta_{temp. \text{ to } GPpT}$ : -0.01, 0.14 to 0.11). Temperature appeared to stimulate GPP at BW ( $\beta_{temp. \text{ to } GPpT}$ : 0.23, 0.09 to 0.37) and to a lesser degree at SH ( $\beta_{temp. \text{ to } GPpT}$ : 0.04, -0.11 to 0.19). Temperature also appeared to stimulate ER at for our west shore sites (BW:  $\beta_{temp. \text{ to } |ERt|}$ : 0.03, -0.03 to 0.08 and SS:  $\beta_{temp. \text{ to } |ERt|}$ : 0.04, 0.01. to 0.08), but potentially suppressed ER at east shore locations (GB:  $\beta_{temp. \text{ to } |ERt|}$ : -0.01, -0.04 to 0.02 and SH:  $\beta_{temp. \text{ to } |ERt|}$ : -0.02, -0.04. to 0.01). Precipitation had a small negative effect on GPP at all locations (BW:  $\beta_{precip. \text{ to } GPpT}$ : -0.03, -0.10 to 0.04, GB:  $\beta_{precip. \text{ to } GPpT}$ : -0.01, -0.08 to 0.07, SH:  $\beta_{precip. \text{ to } GPpT}$ : -0.01, -0.18 to 0.10, and SS:  $\beta_{precip. \text{ to } GPpT}$ : -0.01, -0.18 to 0.10), but a small positive effect on ER at SS only (SS:  $\beta_{precip. \text{ to } |ERt|}$ : 0.01, -0.01 to 0.03)

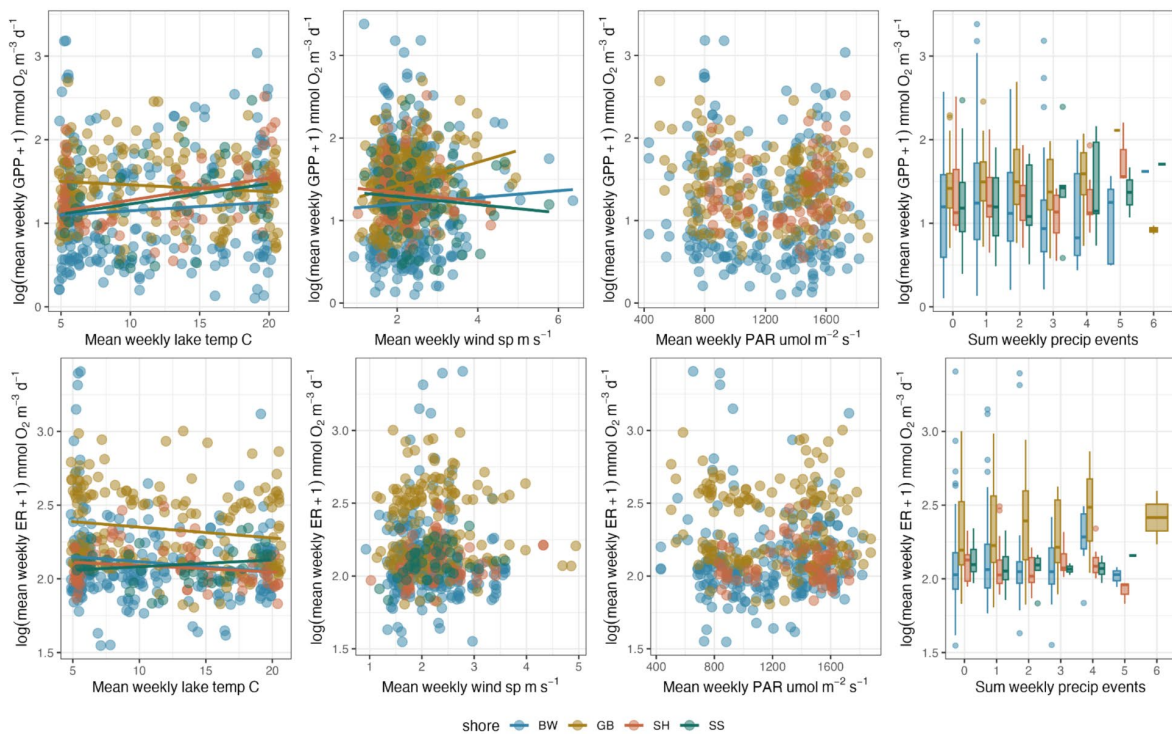


**Figure 40.** Relationships between log-transformed +1 weekly GPP (top) or ER (bottom) and environmental covariates, average weekly, lake water temperature, wind speed, benthic light, and total number of precipitation events at BW (blue), GB (yellow), SH (orange), and SS (green). Solid lines represent statistically significant linear relationships, while dashed lines represent marginal relationships.

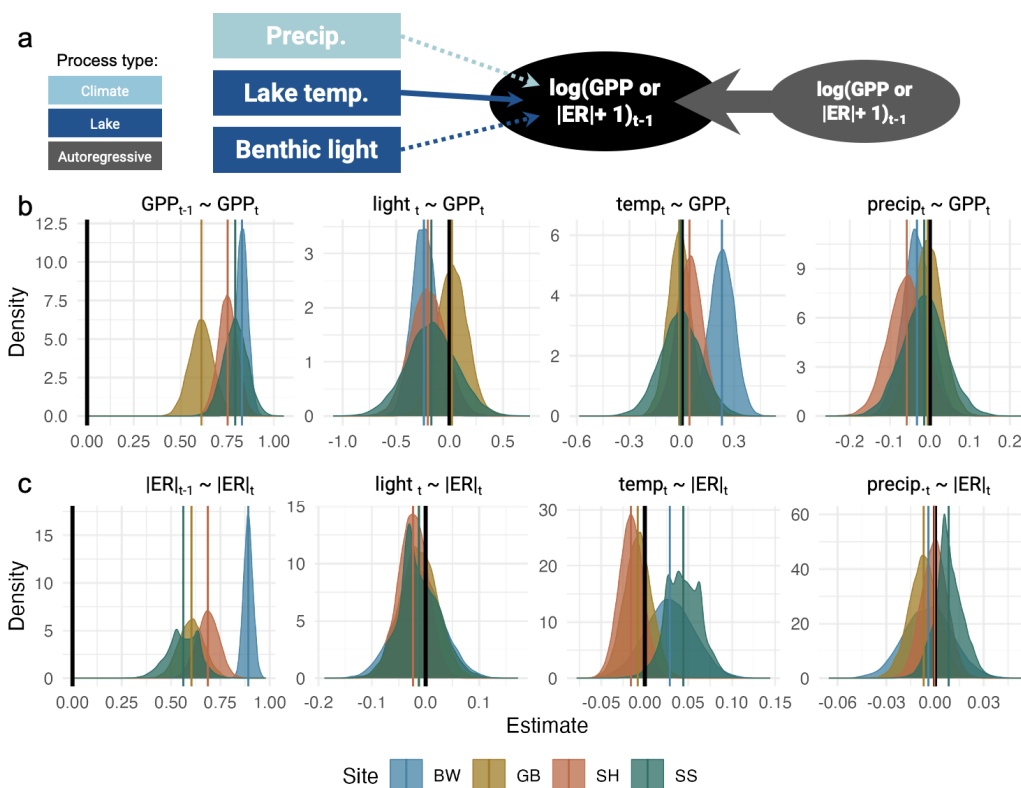


**Figure 41.** Results from Bayesian SEM for log transformed (+1)  $|ER|$  at BW (in blue), GB (in gold), SS (in green), and SH (in orange) for a subset of overlapping data from all four sites (February to September 2023). a) The SEM structure for how  $GPP_t$  or  $|ER|_t$  may be a function of precipitation, lake temperature, benthic light and  $|ER|_{t-1}$ , with mean posterior estimates and standard error color coded by shore in boxes along the path coefficients. Arrow weight represents relationship strength and box color for each parameter represents the type of process associated with a given parameter (light blue for climate processes like precipitation, dark blue for lake, and gray for autoregressive). b) The posterior estimates colored by shore for each parameter relationship. The vertical line marks when posteriors overlap zero for any parameter.

## V.D Conclusion

We observed relatively weak correlations between nearshore metabolism and stream flow and stream temperature. When exploring stronger causal relationships via SEMs that incorporate the combined indirect and direct influence of streamflow on nearshore GPP and  $|ER|$  suggest that streamflow does facilitate GPP, and may indirectly facilitate  $|ER|$  by reducing benthic light at both locations. Benthic metabolism is expected to be a function of light, water temperature, residence time and nutrient availability (Hoellein et al., 2013; Bernhardt et al., 2018; Hotchkiss et al., 2018). However, Lake Tahoe is a large, high elevation lake renowned for its cold water

temperatures and clarity, so much so that it is likely ultraviolet (UV) solar radiation in summertime can suppress GPP and result in benthic algal bleaching (Vinebrooke & Leavitt 1996, Naranjo et al., 2019). We observed confounding indirect impacts of streamflow on benthic light and water temperature. Streamflow reduced benthic light intensity, which may have reduced benthic communities exposure to harmful UV radiation. However, the release from UV photoinhibition may have been restricted by the simultaneous decrease in water temperature, which may thermally limit biologic processes associated with GPP and ER. When considering the causal effect of light, temperature, and precipitation on all four shore locations with overlapping observations, we found that water temperature had a small positive effect on GPP and ER, while benthic light suppressed GPP and ER especially at BW, the effect of precipitation varied with location. Precipitation tended to decrease GPP at all locations and stimulated ER at SS.

This analysis is a step towards linking upland processes (i.e. stream hydrology and stream metabolism) with downstream processes (i.e. nearshore metabolism) to determine the degree of control mountain streams exert on net ecosystem productivity dynamics in the littoral zone at the inflow of watersheds.

## VI. Conclusions and Recommendations

The overarching goal of this project was to develop a process-based understanding of how watershed-to-lake connections drive nearshore algal growth dynamics in Lake Tahoe. We addressed this goal through a combined approach of high-frequency sensor deployment and maintenance, ecosystem metabolism modeling, laboratory incubations, and routine monitoring of water chemistry and other parameters.

We accomplished the following:

1. We generated over two years of daily estimates of ecosystem metabolism (gross primary productivity and ecosystem respiration) from multiple locations on both the east and west shores of Lake Tahoe close to and far away from stream inlets.
2. We measured  $\text{NH}_4^+$  and  $\text{NO}_3^-$  concentrations in surface water samples from both Glenbrook and Blackwood creeks and the nearshore of Lake Tahoe for over two years.
3. We quantified rates of  $\text{NH}_4^+$  and  $\text{NO}_3^-$  uptake in benthic samples of the dominant substrate type collected during peak streamflow, the receding limb, and baseflow conditions in 2023 from multiple locations in the nearshore using established laboratory incubation methods.
4. Finally, we used a combination of time series models and structural equation modeling to integrate the results from objectives 1 and 2 and improve understanding of the direct and indirect effects of hydroclimatic variability on observed patterns in ecosystem metabolism in the nearshore.

The data we collected as part of this project and the ecosystem metabolism estimates we generated demonstrate how variable ecosystem productivity is in time and space in the nearshore of Lake Tahoe. Traditional approaches to quantifying algal activity in the nearshore (i.e., direct sampling of benthic biomass) may miss periods of peak biological activity due to the challenges associated with field sampling. Although maintenance of the sensor arrays during the exceptional winter of 2023 was challenging, we were able to capture the data necessary to estimate a complete time series of metabolic activity across two years with very different hydroclimatic conditions.

To improve the capacity of scientists and managers to monitor enough nearshore locations to capture a broader range of spatial heterogeneity in nearshore productivity and understand the factors controlling it, we recommend the continued and expanded use of high-frequency sensors distributed throughout the nearshore of the lake. We recommend that these sensors are not only at stream inlets, but also capture dynamics at locations further away from inflowing streams. Extending the duration and spatial distribution of high-frequency sensors in the nearshore and collecting additional ancillary data necessary to be able to model metabolism will provide novel insight into nearshore dynamics that have been previously overlooked.

## VII. References

- Adrian, R., O'Reilly, C., Zagarese, H., Baines, S., Hessen, D., Keller, W., et al. (2009). Lakes as sentinels of climate change. *Limnology and Oceanography*, 54, 2283-2297.
- Alavian, V., Jirka, G. H., Denton, R. A., Johnson, M. C., & Stefan, H. G. (1992). Density currents entering lakes and reservoirs. *Journal of Hydraulic Engineering*, 118(11), 1464-1489.
- Allan, J. D., Castillo, M. M., & Capps, K. A. (2021). *Stream ecology: structure and function of running waters*. Springer Nature.
- Appling, A. P., Hall Jr, R. O., Yackulic, C. B., & Arroita, M. (2018). Overcoming equifinality: Leveraging long time series for stream metabolism estimation. *Journal of Geophysical Research: Biogeosciences*, 123(2), 624-645.
- Atkins, K. S., Hackley, S., Allen, B., Watanabe, S., Reuter, J. and S. Schladow. (2021). Variability in periphyton community and biomass over 37 years in Lake Tahoe (CA-NV). *Hydrobiologia* 848:1755–1772.
- Axler, R., Gersberg, R., and C. Goldman. (1982). Inorganic nitrogen assimilation in a subalpine lake. *Limnology and Oceanography* 27: 53–65.
- Axler, R. P., Goldman, C. R., Reuter, J. E., Loeb, S. L., Priscu, J. C., & Carlton, R. G. (1983). Comparative studies of the nitrogen metabolism of phytoplankton and periphyton in oligotrophic lakes. *Using Nuclear Techniques*, 7.
- Barton, K., & Barton, M. K. (2015). Package 'mumin'. Version, 1(18), 439.
- Bates, D., Maechler, M., Bolker, B., Walker, S., Christensen, R. H. B., Singmann, H., ... & Bolker, M. B. (2015). Package 'lme4'. convergence, 12(1), 2.
- Beaudoing, H. and M. Rodell, NASA/GSFC/HSL (2020), GLDAS Noah Land Surface Model L4 3 hourly 0.25 x 0.25 degree V2.1, Greenbelt, Maryland, USA, Goddard Earth Sciences Data and Information Services Center (GES DISC), doi: 10.5067/E7TYRXPJKWOQ
- Bernhardt, E. S., Blaszczak, J. R., Ficken, C. D., Fork, M. L., Kaiser, K. E., & Seybold, E. C. (2017). Control points in ecosystems: moving beyond the hot spot hot moment concept. *Ecosystems*, 20, 665-682.
- Bernhardt, E. S., Heffernan, J. B., Grimm, N. B., Stanley, E. H., Harvey, J. W., Arroita, M., et al. (2018). The metabolic regimes of flowing waters. *Limnology and Oceanography*, 63, S99-S118.
- Bernot, M. J., Sobota, D. J., Hall Jr, R. O., Mulholland, P. J., Dodds, W. K., Webster, J. R., ... & Wilson, K. Y. M. (2010). Inter-regional comparison of land-use effects on stream metabolism. *Freshwater Biology*, 55(9), 1874-1890.
- Blaszczak, J. R., Yackulic, C. B., Shriver, R. K., & Hall Jr, R. O. (2023). Models of underlying autotrophic biomass dynamics fit to daily river ecosystem productivity estimates improve understanding of ecosystem disturbance and resilience. *Ecology Letters*, 26(9), 1510-1522.
- Bolker, B. M., Brooks, M. E., Clark, C. J., Geange, S. W., Poulsen, J. R., Stevens, M. H. H., & White, J. S. S. (2009). Generalized linear mixed models: a practical guide for ecology and evolution. *Trends in Ecology & Evolution*, 24(3), 127-135.
- Brooks, P. D., & Williams, M. W. (1999). Snowpack controls on nitrogen cycling and export in seasonally snow-covered catchments. *Hydrological processes*, 13(14-15), 2177-2190.
- Brooks, P. D., Grogan, P., Templer, P. H., Groffman, P., Öquist, M. G., & Schimel, J. (2011). Carbon and nitrogen cycling in snow-covered environments. *Geography Compass*, 5(9),

- 682-699.
- Brown, C. J., Saint Ange, C., Connolly, R. M., Hasan, S., Jackson, S., McMahon, J. M., & Smart, J. C. (2023). Ecosystem services in connected catchment to coast ecosystems: Monitoring to detect emerging trends. *Science of the Total Environment*, 869, 161670.
- Bürkner, P. (2021). Bayesian Item Response Modeling in R with brms and Stan. *Journal of Statistical Software*, 100(5), 1-54. doi:10.18637/jss.v100.i05
- California Department of Water Resources. (2023). WY 2023 Hydrometeorology Summary. Retrieved from [https://snow.water.ca.gov/service/plotly/data/download?dash=hydromet\\_summary&file=WY2023-Hydrometeorology-Summary.pdf](https://snow.water.ca.gov/service/plotly/data/download?dash=hydromet_summary&file=WY2023-Hydrometeorology-Summary.pdf)
- Carpenter, B., Gelman, A., Hoffman, M., et al. (2017). Stan: A probabilistic programming language. *Journal of Statistical Software* 76: 1–32.
- Carter, M. R., & Gregorich, E. G. (Eds.). (2007). *Soil sampling and methods of analysis*. CRC press.
- Casson, N. J., Contosta, A. R., Burakowski, E. A., Campbell, J. L., Crandall, M. S., Creed, I. F., ... & Nelson, S. J. (2019). Winter weather whiplash: Impacts of meteorological events misaligned with natural and human systems in seasonally snow-covered regions. *Earth's Future*, 7(12), 1434-1450.
- Cavalcanti, J. R., da Motta-Marques, D., & Fragoso Jr, C. R. (2016). Process-based modeling of shallow lake metabolism: Spatio-temporal variability and relative importance of individual processes. *Ecological modeling*, 323, 28-40.
- Chmiel, H. E., Hofmann, H., Sobek, S., Efremova, T., & Pasche, N. (2020). Where does the river end? Drivers of spatiotemporal variability in CO<sub>2</sub> concentration and flux in the inflow area of a large boreal lake. *Limnology and Oceanography*, 65(6), 1161-1174.
- Coats, R., Lewis, J., Alvarez, N., & Arneson, P. (2016). Temporal and Spatial Trends in Nutrient and Sediment Loading to Lake Tahoe, California-Nevada, USA. *JAWRA Journal of the American Water Resources Association*, 52(6), 1347-1365.
- Dai, A., Zhao, T., & Chen, J. (2018). Climate change and drought: a precipitation and evaporation perspective. *Current Climate Change Reports*, 4, 301-312.
- Devlin, S. P., Vander Zanden, M. J., & Vadeboncoeur, Y. (2016). Littoral-benthic primary production estimates: Sensitivity to simplifications with respect to periphyton productivity and basin morphometry. *Limnology and Oceanography: Methods*, 14(2), 138-149.
- Dodds, W. K., Biggs, B. J., & Lowe, R. L. (1999). Photosynthesis-irradiance patterns in benthic microalgae: variations as a function of assemblage thickness and community structure. *Journal of phycology*, 35(1), 42-53.
- Dodds, W. K., Bruckerhoff, L., Batzer, D., Schechner, A., Pennock, C., Renner, E., ... & Grieger, S. (2019). The freshwater biome gradient framework: predicting macroscale properties based on latitude, altitude, and precipitation. *Ecosphere*, 10(7), e02786.
- Domagalski, J. L., Morway, E., Alvarez, N. L., Hutchins, J., Rosen, M. R., & Coats, R. (2021). Trends in nitrogen, phosphorus, and sediment concentrations and loads in streams draining to Lake Tahoe, California, Nevada, USA. *Science of The Total Environment*, 752, 141815.
- Dugan, H. A., Woolway, R. I., Santoso, A. B., Corman, J. R., Jaimes, A., Nodine, E. R., ... & Weathers, K. C. (2016). Consequences of gas flux model choice on the interpretation of metabolic balance across 15 lakes. *Inland Waters*, 6(4), 581-592.

- Feistel, R. (2008). A Gibbs function for seawater thermodynamics for -6 to 80 C and salinity up to 120 g kg<sup>-1</sup>. *Deep Sea Research Part I: Oceanographic Research Papers*, 55(12), 1639-1671.
- Fox, J., & Weisberg, S. (2019). Using car functions in other functions. CRAN R.  
Fuka, D. R., Walter, M. T., Archibald, J. A., Steenhuis, T. S., & Easton, Z. M. (2018). *EcoHydrology: a community modeling foundation for eco-hydrology*. R package version 0.4, 12.
- Gardner, James V., Mayer, Larry A., Hughes-Clarke, John, 1998, Cruise Report RV Inland Surveyer Cruise IS-98; the Bathymetry of Lake Tahoe, California-Nevada, August 2 through August 17, 1998, Lake Tahoe, California and Nevada: U. S. Geological Survey Open-File Report 98-509, 28 pp., <https://pubs.usgs.gov/of/1998/0509/>.
- Glibert, P., F. Wilkerson, R. Dugdale, and others. 2016. Pluses and minuses of ammonium and nitrate uptake and assimilation by phytoplankton and implications for productivity and community composition, with emphasis on nitrogen-enriched conditions. *Limnology & Oceanography*, 61, 165–197.
- Goldman, C. R. (1988). Primary productivity, nutrients, and transparency during the early onset of eutrophication in ultra-oligotrophic Lake Tahoe, California-Nevada 1. *Limnology and oceanography*, 33(6), 1321-1333.
- Hackley, S., B. Allen, K. Senft, B. Berry, G. Schladow, A. Wong, Y. Chen, Q. Yu, Y. Jin, and M. Bruno. (2020). A Sustainable Method for the Rapid Assessment of the Extent and Causes of Metaphyton in Lake Tahoe. Final Report prepared for the Nevada Division of State Lands.
- Hagedorn, F., Kaiser, K., Feyen, H., & Schleppei, P. (2000). Effects of redox conditions and flow processes on the mobility of dissolved organic carbon and nitrogen in a forest soil (Vol. 29, No. 1, pp. 288-297). American Society of Agronomy, Crop Science Society of America, and Soil Science Society of America.
- Hale, K. E., Jennings, K. S., Musselman, K. N., Livneh, B., & Molotch, N. P. (2023). Recent decreases in snow water storage in western North America. *Communications Earth & Environment*, 4(1), 170.
- Hall, Jr, R. O., Baker, M. A., Arp, C. D., & Koch, B. J. (2009). Hydrologic control of nitrogen removal, storage, and export in a mountain stream. *Limnology and Oceanography*, 54(6), 2128-2142.
- Hammond, J. C., Saavedra, F. A., & Kampf, S. K. (2018). How does snow persistence relate to annual streamflow in mountain watersheds of the western US with wet maritime and dry continental climates?. *Water Resources Research*, 54(4), 2605-2623.
- Hanson, P. C., Pace, M. L., Carpenter, S. R., Cole, J. J., & Stanley, E. H. (2015). Integrating landscape carbon cycling: research needs for resolving organic carbon budgets of lakes. *Ecosystems*, 18, 363-375.
- Harpold, A., Brooks, P., Rajagopal, S., Heidbuchel, I., Jardine, A., & Stielstra, C. (2012). Changes in snowpack accumulation and ablation in the intermountain west. *Water Resources Research*, 48(11).
- Harpole, W. S., Ngai, J. T., Cleland, E. E., Seabloom, E. W., Borer, E. T., Bracken, M. E., ... & Smith, J. E. (2011). Nutrient co-limitation of primary producer communities. *Ecology letters*, 14(9), 852-862.
- Hayvaert, A., Fitzgerald, B., Morton, C. McGwire, R., and R. Susfalk. 2016. Pilot Implementation of the Lake Tahoe Nearshore Monitoring Framework for Clarity Metrics.

- Final Report prepared for the Nevada Division of State Lands.
- Hoellein, T. J., Bruesewitz, D. A., & Richardson, D. C. (2013). Revisiting Odum (1956): A synthesis of aquatic ecosystem metabolism. *Limnology and Oceanography*, 58(6), 2089-2100.
- Hofmann, H., Lorke, A., & Peeters, F. (2008). Temporal scales of water-level fluctuations in lakes and their ecological implications (pp. 85-96). Springer Netherlands.
- Hotchkiss, E. R., Sadro, S., & Hanson, P. C. (2018). Toward a more integrative perspective on carbon metabolism across lentic and lotic inland waters. *Limnology and Oceanography Letters*, 3(3), 57-63.
- Immerzeel, W. W., Lutz, A. F., Andrade, M., Bahl, A., Biemans, H., Bolch, T., ... & Baillie, J. E. M. (2020). Importance and vulnerability of the world's water towers. *Nature*, 577(7790), 364-369.
- Jankowski, K. J., Mejia, F. H., Blaszcak, J. R., & Holtgrieve, G. W. (2021). Aquatic ecosystem metabolism as a tool in environmental management. *Wiley Interdisciplinary Reviews: Water*, 8(4), e1521.
- Johengen, T. H., Biddanda, B. A., & Cotner, J. B. (2008). Stimulation of Lake Michigan plankton metabolism by sediment resuspension and river runoff. *Journal of Great Lakes Research*, 34(2), 213-227.
- Johnson, L. T., Tank, J. L., & Arango, C. P. (2009). The effect of land use on dissolved organic carbon and nitrogen uptake in streams. *Freshwater Biology*, 54(11), 2335-2350.
- Jones, N. E. (2010). Incorporating lakes within the river discontinuum: longitudinal changes in ecological characteristics in stream-lake networks. *Canadian Journal of Fisheries and Aquatic Sciences*, 67(8), 1350-1362.
- Kirchner, J. W., Godsey, S. E., Solomon, M., Osterhuber, R., McConnell, J. R., & Penna, D. (2020). The pulse of a montane ecosystem: coupling between daily cycles in solar flux, snowmelt, transpiration, groundwater, and streamflow at Sagehen Creek and Independence Creek, Sierra Nevada, USA. *Hydrology and Earth System Sciences*, 24(11), 5095-5123.
- Kuznetsova, A., Brockhoff, P. B., & Christensen, R. H. B. (2017). lmerTest package: tests in linear mixed effects models. *Journal of statistical software*, 82(13).
- Lefcheck, J. S. (2016). piecewiseSEM: Piecewise structural equation modeling in r for ecology, evolution, and systematics. *Methods in Ecology and Evolution*, 7(5), 573-579.
- Lefcheck, J. S., Orth, R. J., Dennison, W. C., Wilcox, D. J., Murphy, R. R., Keisman, J., ... & Batiuk, R. A. (2018). Long-term nutrient reductions lead to the unprecedented recovery of a temperate coastal region. *Proceedings of the National Academy of Sciences*, 115(14), 3658-3662.
- Langlois, J. L., Johnson, D. W., & Mehuys, G. R. (2005). Suspended sediment dynamics associated with snowmelt runoff in a small mountain stream of Lake Tahoe (Nevada). *Hydrological Processes: An International Journal*, 19(18), 3569-3580.
- Lee, J. Y., Marotzke, J., Bala, G., Cao, L., Corti, S., Dunne, J. P., ... & Jones, C. (2021). A., Maycock JM, O. Ndiaye, S. Panickal, T. Zhou Future Global Climate: Scenario-Based Projections and Near-Term Information/Climate Change 2021: The Physical Science Basis. Contribution of Working Group I to the Sixth Assessment Report of the Intergovernmental Panel on Climate Change.
- Leonard, R. L., Kaplan, L. A., Elder, J. F., Coats, R. N., & Goldman, C. R. (1979). Nutrient transport in surface runoff from a subalpine watershed, Lake Tahoe Basin, California.

- Ecological monographs, 49(3), 281-310.
- Leonard, R. L., & Goldman, C. R. (1981). Interagency Tahoe Monitoring Program: First Annual Report, Water Year 1980. Tahoe Research Group, Univ. of Calif., Davis.
- Li, D., Wrzesien, M. L., Durand, M., Adam, J., & Lettenmaier, D. P. (2017). How much runoff originates as snow in the western United States, and how will that change in the future?. *Geophysical Research Letters*, 44(12), 6163-6172.
- Loeb, S. L., & Goldman, C. R. (1979). Water and nutrient transport via groundwater from Ward Valley into Lake Tahoe 1. *Limnology and Oceanography*, 24(6), 1146-1154.
- Loeb, S. L., Reuter, J. E., & Goldman, C. R. (1983). Littoral zone production of oligotrophic lakes. In *Periphyton of freshwater ecosystems* (pp. 161-167). Springer, Dordrecht.
- Loeb, S. L. (1986). Algal Biofouling of Oligotrophy Lake Tahoe: Causal Factors Affecting Production. In *Studies in environmental science* (Vol. 28, pp. 159-173). Elsevier.
- Lohse, K. A., Brooks, P. D., McIntosh, J. C., Meixner, T., & Huxman, T. E. (2009). Interactions between biogeochemistry and hydrologic systems. *Annual Review of Environment and Resources*, 34, 65-96.
- Lottig, N. R., Phillips, J. S., Batt, R. D., Scordo, F., Williamson, T. J., Carpenter, S. R., ... & Zwart, J. (2022). Estimating pelagic primary production in lakes: Comparison of <sup>14</sup>C incubation and free-water O<sub>2</sub> approaches. *Limnology and Oceanography: Methods*, 20(1), 34-45.
- Lyon, S. W., Troch, P. A., Broxton, P. D., Molotch, N. P., & Brooks, P. D. (2008). Monitoring the timing of snowmelt and the initiation of streamflow using a distributed network of temperature/light sensors. *Ecohydrology: Ecosystems, Land and Water Process Interactions, Ecohydrogeomorphology*, 1(3), 215-224.
- Maranger, R., Jones, S. E., & Cotner, J. B. (2018). Stoichiometry of carbon, nitrogen, and phosphorus through the freshwater pipe. *Limnology and Oceanography Letters*, 3(3), 89-101.
- MacIntyre, S., Sickman, J. O., Goldthwait, S. A., & Kling, G. W. (2006). Physical pathways of nutrient supply in a small, ultraoligotrophic arctic lake during summer stratification. *Limnology and Oceanography*, 51(2), 1107-1124.
- McCullough, I. M., Cheruvilil, K. S., Collins, S. M., & Soranno, P. A. (2019). Geographic patterns of the climate sensitivity of lakes. *Ecological Applications*, 29(2), e01836.
- Messerli, B., Viviroli, D., & Weingartner, R. (2004). Mountains of the world: vulnerable water towers for the 21st century. *AMBIO: A Journal of the Human Environment*, 33(sp13), 29-34.
- Mulholland, P. J., & Hill, W. R. (1997). Seasonal patterns in streamwater nutrient and dissolved organic carbon concentrations: Separating catchment flow path and in-stream effects. *Water resources research*, 33(6), 1297-1306.
- Musselman, K. N., Addor, N., Vano, J. A., & Molotch, N. P. (2021). Winter melt trends portend widespread declines in snow water resources. *Nature Climate Change*, 11(5), 418-424.
- Murphy, D. D., & Knopp, C. M. (2000). Lake Tahoe watershed assessment: volume II. appendixes. General Technical Report-Pacific Southwest Research Station, USDA Forest Service, (PSW-GTR-176).
- Naranjo, R., Niswonger, R. G., Smith, D., Rosenberry, D., & Chandra, S. (2019). Linkages between hydrology and seasonal variations of nutrients and periphyton in a large oligotrophic subalpine lake. *Journal of Hydrology*, 568, 877-890.
- Naranjo, R., Work, P., Heyvaert, A., Schladow, G., Cortes, A., Watanabe, S., Tanaka, L.,

- and Elci, S. (2022). Seasonal and long-term clarity trend assessment of Lake Tahoe, California–Nevada: U.S. Geological Survey Scientific Investigations Report 2022–5070, 86 p., <https://doi.org/10.3133/sir20225070>.
- Ngai, K. L. C., Shuter, B. J., Jackson, D. A., & Chandra, S. (2013). Projecting impacts of climate change on surface water temperatures of a large subalpine lake: Lake Tahoe, USA. *Climatic Change*, 118, 841-855.
- Odum, H. T. (1956). Primary production in flowing waters 1. *Limnology and oceanography*, 1(2), 102-117.
- Oleksy, I. A., Jones, S. E., & Solomon, C. T. (2021). Hydrologic setting dictates the sensitivity of ecosystem metabolism to climate variability in lakes. *Ecosystems*, 1-18
- Ormerod, S. J., Dobson, M., Hildrew, A. G., & Townsend, C. (2010). Multiple stressors in freshwater ecosystems. *Freshwater Biology*, 55, 1-4.
- Pearson, C. and J. Huntington. 2019. Remote Sensing and Cloud Computing to Support Lake Tahoe Nearshore Monitoring. Final Report prepared for the Nevada Division of State Lands.
- Périllon, C., Pöschke, F., Lewandowski, J., Hupfer, M., Hilt, S., (2017). Stimulation of epiphyton growth by lacustrine groundwater discharge to an oligo-mesotrophic hard-water lake. *Freshwater Sci.* 36 (3), 555–570.
- Peterson, B. J., Wollheim, W. M., Mulholland, P. J., Webster, J. R., Meyer, J. L., Tank, J. L., ... & Morrall, D. D. (2001). Control of nitrogen export from watersheds by headwater streams. *Science*, 292(5514), 86-90.
- Phillips, J. S. (2020). Time-varying responses of lake metabolism to light and temperature. *Limnology and Oceanography*, 65(3), 652-666.
- Poff, N. L., & Ward, J. V. (1992). Heterogeneous currents and algal resources mediate in situ foraging activity of a mobile stream grazer. *Oikos*, 465-478.
- Nielson, J. R., & Henderson, S. M. (2023). Periodic boundary layer separation and lateral intrusions observed above a sloping lakebed. *Limnology and Oceanography*, 68(1), 26-39.
- Reidmiller, D. R., Avery, C. W., Easterling, D. R., Kunkel, K. E., Lewis, K. L., Maycock, T. K., & Stewart, B. C. (2017). Impacts, risks, and adaptation in the United States: Fourth national climate assessment, volume II.
- Reuter, J., Loeb, S., and C. Goldman. 1986. Inorganic nitrogen uptake by epilithic periphyton in a N-deficient lake. *Limnology & Oceanography* 31: 149–160.
- Reuter, J. E., & Miller, W. W. (2000). Aquatic resources, water quality, and limnology of Lake Tahoe and its upland watershed. *Lake Tahoe watershed assessment*, 1, 215-399.
- Roberts, D. C., Forrest, A. L., Sahoo, G. B., Hook, S. J., & Schladow, S. G. (2018). Snowmelt timing as a determinant of lake inflow mixing. *Water Resources Research*, 54(2), 1237-1251.
- Rose, K. C., Williamson, C. E., Schladow, S. G., Winder, M., & Oris, J. T. (2009). Patterns of spatial and temporal variability of UV transparency in Lake Tahoe, California-Nevada. *Journal of Geophysical Research: Biogeosciences*, 114(G2).
- Rosenberry, D. O., Lewandowski, J., Meinikmann, K., & Nützmann, G. (2015). Groundwater—the disregarded component in lake water and nutrient budgets. Part 1: effects of groundwater on hydrology. *Hydrological processes*, 29(13), 2895-2921.
- Sadro, S., Melack, J. M., Sickman, J. O., & Skeen, K. (2019). Climate warming response of mountain lakes affected by variations in snow. *Limnology and Oceanography Letters*,

- 4(1), 9-17.
- Sartory, D. P. (1985). The determination of algal chlorophyllous pigments by high performance liquid chromatography and spectrophotometry. *Water Research*, 19(5), 605-610.
- Savoy, P., Bernhardt, E., Kirk, L., Cohen, M. J., & Heffernan, J. B. (2021). A seasonally dynamic model of light at the stream surface. *Freshwater Science*, 40(2), 286-301.
- Scordo, F., Lottig, N. R., Fiorenza, J. E., Culpepper, J., Simmons, J., Seitz, C., ... & Chandra, S. (2022). Hydroclimate Variability Affects Habitat-Specific (Open Water and Littoral) Lake Metabolism. *Water Resources Research*, 58(1), e2021WR031094.
- Schindler, D. W. (2001). The cumulative effects of climate warming and other human stresses on Canadian freshwaters in the new millennium. *Canadian Journal of Fisheries and Aquatic Sciences*, 58(1), 18-29.
- Scott, D. N., & Wohl, E. E. (2017). Evaluating carbon storage on subalpine lake deltas. *Earth Surface Processes and Landforms*, 42(10), 1472-1481.
- Scordo, F., Lottig, N. R., Fiorenza, J. E., Culpepper, J., Simmons, J., Seitz, C., ... & Chandra, S. (2022). Hydroclimate variability affects habitat-specific (open water and littoral) lake metabolism. *Water Resources Research*, 58(1), e2021WR031094.
- Seybold, E., & McGlynn, B. (2018). Hydrologic and biogeochemical drivers of dissolved organic carbon and nitrate uptake in a headwater stream network. *Biogeochemistry*, 138, 23-48.
- Seybold, E. C., Dwivedi, R., Musselman, K. N., Kincaid, D. W., Schroth, A. W., Classen, A. T., ... & Adair, E. C. (2022). Winter runoff events pose an unquantified continental-scale risk of high wintertime nutrient export. *Environmental Research Letters*, 17(10), 104044.
- Sickman, J. O., Melack, J. M., & Stoddard, J. L. (2002). Regional analysis of inorganic nitrogen yield and retention in high-elevation ecosystems of the Sierra Nevada and Rocky Mountains. *The Nitrogen Cycle at Regional to Global Scales*, 341-374.
- Sickman, J. O., Leydecker, A. L., Chang, C. C., Kendall, C., Melack, J. M., Lucero, D. M., & Schimel, J. (2003). Mechanisms underlying export of N from high-elevation catchments during seasonal transitions. *Biogeochemistry*, 64(1), 1-24.
- Siirila-Woodburn, E. R., Rhoades, A. M., Hatchett, B. J., Huning, L. S., Szinai, J., Tague, C., ... & Kaatz, L. (2021). A low-to-no snow future and its impacts on water resources in the western United States. *Nature Reviews Earth & Environment*, 2(11), 800-819.
- Steele, J. H. (1962). Environmental control of photosynthesis in the sea. *Limnology and oceanography*, 7(2), 137-150.
- Steissberg, T. E., Hook, S. J., & Schladow, S. G. (2005). Characterizing partial upwellings and surface circulation at Lake Tahoe, California–Nevada, USA with thermal infrared images. *Remote sensing of environment*, 99(1-2), 2-15.
- Staehr, P. A., Brighenti, L. S., Honti, M., Christensen, J., & Rose, K. C. (2016). Global patterns of light saturation and photoinhibition of lake primary production. *Inland Waters*, 6(4), 593-607.
- Stewart, I. T. (2009). Changes in snowpack and snowmelt runoff for key mountain regions. *Hydrological Processes: An International Journal*, 23(1), 78-94.
- Stoddard, J. L. (1995). Episodic acidification during snowmelt of high elevation lakes in the Sierra Nevada mountains of California. *Water, Air, and Soil Pollution*, 85, 353-358.
- Vachon, D., & Prairie, Y. T. (2013). The ecosystem size and shape dependence of gas transfer velocity versus wind speed relationships in lakes. *Canadian Journal of Fisheries and Aquatic Sciences*, 70(12), 1757-1764.

- Vadeboncoeur, Y., Jeppesen, E., Zanden, M. J. V., Schierup, H. H., Christoffersen, K., & Lodge, D. M. (2003). From Greenland to green lakes: cultural eutrophication and the loss of benthic pathways in lakes. *Limnology and oceanography*, 48(4), 1408-1418.
- Vadeboncoeur, Y., Kalff, J., Christoffersen, K., & Jeppesen, E. (2006). Substratum as a driver of variation in periphyton chlorophyll and productivity in lakes. *Journal of the North American Benthological Society*, 25(2), 379-392.
- Vadeboncoeur, Y., Moore, M. V., Stewart, S. D., Chandra, S., Atkins, K. S., Baron, J. S., ... & Yamamuro, M. (2021). Blue waters, green bottoms: Benthic filamentous algal blooms are an emerging threat to clear lakes worldwide. *BioScience*, 71(10), 1011-1027.
- Vander Zanden, M. J., & Vadeboncoeur, Y. (2020). Putting the lake back together 20 years later: what in the benthos have we learned about habitat linkages in lakes?. *Inland Waters*, 10(3), 305-321.
- Venables, W. N., & Ripley, B. D. (2002). *Modern applied statistics with S* fourth edition by world.
- Vinebrooke, R. D., & Leavitt, P. R. (1996). Effects of ultraviolet radiation on periphyton in an alpine lake. *Limnology and Oceanography*, 41(5), 1035-1040.
- Ward, N. K., Brentrup, J. A., Richardson, D. C., Weathers, K. C., Hanson, P. C., Hewett, R. J., & Carey, C. C. (2022). Dynamics of the stream–lake transitional zone affect littoral lake metabolism. *Aquatic Sciences*, 84(3), 31.
- Watanabe, S. and G. Schladow. 2023. Lake Tahoe UV Radiation Profile data ver 1. Environmental Data Initiative. <https://doi.org/10.6073/pasta/cd6d77f5642d0f31f7edbf798bec5d38> (Accessed 2024-03-12).
- Wells, M. L., Trainer, V. L., Smayda, T. J., Karlson, B. S., Trick, C. G., Kudela, R. M., ... & Cochlan, W. P. (2015). Harmful algal blooms and climate change: Learning from the past and present to forecast the future. *Harmful algae*, 49, 68-93.
- Williamson, C. E., Saros, J. E., Vincent, W. F., & Smol, J. P. (2009). Lakes and reservoirs as sentinels, integrators, and regulators of climate change. *Limnology and Oceanography*, 54(6part2), 2273-2282.
- Wilkinson, G. M., Pace, M. L., & Cole, J. J. (2013). Terrestrial dominance of organic matter in north temperate lakes. *Global Biogeochemical Cycles*, 27(1), 43-51.
- Winslow L., Read J., Woolway R., Brentrup J., Leach T., Zwart J., Albers S., and Collinge D. (2019). rLakeAnalyzer: Lake Physics Tools. R package version 1.11.4.. <https://CRAN.R-project.org/package=rLakeAnalyzer>.
- Xia, Y., Mitchell, K., Ek, M., Sheffield, J., Cosgrove, B., Wood, E., ... & Mocko, D. (2012). Continental-scale water and energy flux analysis and validation for the North American Land Data Assimilation System project phase 2 (NLDAS-2): 1. Intercomparison and application of model products. *Journal of Geophysical Research: Atmospheres*, 117(D3).

## Appendix 1. Supplementary Figures

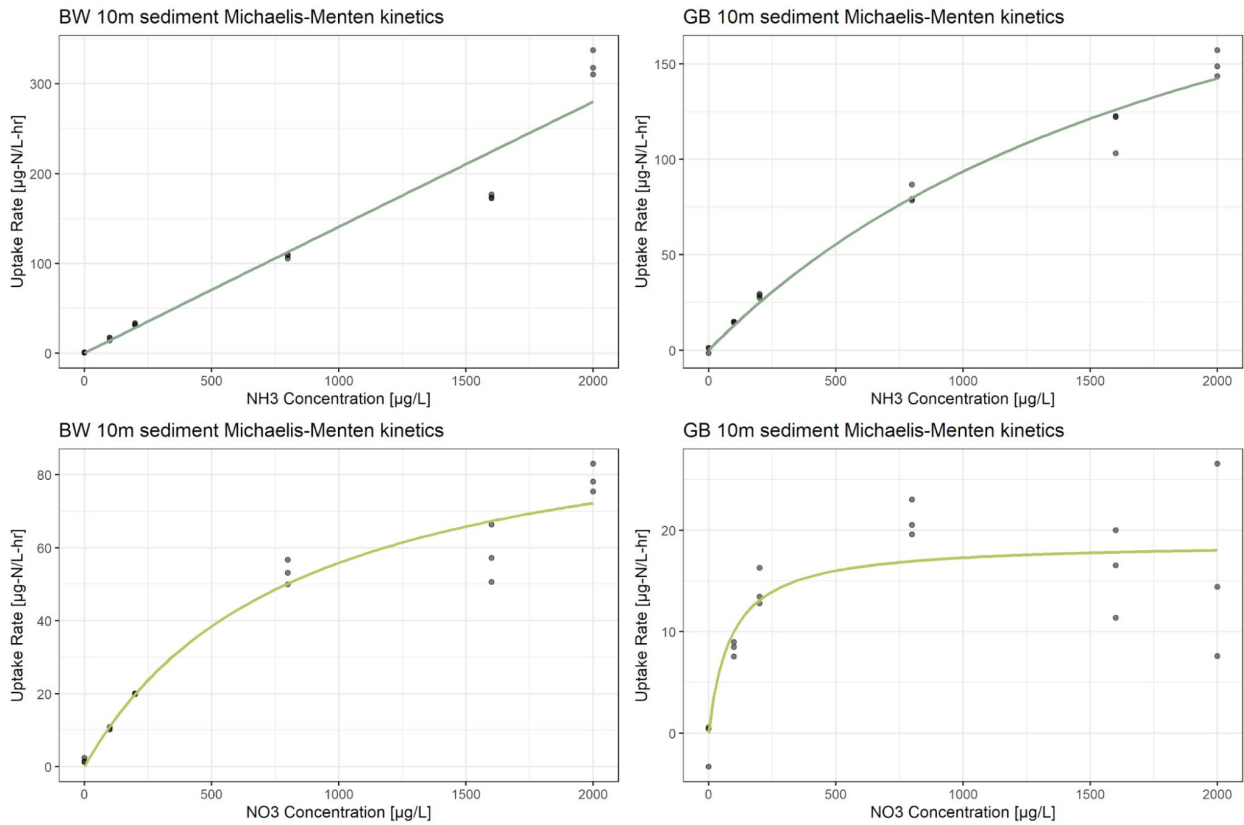


**Figure S1.** Example Michaelis-Menten uptake kinetics models for ammonium and nitrate fit to incubation data from July across GB and BW for sediment from 10m depth. NH<sub>3</sub> (ammonia) as labeled in the figure was adjusted to NH<sub>4</sub> (ammonium) in the analyses. Not all incubations reached saturation (indicated by a straight line), while others did (indicated by a saturating curve such as for NO<sub>3</sub> from GB 10m in the lower right hand corner).